UNIVERSITÉ D'ORLÉANS

ÉCOLE DOCTORALE
SANTE, SCIENCES BIOLOGIQUES ET CHIMIE DU VIVANT

Centre de Biophysique Moléculaire

THÈSE présentée par :

Alexandra Foucault-Collet

soutenue le : 23 Septembre 2013

pour obtenir le grade de : **Docteur de l'université d'Orléans**

Discipline/ Spécialité : Biologie / Biochimie

Luminescent Lanthanide Metal-Organic Frameworks and Dendrimer Complexes for Optical biological imaging

THÈSE dirigée par :

M. Stéphane Petoud	Directeur de recherche Inserm

RAPPORTEURS :

M. Ludovic Julien	Professeur, Université Pierre et Marie Curie
M. Christopher Orvig	Professor, University of British Columbia

---

JURY :

M. Richard Daniellou	Professeur, Université d'Orléans, Président du jury
M. Ludovic Jullien	Professeur , Université Pierre et Marie Curie
M. Christopher Orvig	Professeur, University of British Columbia
M. Christian Amatore	Directeur de recherche CNRS, Ecole Normale Supérieure
M. Nathaniel Rosi	Professeur, University of Pittsburgh
M. Stéphane Petoud	Directeur de recherche Inserm, CBM

Acknowledgements

Je voudrais tout d'abord remercier les membres du jury qui me font l'honneur d'avoir accepté de juger mon travail: Pr Ludovic Julien et le Pr Christopher Orvig ainsi que le Dr Christian Amatore, Pr Richard Daniellou, Pr Nathaniel Rosi.

Je remercie également le Pr Jean-Claude Beloeil et Dr Eva Jakab-Toth de m'avoir permis d'effectuer cette thèse au sein du Centre de Biophysique Moléculaire.

Je remercie chaleureusement mon directeur de thèse, le Pr Stéphane Petoud. Merci de ton aide, ton soutien, ta compréhension et ta gentillesse. Merci de m'avoir laissé une aussi grande liberté dans mon travail durant ces 3 ans. J'espère que cette page qui se tourne ne sera que le début d'une fructueuse collaboration!

Merci à toute l'équipe qui a été comme une deuxième famille durant ces 3 années:

- Dr Ulysse Asseline, merci pour votre oeil avisé et vos conseils expérimentés qui m'auront été bien utiles et pour le temps passé à corriger cette thèse!
- Pr Josef Hamacek, toi qui est toujours partant pour une bataille de boules de neige, un bowling ou un lasergame, merci pour ton humour et ta bonne humeur!
- Dr Svetlana Eliseeva, myfriend! I'm so happy to meet you, I have lot of respect for your human and scientific qualities. Thank you for all nice moment with you.
- Dr Sandrine Villette, merci pour ton aide et ton amitié, toi qui a été là depuis le tout début et m'a beaucoup appris. Merci aussi de m'avoir fait découvrir l'univers du synchrotron.
- Dr Emi Evangelio,muchas gracias Chica por haberme enseñado algunas palabras en español! Merci aussi pour ta bonne humeur et ta joie de vivre communicative et les "chocolatito" qui remontent le moral quand "on en peux pas plus"!
- Agnès Pallier, merci pour ta patience, ta gentillesse et les heures passées à essayer de déboucher l'ICP à cause de mes solutions divers et variées!
- Iuliia Nazarenko, merci pour tes petites attentions (je me souviens particulièrement du jour où tu nous as offert des tulipes!), je te souhaite de passer 3 ans aussi enrichissants que ceux que je viens de passer.
- Dr Virginie Placide, que j'ai mis à contribution alors qu'elle vient de rejoindre l'équipe! Merci pour ton aide!

Merci au Dr Fabienne Brulé de m'avoir donné l'opportunité de pouvoir découvrir l'enseignement. Merci également Arnaud et Mélanie pour leur aide si précieuse lors des TP.

Je remercie David Gosset pour son aide précieuse sur la plateforme cytométrie et imagerie cellulaire, Rudy Clémençon pour son aide à l'animalerie ainsi que le Dr Mathieu Réfrégiers pour son acceuil chaleureux et son aide lors des créneaux au synchrotron SOLEIL.

Je remercie également Annie Richard du Centre de microscopie électronique à l'université d'Orléans pour sa gentillesse et son efficacité lors des sessions MEB. Ainsi que le Dr Mathieu Allix et le Dr Emmanuel Veron du CEMHTI pour les mesures de rayons X, le MET et l'enthousiasme et la disponibilité dont ils ont fait preuve pour nous aider dans ce projet.

Je souhaite remercier nos collaborateurs à Pittsburgh, Pr Nathaniel Rosi, Dr Hyounsoo Hu, Kristy Gogick et Tao Li pour la synthèse des molécules et autres manipulations urgentes (pas toujours facile de travailler dans l'urgence avec 6 heures de décalage horaire).

Un petit mot pour mes amis: Alan Guichard, pour les coups de main avec les souris et les très longues heures du vendredi soir sur le vidéomiroscope; ainsi qu'Axelle Hubert, ma voisine de couloir pour son soutien et nos petites blagues qui remontent le moral!

Merci à mes parents, Jean-Louis et Isabelle, et à mon frère Valentin à qui je dédie cette thèse.

Une pensée également pour mon amie Tiphaine qui m'aura bien soutenue ces dernières semaines!

Je voudrais également dédier cette thèse à mon incroyable mari Guillaume sans qui je n'aurais probablement pas écris ces pages aujourd'hui...Merci pour ton soutiens sans faille.

Because it was a kind of magic…

Résumé

Les composés à base de lanthanides luminescents possèdent des propriétés uniques offrant de nombreux avantages pour l'étude de problèmes biologiques et pour le diagnostic. Ils résistent notamment à la photodécomposition, possèdent des temps de vie de luminescence longs ainsi que des bandes d'émissions étroites qui ne se recouvrent pas.

De plus, certains lanthanides émettent dans le proche infrarouge, ce qui les rend particulièrement intéressants pour des applications d''imagerie *in vivo*.

De part l'interdiction des transitions $f \rightarrow f$, les cations lanthanides ont des coefficients d'extinction très faibles. C'est la raison pour laquelle, il est nécessaire d'utiliser un ou plusieurs sensibilisateur(s) (comme un chromophore organique) pour exciter le lanthanide par « effet antenne ».

Nous proposons ici de nouveaux composés émettant dans le proche infrarouge dont la structure permet d'incorporer une densité importante de lanthanides et de sensibilisateurs par unité de volume : i) les nano-MOF Yb-PVDC-3 constitués de chromophores dérivés de dicarboxylates de phenylènevinylène qui sensibilisent les cations Yb^{3+} du réseau. ii) les complexes formés avec des ligands dendrimères dérivés de polyamidoamine de génération 3 capables de sensibiliser 8 lanthanides (Eu^{3+}, Yb^{3+}, Nd^{3+}) par le biais de 32 antennes dérivées du groupe 1,8-naphthalimide.

La caractérisation physique, photophysique et la biocompatibilité de ces composés ont été réalisées. Ils ont montré une bonne stabilité dans différents environnements. Leur faible cytotoxicité a permis d'obtenir des images de microscopie proche infrarouge sur cellules vivantes.

La preuve de principe que les nano-MOFs et les dendrimères complexant des lanthanides peuvent être utilisés comme rapporteurs luminescents *in cellulo* et *in vivo* a été ici établie. Les résultats obtenus valident la stratégie d'utiliser ce type de matériel pour augmenter le nombre de photons émis par unité de volume afin d'obtenir une meilleure sensibilité de détection.

<u>Mots clés:</u> imagerie - proche-infrarouge - lanthanides - dendrimères - réseaux métallo-organiques

Abstract

Unique properties of luminescent lanthanides reporters explain their emergence for bioanalytical and optical imaging applications. Lanthanide ions possess long emission lifetimes, a good resistance to photodecomposition and sharp emission bands that do not overlap.

In addition, several lanthanides emit in the near infrared (NIR) region of the electromagnetic spectrum making them very interesting for *in vivo* imaging. Free lanthanide cations have low extinction coefficients due to the forbidden nature of the $f \rightarrow f$ transition. Therefore, lanthanides must be sensitized using a photonic converter such as an organic chromophore through the "antenna effect".

We report here new near-infrared emitting compounds whose structure allows to incorporate a high density of lanthanide cations and sensitizers per unit volume: i) nano-MOF Yb-PVDC-3 based on Yb^{3+} sensitized by phenylenevinylene dicarboxylates. ii) polymetallic dendrimer complexes formed with derivatives of new generation-3 polyamidoamine dendrimers. In these complexes, 8 lanthanide ions (Eu^{3+}, Yb^{3+}, Nd^{3+}) can be sensitized by the 32 antenna derived from 1,8-naphthalimide.

These two families of compounds were fully characterised for their physical, photophysical properties as well as for their biological respective compatibilities. They are stable in various media and their low cytotoxicity and emission of a sufficient number of photons are suitable for near-infrared live cell imaging.

One of the main goal outcomes of this work is the establishment of the proof of principle that nano-MOFs and lanthanide derived dendrimers can be used for the sensitization of NIR emitting lanthanides to create a new generation of NIR optical imaging agents suitable for both *in cellulo* and *in vivo*applications.The present work also validates the efficiency of the strategy to use both types of nanoscale systems described here to increase the number of emitted photons per unit volume for an improved detection sensitivity and to compensate for low quantum yields.

Key words: imaging - near-infrared - lanthanides - dendrimers - Metal Organic Frameworks.

General introduction

Optical fluorescence imaging has become an essential tool allowing to study in real time biological systems and their functions from the single cell to the whole animal. For clinical purposes, this technique is very promising by providing quantitative and high sensitivity detection sensitivity not only for the diagnostic but also for the monitoring of therapy efficacy.

A large variety of fluorescent reporters are described in the literature as organic fluorophores. These compounds are often suffering from rapid photobleaching which can be a major limitation for long time scale or repeated studies. Semi-conductor nanocrystals (Quantum Dots) are highly photostable but present significant risks of toxicity due to the potential release of their toxic constituting metal such as Cd^{2+} or Se^{n+} ions.

Luminescent lanthanide complexes are emerging as new reporters for optical imaging applications. They possess several advantages for the study and analysis of biological problems where the analyte is typically present with in a complex mixture of molecules. They emit as sharp emission bands that allow spectral discrimination and whose wavelengths are independent from experimental conditions, long luminescence lifetimes (few tens of nanoseconds to several milliseconds) and are, for most of them, highly resistant to the photodecomposition.

In addition, several lanthanides (Yb^{3+}, Nd^{3+}, Ho^{3+}, Tm^{3+}, Pr^{3+}) emit in the near infrared (NIR) domain, making them very interesting for *in vivo* imaging. Indeed, NIR light can cross important depths of biological tissue and allows detection in a wavelength range almost free of autofluorescence, increasing the signal-to-noise and the detection sensitivity. Furthermore, NIR photons interact less with the biological material in comparison to visible photons, thus decreasing the risk of disturbing or damaging the biological systems being observed.

Free lanthanide cations have low extinction coefficients due to the forbidden nature of the $f \rightarrow f$ transitions. Therefore, lanthanides must be sensitized using a photonic converter such as an organic chromophore through the “antenna effect”. Antenna (chromophore and ligand) must be placed in sufficiently close proximity to the lanthanide to provide sensitization, resulting in the compound to emit a sufficient number of photons for detection.

One current limitation of near-infrared emitting lanthanide complexes that strongly limit their applications is their low quantum yields. To compensate for this disadvantage, we propose a strategy that aims at the creation of novel macromolecules and nanoparticles such as

dendrimers and metal organic frameworks (MOFs) to multiply the number of chromophoric sensitizers and the number of NIR-emitting lanthanides per molecule to enhance the number of emitted photons per unit volume.

Dendrimers are widely described in the literature as being biocompatible compounds available for several biological application fields such as drug delivery, gene transfection and imaging agents.

These two families of molecules are chemically very different but both allow to test the concept of concentrating a high number of antennae and lanthanide cations in a same compound to in order to increase the emission signal.

As a major achievement presented in this work, we have demonstrated for the first time the proof of principle of using of lanthanide based near-infrared emitting dendrimer complexes and MOFs for biological imaging (*in cellulo* and *in vivo*) using a single photon classical source of microscopy excitation.

In the first part, a new nanoMOFs based on chromophore PVDC (a derivative of the phenylene chromophore) and Yb^{3+} was physically and photophysically characterized. The good stability of this compound was studied in different solution environments before experiments it in living cells.

In a second part, abilities of two different generation-3 dendrimer complexes were evaluated as near-infrared imaging agents. The compounds were photophysically characterized and studied for their behavior in living cells. Strong NIR emission intensities monitored *in vitro* and *in vivo* making them good candidates for tumor diagnostic (using specific targeting).

Results obtained validate the efficiency of the strategy to use this type of material for increasing the number of emitted photons per unit volume for higher detection sensitivity.

The third part of the thesis is devoted to the observation of a very surprising behavior of 1,8-naphthalimide derivatived dendrimer complexes behavior in cells under blue light excitation.

Table of contents

Abbreviations:

A.U.: Arbitrary Units

BODIPY : Borondipyrromethane

BP: Band Pass

BSA: Bovine Serum Albumin

Ca : calcium

CBM : centre de Biophysique Moléculaire

CCD: Charge-Coupled Device

Cd : Cadmium

CEMHTI : Conditions Extrêmes et Matériaux : Haute Température et Irradiation

CLSM : Confocal Laser Scanning Microscopy

cm : Centimeter

CNRS : Centre National de la Recherche Scientifique

CO_2 : Carbon dioxide

CTAB : Cetyl trimethylammonium bromide

cTDNA: Calf Thymus DNA

Cy : Cyanine

DAB: Diaminobutane

DIC: Differential Interference Contrast

DISCO : Dichroïsm Imagerie, Spectrométrie de masse pour la chimie et la biologie

DMEM: Dulbecco's modified Eagle's medium

DNA: Deoxyribonucleic Acid

DCDHF-DA: 2',7'-dichlorodihydrofluorescein diacetate

DMF : Dimethylformamide

DMSO: Dimethylsulfoxide

EDTA: Ethylene Diamine Tetraacetic Acid

EMCCD : Electron Multiplying Charge-Coupled Device

EPFL : École Polytechnique Féderale de Lausanne

EPR effect : Enhanced Permeability and Retention Effect

Eu: Europium

Er: Erbium

ER : Endoplasmic reticulum

FACS: Fluorescence-activated Cell Sorting

FBS: Fetal BovineSerum

FDA: Food and Drug Administration

FITC: Fluorescein isothiocyanate

G*x* : Generation *x* dendrimer

Gd: Gadolinium

Hb : Hemoglobin

HbO_2 : Oxygenated hemoglobin

HDD : High Dynamic Detection

HEPES : 4-(2-hydroxyethyl)-1-piperazineethanesulfonic acid

Ho: Holmium

HRMS : High resolution mass spectrometry

H&E: Hematoxylin and Eosin

ICP: Inductively Coupled Plasma

IF: Intensity of Fluorescence

ICG: Indocyanine Green

In : Indium

INSERM : Institut National de la Santé et de la Recherche Médicale

IV : Intravenous

KD: Dissociation constant

KDa: kilo Dalton

kV : kiloVolt

LASER : Light Amplification by Stimulated Emission of Radiation

LED: Light-Emitting Diode

Ln : Lanthanide

LP: Long Pass

M : Molar

mA : MiliAmper

MEM : Mimimum Essential Medium

MHz : MegaHertz

MIL: Materials of Institut Lavoisier

MOF: Metal Organic Frameworks

MRI : Magnetic Resonance Imaging

ms : Millisecond

MWCO : Molecular Weight Cut Off

NA : Numerical Aperture

Nap : Maphthalimide

Nd: Neodimium

NIR: Near infrared

nm : Nanometer

nMOF: Nano-MOF (NMOF)

NMR : Nuclear magnetic resonance

NSF : Nephrogenic Systemic Fibrosis

OCT : Optimum cutting temperature

OptiMEM : Opti-Minimum Essential Medium

PAMAM : Polyaminoamide

PBS : Phosphate buffer saline

PFA: Paraformaldehyde

PhD : *Philosophiæ Doctor* (doctor of philosophy)

PEG: Polyethylene glycol

PET : Positron Emission Tomography

PPCy : Pyrrolopyrrole cyanine dyes

PPI: Polypropylenemine

Pr : Prazeodim

PVDC: Phenylenevinylene dicarboxylate

PXRD : Powder X-ray diffraction

QDs: Quantum Dots

RGD : Arginine-glycine-aspartic acid

ROS: Reactive Oxygen Species

RPMI: Roswell Park Memorial Institute

RU: Resonance Units

S: **S**inglet state

SBUs : Secondary building units

SD: Standard deviation

Se : Selenium

SEM: Scanning Electron Microscopy

SPECT : Single photon emission computed tomography

T : Triplet state

TEM : TransmittedElectron Microscopy

Tm : Thulium

UV: Ultraviolet

Vis : Visible

W : Watt

Yb: Ytterbium

Z : Atomic number

3D: Three-dimensional

λex : Excitation wavelength

λem : Emission wavelength

τ_x : Luminescent lifetimes

Φ: Quantum yield

ε : Molecular extinction coefficients

Å : Ångström

Figures:

Appendix 4: G3P-NH_2 and G3P-NB dendrimer synthesis

Appendix 5: Emission intensity variations of Eu-G3P-NB (A.U.) as function of pH

Appendix 6: excitation and emission spectra of Nd^{3+} dendrimers.

Appendix 7: Emission and excitation spectra of Yb^{3+} dendrimers.

Appendix 8. Decay of the intensity with time of the luminescence arising from Eu^{3+} cations located in the polymetallic complex formed by reaction of a generation-3 PAMAM dendrimer whose branches have been functionalized with 32 2,3-naphthalimide groups.

1-Bibliographic overview and introduction

The present work was aiming at establishing a proof of concept that luminescent lanthanide complexes and nanomaterials emitting in the near-infrared can be used as efficient luminescence imaging agents in cells and small animal models.

This chapter contains a bibliographic overview allowing to locate this PhD project in its context of actual concern about the lack of efficient NIR imaging agents for diagnostic and fluorescence imaging.
After the description of the advanatages of NIR fluorescence imaging, the most used NIR emitting organic fluorophores and quantum dots for biological imaging applications will be rapidly described. Lanthanide cations properties will be presented in more details to explain why they are interesting and the challenges of creating new NIR emitting lanthanide complexes as efficient imaging agents for biological imaging.
A paragraph will be devoted to describe the main goal of this work before presenting obtained results.

1.1-Fluorescence imaging

Fluorescence imaging is increasingly used for the location of biological entities or for the real-time monitoring of biological functions of specific targets *in celullo* and *in vivo* (Willmann, van Bruggen *et al*. 2008). This technique that does not involve ionizing radiations is quite inexpensive and requires only small quantities of imaging agents (in comparison to magnetic resonance imaging (MRI) technique for example).
Fluorescence imaging has demonstrated its efficiency in clinical medicine and has become a non-invasive complement to positron emission tomography (PET), single photon emission computed tomography (SPECT) and MRI imaging in small animals with the ultimate goal of validation clinical uses and drug developments in humans (Hargreaves 2008; Leung, Chopra *et al.* 2012). Indeed, several recent studies have shown the advantages of fluorescence imaging assisted surgery for ovarian tumor resection (van Dam, Themelis *et al.* 2011) or hepatic resection for colorectal cancer metastases (van der Vorst, Schaafsma *et al.* 2013).

Principal limitations of these techniques are the limited depth of penetration of the light in tissues and the intrinsic fluorescence of biomolecules that interfere with the fluorescence signal arising from the fluorophores that absorb visible light (350-650nm) (Frangioni 2003).

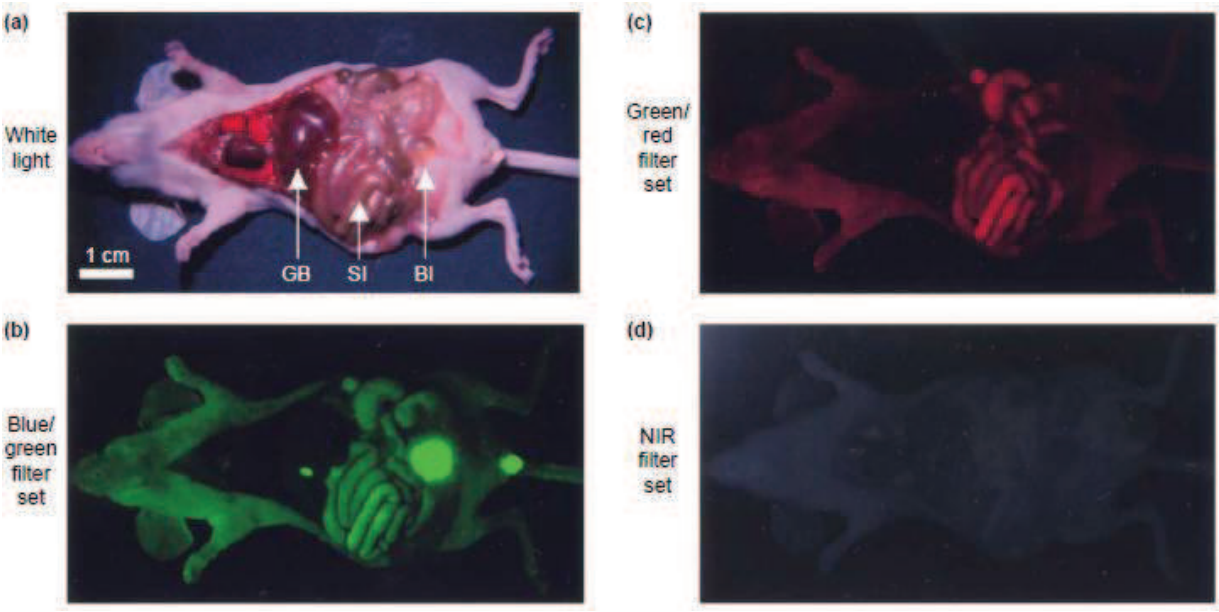

Figure 1.1. Images showing the autofluorescence of vital organs and bodily fluids. (a) White light. (b) λex: 460-500 nm- λem: 505-560 nm; (c) λex: 525-555 nm- λem:590-650 nm; (d) λex: 725-775 nm- λem: 790-830 nm (Frangioni 2003)

The use of near-infrared (NIR) fluorescence (650-1100 nm) allows the detection in an environment possessing low or absence of background of autofluorescence (Figure 1.1). This advantage allows easier discrimination between the fluorescence signal emitted by the fluorophore and the biological autofluorescence background, leading to enhanced signal to noise ratio and improved detection sensitivity.

1.2-Near-infrared imaging

The near-infrared (NIR) region of the electromagnetic spectrum is highly advantageous for biological imaging applications because it allows to overcome the limitations of visible fluorescence imaging as previously described in this chapter.

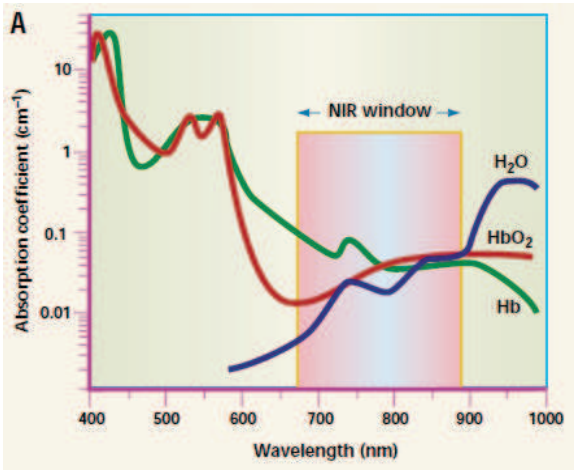

Figure 1.2. Absorption coefficients for hemoglobin (Hb), oxygenated hemoglobin (HbO_2), and H_2O showing the low absorption of biological species in the NIR Window. Adapted from (Mahmood and Weissleder 2003)

The main components of biological tissue possess low absorption coefficients in the NIR in comparison to the visible range. (Figure 1.2). NIR photons are poorly absorbed by tissue which allows a deeper light penetration for non-invasive imaging and diagnostic. Mahmood and Weissleder have reported that a fluorescent probewhich absorb in the 700-800 nm range could in theory penetrate 10-15 cm trough tissues (Mahmood and Weissleder 2003).

Additionally, NIR light scatters less than visible light and therefore results in the increased resolution of the optical image (Frangioni 2003; Taik Lim, Kim *et al*. 2003; Kim, Lim *et al.* 2004). Finally, NIR photons interact less with biological material compared to visible photons, thus decreasing the risk of disturbing or damaging the biological systems being observed.

1.2.1-Fluorescence reporters properties.

Fluorescence/luminescence efficacy of traditional organic fluorophores is characterized by its quantum yield (Φ), which is defined as the ratio between the number of emitted photons over the number of absorbed photons.

High quantum yield, high molar extinction coefficient, good resistance to photobleaching combined with NIR excitation and emission wavelengths (for a deeper sensitive detection without autofluorescence background) constitute typical characteristics of an ideal fluorescent agent.

1.2.2- NIR emitted Organic fluorophores

Organic fluorophores are commonly used for fluorescence imaging *in vivo*. The most used organic fluorescent agents with NIR photophysical properties fit into three categories: cyanines, squaraines and BODIPYs (Figure 1.3) (Luo, Zhang *et al.* 2011).

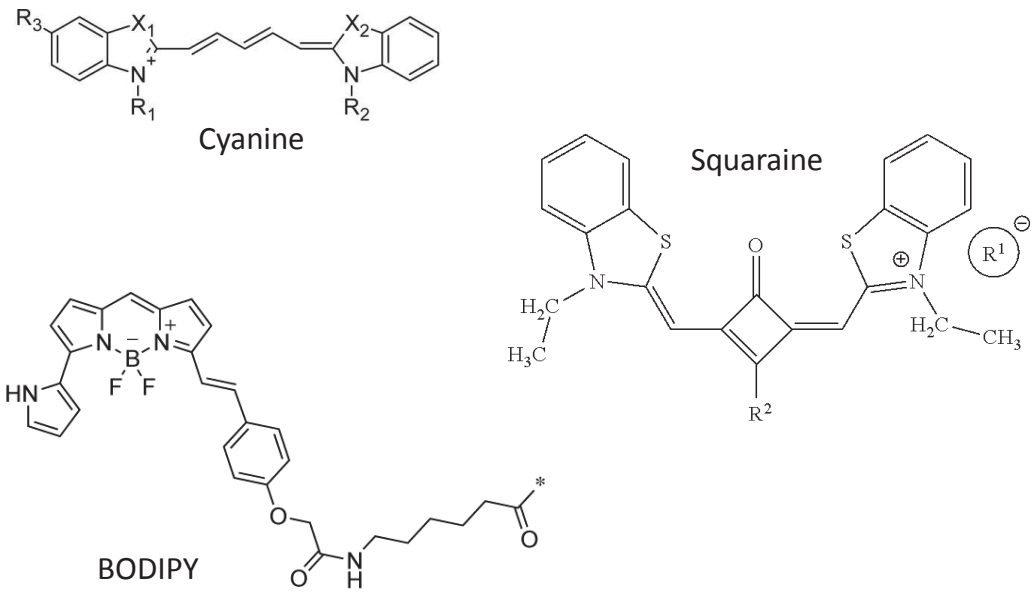

Figure 1.3. Structures of three examples of near infrared emitting organic fluorophores: cyanine, squaraine and BODIPY

Squaraine dyes are a class of dyes constituted by an oxocyclobutenolate core with aromatic heterocyclic moieties on each end of the molecule. Their planar and highly conjugated architecture result in poor water solubility. Several research groups are working towards the improvement of water solubility to allow their use as NIR imaging agent in biological systems (Pansare, Hejazi *et al*. 2012).

BODIPY (borondipyrromethane) dyes have relatively sharp absorption and emission bands and high quantum yield values. However, they have low extinction coefficients (in comparison to cyanines) and have also very low solubility in water (Escobedo, Rusin *et al.* 2010).

Cyanines (Cy) are largely described in the literature as efficient fluorescent probes (Mujumdar, Ernst *et al.* 1993).

Their structures include two aromatic nitrogen heterocycles linked together with a polymethine bridge whose length is proportional to the emission wavelength (Resch-Genger, Grabolle *et al.* 2008).

Two NIR emitting cyanine, Cy5 and Cy7, possess absorption and emission wavelengths at 650-667 nm and 747-774 nm respectively (Gruber, Hahn *et al*. 2000).

The Indocyanine green (ICG) possesses a maximum of absorption around 800 nm and emits fluorescence between 750 and 950 nm, and is FDA (Food and Drug Administration) approved it since 1959 for human injection. Today, ICG is frequently used in clinical medicine for ophtalmology, angiography (Figure 1.4) or evaluation of cardiac and hepatic functions (Owens 1996).

ICG is also emerging as NIR probe for fluorescence assisted surgery, especially for tumor resection. (Alander, Kaartinen *et al.* 2012)

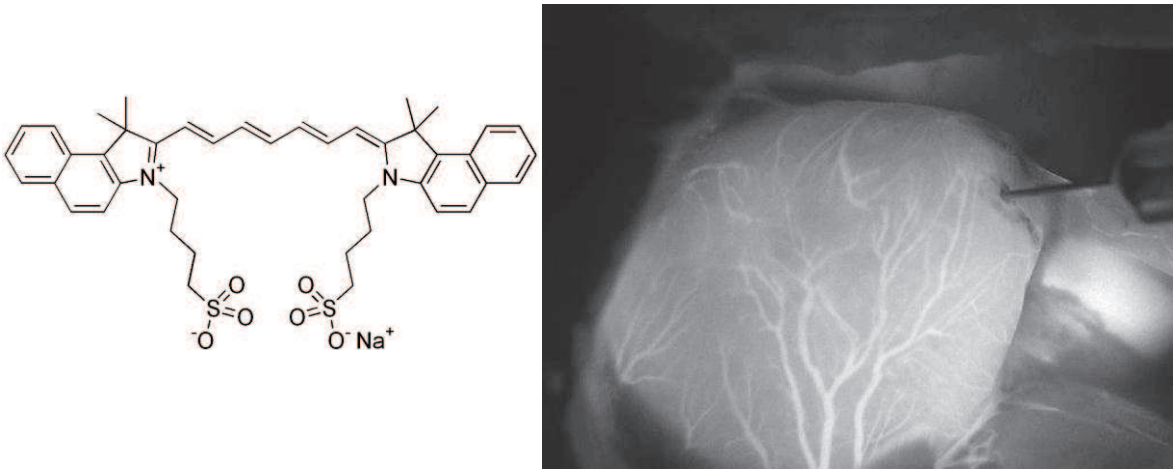

Figure 1.4. Chemical structure (left) and typical ICG angiography of rat heart (right). (Alander, Kaartinen *et al.* 2012)

Fisher *et al.,* reported the synthesis of a new class of NIR emitting cyanine fluorophores: pyrrolopyrrole cyanine dyes (PPCy). Variation of the heterocyclic peripheral groups of the chromophore allowed to tune the maxima of absorption spectra between 684 and 864 nm (Fischer, Isomaki-Krondahl *et al*. 2009).

The common weakness of all these organic fluorophores are their high sensitivity to the rapid photobleaching which is oftena major limitation for optical imaging experiments. The decrease of the signal to noise ratio during the experiments makes the discrimination between the signal and the background very difficult. The fact that the NIR signal intensity will change over time prevent the use of such NIR reporters for quantitative detections.

1.2.3-Quantum Dots

Quantum Dots (QDs) are semiconductors nanocrystals, usually constituted from CdSe coated with a shell of ZnS, which present specific photophysical properties due to quantum confinement effects. They emit different wavelength from the visible to the NIR part of the light spectrum (Figure 1.5). The emission wavelength is controlled by the size of the particules (the smaller the particles, the higher is the energy (Shao, Gao *et al.* 2011).

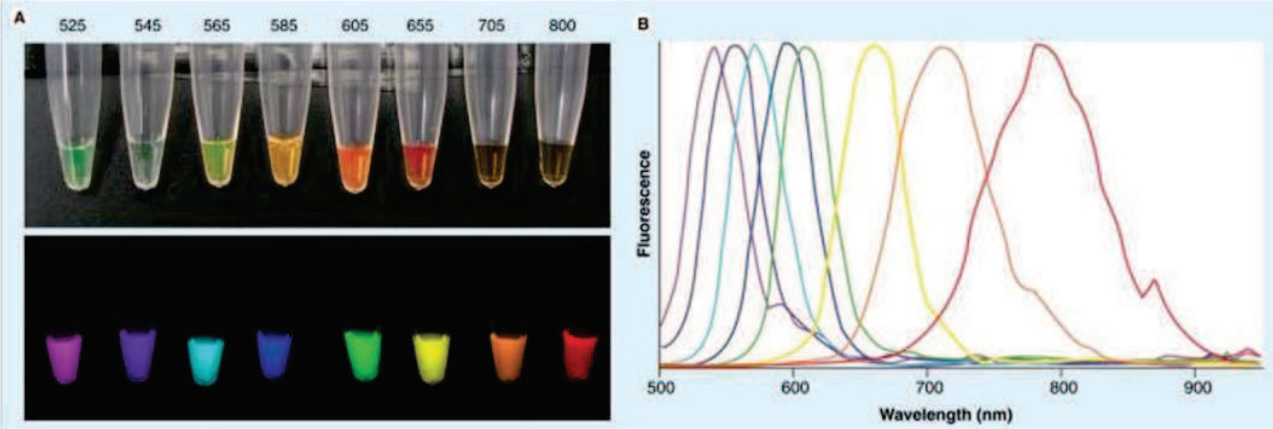

Figure 1.5. Spectral range of Quantum Dots emission spectra. A) Picture of QD solutions: QD 525, 548, 565, 585, 605, 655, 700 and 800 (top) and their corresponding fluorescence emission under blue light excitation (bottom). B), Fluorescence emission spectra of each quantum dots.

In addition to be relatively resistant to photobleaching (Winnik and Maysinger 2012), QDs have high molecular extinction coefficients (from 0.5 to $5 \cdot 10^6$ $M^{-1}cm^{-1}$) in comparison to organic fluorophores (from 5 to $10 \cdot 10^4$ $M^{-1}cm^{-1}$) and quantum yields ranging from 20% to 60% indicating that they are very bright reporters (Gao, Yang *et al.* 2005).

Quantum Dots were found to be toxic in biological experiments, with the release of constituent metals (generally cadmium and selenium), after degradation of the coating of their core *in cellulo* and *in vivo* (Hardman 2006). Cadmium, a probable carcinogen, has a biological half-life of 15-20 years in humans, can cross the blood-brain barrier and the placenta, and is systemically distributed in all organism with liver and kidney preferential accumulation (Winnik and Maysinger 2012).

Given the limitations of organic fluorophores and semi-conductor nanocrystals, only very few candidates could lead to satisfactory results. This situation explains the limited use of NIR imaging for biological studies and diagnostic despite the advantages of these photons. As of

today, it is difficult for example to find equipment commercially available which is suitable for such imaging modality. It is good to keep in mind that the limitation is in the reagents and not in the technology as optics and current CCD sensors in cameras can all detect wavelengths ranging from visible light up to 1100 nm.

1.2.4-Luminescent lanthanides

Luminescent lanthanides offer an exciting alternative to the existing NIR emitting probes described previously. Their unique properties, described in the next paragraph, have generated a growing interest for biomedical analysis and imaging (Bünzli 2010).

1.3-Lanthanide cations

Lanthanides are a special group of elements within the Mendeleev classification (Figure 1.6) from lanthane (Z=57) to lutetium (Z=71). Lanthanides usually exist as trivalent cations (noted Ln(III) or Ln^{3+}) with electronic configuration varying from [Xe] $4f^0$ to [Xe] f^{14}. The trivalent cations emit luminescence light at well-defined wavelengths, except La^{3+} and Lu^{3+}.

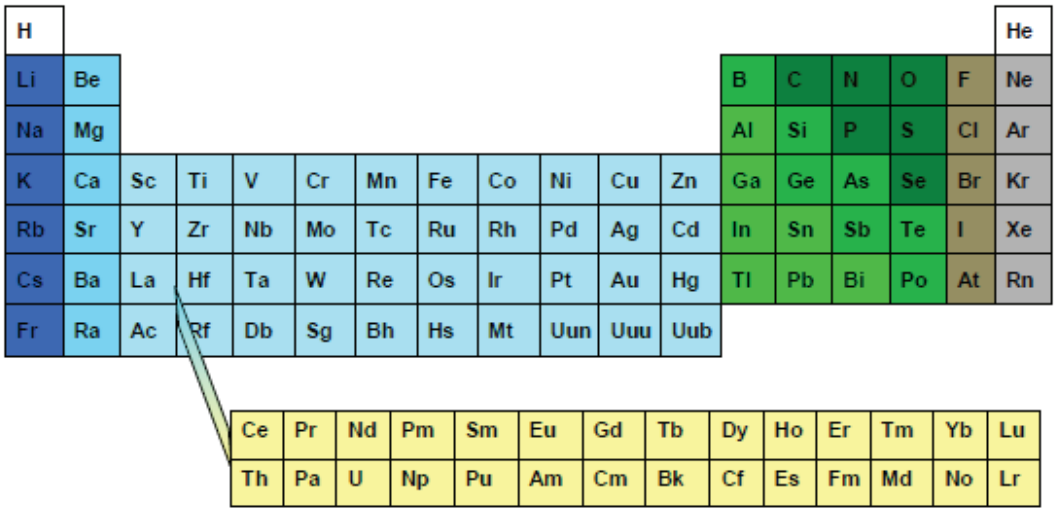

Figure 1.6. Mendeleev's periodic table.

1.3.1-Advantages of lanthanide luminescence for biological imaging

The luminescence properties of lanthanide are especially well adapted for the study and analysis of biological systems as they possess several specific advantages.

Their emission bands are sharp and do not overlap (Figure 1.7) and their wavelengths do not vary with experimental conditions such as pH, solvent, temperature and biological environment. These sharp bands allow for an efficient spectral discrimination from the background for example, by the choice of a specific interferential filter for microscopy. Due to their emission in the NIR, neodymium (Nd^{3+}), holmium (Ho^{3+}), erbium (Er^{3+}), thulium (Tm^{3+}) and ytterbium (Yb^{3+}), are attractive to lanthanide coordination chemists and spectroscopists for development of new NIR emitting probes.

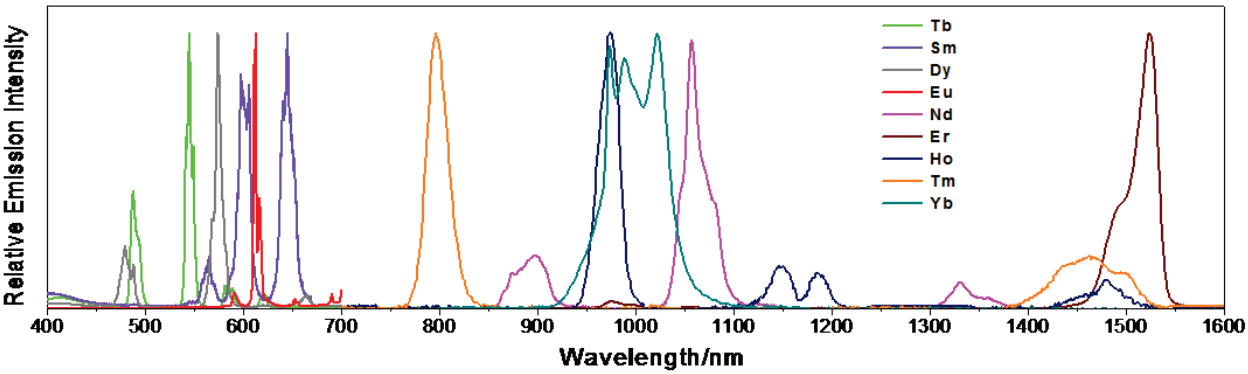

Figure 1.7. Normalized emission spectra of luminescent lanthanide complexes in solution (Petoud, Cohen *et al.* 2003; Zhang, Badger *et al.* 2005).

Lanthanide cations have also much longer luminescence lifetimes (few tens of nanoseconds to several milliseconds) than organic fluorophores (from picoseconds to nanoseconds) (Horrocks and Sudnick 1979). The long lifetimes can allow the discrimination of the Ln^{3+} emission signal from biological autofluorescence background by collecting the lanthanide signal through time resolved measurements (Figue 1.8).

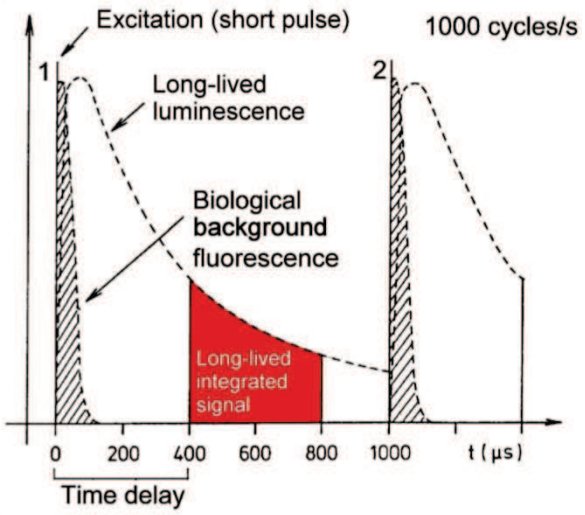

Figure 1.8. Graphical representation of the principle of time-resolved measurements for the discrimination of the Ln3+ emission signal from autofluorescence background (Bünzli 1989).

Another important advantage of lanthanide cations as imaging agents is their strong resistance to photobleaching (in contrast to organic fluorophores), allowing long and repeated exposures to excitation light. This property is also advantageous for long term storage.

All these unique advantages make NIR emitting lanthanide compounds, promising imaging agents as an alternative to the classical organic fluorophore and QDs. However, lanthanide cations have the particularity to absorb very low amount of light. In order to take advantage of their properties, they need to be sensitized.

1.3.2-Challenge of lanthanide luminescence

Since $f \rightarrow f$ transitions are forbidden by the Laporte rules, free lanthanide cations have low extinction coefficients and cannot be directly excited (Weissman 1942).

This limitation can be overcome by placing the lanthanide cations in close proximity to a sensitizer (antenna or chromophore), which will be able to absorb excitation light and efficiently convert the resulting energy to the lanthanide cations. This phenomenon, so called "antenna effect" is illustrated in the (Figure 1.9).

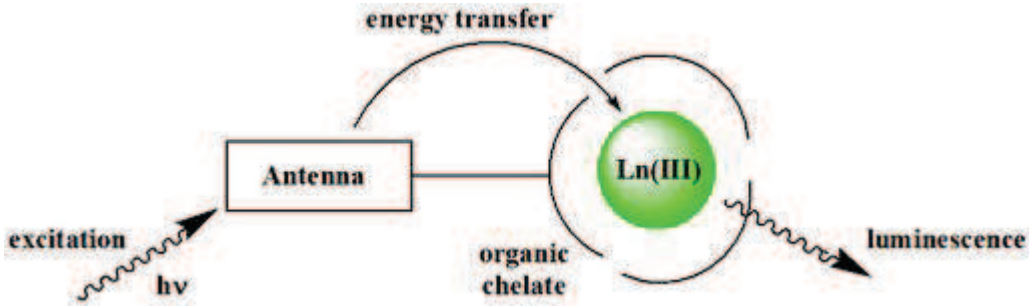

Figure 1.9: Illustration of the "antenna effect" from Prof K. Raymond group research web site (http://www.cchem.berkeley.edu/knrgrp/ln.html)

Upon excitation, the antenna will absorb photons resulting in a higher energy state and transfers the resulting energy from its excited singlet or triplet state to the lanthanide which will emit its specific luminescence. (Figure 1.10).

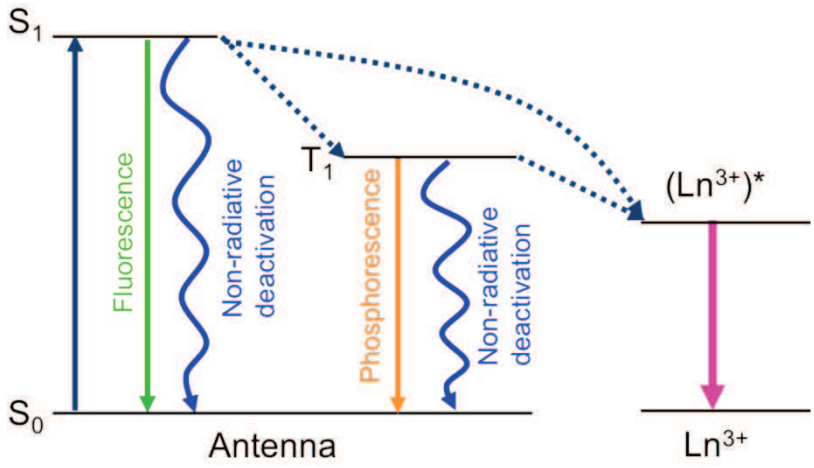

Figure 1.10. Jablonski diagram illustrating the mechanism of sensitization of Ln^{3+} through the antenna effect and potential relaxation through radiative (fluorescence and phosphorescence) and non radiative deactivations. S: singlet state; T: triplet state.

The coordination environment around lanthanide cations impacts significantly its luminescence properties. Indeed, -OH, -NH, and -CH vibrations can quench luminescence intensity and decrease luminescence lifetime (Eliseeva and Bünzli 2010).

Design of antenna represents a real challenge to combine effective sensitization and shielding of lanthanide cations.

Even if several lanthanide complexes emitting in the NIR have been described in the literature (Korovin, Rusakova *et al*. 2002; Zhang, Badger *et al*. 2005; Comby, Imbert *et al*. 2006; Zhang and Petoud 2008; Eliseeva and Bünzli 2010; Bünzli and Eliseeva 2013), as of today, there is

only one reports the use of a Yb^{3+} complex on HeLa cells and mice brain slices under two-photons excitation (D'Aléo, Bourdolle *et al.* 2012).

1.4-Goals of this work

The main goal of the thesis project was to establish the prof of principle that lanthanide compounds can be used as NIR imaging agents *in cellulo* and *in vivo*.

The present work will take advantage of a strategy which consists to increase the density of the number of chromophore and lanthanides cations per unit volume to augment the number of emitted photons and the detection sensitivity in order to overcome the negative effects of low quantum yields.

Lanthanide containing MOFs and polymetallic derivative of polyamidoamine (PAMAM) dendrimers will be used as a basis for the construction of NIR luminescent reporters. These two families of compound are chemically very different and are complementary candidates to test our hypothesis.

To the best of our knowledge, there is no report at this time NIR emitting reporters based on lanthanide compounds that can be excited with a single photons for living cells and/or organism.

The work will organized in three chapters:

- The first part will focus on MOFs. After a bibliographic introduction centered on the use of MOFs for biological applications, this chapter will describe the characterization of the new nano-Yb-PVDC-3 and show its ability to be imaged in living cells through the Yb^{3+} NIR emission.
- The second part will started with a non exhaustive bibliographic overview of PAMAM dendrimers biomedical applications, following by the study of two luminescent PAMAM dendrimers (Ln-G3P-NH2 and Ln-G3P-NB) and their behavior evaluation in biological environment. Even if dendrimers derivatives are very different of previously described nano-MOFs, they have also proven their ability to be image *in cellulo* and *in vivo* as NIR emitting reporters.
- The last part will be devoted to the description and discussion of a massive increase of luminescence signal of the dendrimers incorporated in living cells when placed under blue light. Several experiments *in cellulo* and *in vitro* allowed to establish and/or reject hypothesis in order to obtain some level of explanation of this phenomenon.

To conclude, the two efficient systems will be discussed with their respective advantages and drawbacks and potential applications adapted to their specificity will be discussed with the perspective of theranostic field.

References

- Alander, J. T., I. Kaartinen, *et al*. (2012). "A review of indocyanine green fluorescent imaging in surgery." Int J Biomed Imaging**2012**: 940585.
- Bünzli, J.-C. G. (1989). Luminescent Probes. Lanthanide Probes in Life, Chemical and Earth Sciences. J.-C. G. Bünzli and G. R. Choppin. Amsterdam, Elsevier Science Publishers B.V.**:** 219-293.
- Bünzli, J.-C. G. and S. V. Eliseeva (2013). "Intriguing aspects of lanthanide luminescence." Chemical Science DOI: 10.1039/c3sc22126a.
- Bünzli, J. C. (2010). "Lanthanide luminescence for biomedical analyses and imaging." Chem Rev**110**(5): 2729-2755.
- Comby, S., D. Imbert, *et al*. (2006). "Stable 8-hydroxyquinolinate-based podates as efficient sensitizers of lanthanide near-infrared luminescence." Inorg Chem**45**(2): 732-743.
- D'Aléo, A., A. Bourdolle, *et al*. (2012). "Ytterbium-based bioprobes for near-infrared two-photon scanning laser microscopy imaging." Angew Chem Int Ed Engl**51**(27): 6622-6625.
- Eliseeva, S. V. and J.-C. G. Bünzli (2010). "Lanthanide luminescence for functional materials and bio-sciences." Chem Soc Rev**39**(1): 189-227.
- Escobedo, J. O., O. Rusin, *et al*. (2010). "NIR dyes for bioimaging applications." Curr Opin Chem Biol**14**(1): 64-70.
- Fischer, G. M., M. Isomaki-Krondahl, *et al*. (2009). "Pyrrolopyrrole cyanine dyes: a new class of near-infrared dyes and fluorophores." Chemistry**15**(19): 4857-4864.
- Frangioni, J. V. (2003). "In vivo near-infrared fluorescence imaging." Curr Opin Chem Biol**7**(5): 626-634.
- Gao, X., L. Yang, *et al*. (2005). "In vivo molecular and cellular imaging with quantum dots." Curr Opin Biotechnol**16**(1): 63-72.
- Gruber, H. J., C. D. Hahn, *et al*. (2000). "Anomalous fluorescence enhancement of Cy3 and cy3.5 versus anomalous fluorescence loss of Cy5 and Cy7 upon covalent linking to IgG and noncovalent binding to avidin." Bioconjug Chem**11**(5): 696-704.
- Hardman, R. (2006). "A toxicologic review of quantum dots: toxicity depends on physicochemical and environmental factors." Environ Health Perspect**114**(2): 165-172.
- Hargreaves, R. J. (2008). "The role of molecular imaging in drug discovery and development." Clin Pharmacol Ther**83**(2): 349-353.
- Horrocks, W. D. and D. R. Sudnick (1979). "Lanthanide ion probes of structure in biology. Laser-induced luminescence decay constants provide a direct measure of the number of metal-coordinated water molecules." J Am Chem Soc**101**(2): 334-340.

- Kim, S., Y. T. Lim, *et al*. (2004). "Near-infrared fluorescent type II quantum dots for sentinel lymph node mapping." Nat Biotechnol**22**(1): 93-97.
- Korovin, Y. V., N. V. Rusakova, *et al.* (2002). "Luminescence of ytterbium and neodymium in complexes with bis-macrocyclic ligands." Journal of Applied Spectroscopy**69**(6): 841-844.
- Leung, K., A. Chopra, *et al*. (2012). "Essential parameters to consider for the characterization of optical imaging probes." Nanomedicine (Lond)**7**(7): 1101-1107.
- Luo, S., E. Zhang, *et al.* (2011). "A review of NIR dyes in cancer targeting and imaging." Biomaterials**32**(29): 7127-7138.
- Mahmood, U. and R. Weissleder (2003). "Near-infrared optical imaging of proteases in cancer." Mol Cancer Ther**2**(5): 489-496.
- Mujumdar, R. B., L. A. Ernst, et al. (1993). "Cyanine dye labeling reagents: sulfoindocyanine succinimidyl esters." Bioconjug Chem**4**(2): 105-111.
- Owens, S. L. (1996). "Indocyanine green angiography." Br J Ophthalmol**80**(3): 263-266.
- Pansare, V., S. Hejazi, *et al*. (2012). "Review of Long-Wavelength Optical and NIR Imaging Materials: Contrast Agents, Fluorophores and Multifunctional Nano Carriers." Chem Mater**24**(5): 812-827.
- Petoud, S., S. M. Cohen, *et al*. (2003). "Stable lanthanide luminescence agents highly emissive in aqueous solution: multidentate 2-hydroxyisophthalamide complexes of Sm(3+), Eu(3+), Tb(3+), Dy(3+)." J Am Chem Soc**125**(44): 13324-13325.
- Resch-Genger, U., M. Grabolle, *et al*. (2008). "Quantum dots versus organic dyes as fluorescent labels." Nat Methods**5**(9): 763-775.
- Shao, L., Y. Gao, *et al*. (2011). "Semiconductor quantum dots for biomedicial applications." Sensors (Basel)**11**(12): 11736-11751.
- Taik Lim, Y., S. Kim, *et al*. (2003). "Selection of quantum dot wavelengths for biomedical assays and imaging." Mol Imaging**2**(1): 50-64.
- Van Dam, G. M., G. Themelis, *et al*. (2011). "Intraoperative tumor-specific fluorescence imaging in ovarian cancer by folate receptor-alpha targeting: first in-human results." Nat Med**17**(10): 1315-1319.
- Van der Vorst, J. R., B. E. Schaafsma, *et al.* (2013). "Near-infrared fluorescence-guided resection of colorectal liver metastases." Cancer**119**(18): 3411-8.
- Weissman, S. I. (1942). "Intramolecular energy transfer the fluorescence of complexes of europium." J Chem Phys**10**(4): 214-217.
- Willmann, J. K., N. van Bruggen, *et al*. (2008). "Molecular imaging in drug development." Nat Rev Drug Discov**7**(7): 591-607.
- Winnik, F. M. and D. Maysinger (2012). "Quantum Dot Cytotoxicity and Ways To Reduce It." Acc Chem Res**46**(3): 672-80.

- Zhang, J., P. D. Badger, *et al*. (2005). "Sensitization of near-infrared-emitting lanthanide cations in solution by tropolonate ligands." Angew Chem Int Ed Engl**44**(17): 2508-2512.
- Zhang, J., P. D. Badger, *et al.* (2005). "Sensitization of near-infrared-emitting lanthanide cations in solution by tropolonate ligands." Angew Chem Int Ed Engl**44**(17): 2508-2512.
- Zhang, J. and S. Petoud (2008). "Azulene-moiety-based ligand for the efficient sensitization of four near-infrared luminescent lanthanide cations: Nd^{3+}, Er^{3+}, Tm^{3+}, and Yb^{3+}." Chemistry**14**(4): 1264-1272.

Résumé Français

Le premier chapitre de cette thèse est consacré à présenter l'état de l'art dans le domaine de l'imagerie de fluorescence proche infrarouge afin de replacer le travail réalisé dans le contexte scientifique actuel.

L'imagerie de fluorescence est une technique émergeante dans le domaine des applications biomédicales dans la mesure où elle permet de suivre des cibles spécifiques *in cellulo* et *in vivo* tout en offrant une grande sensibilité spatio-temporelle. En plus d'être non ionisante, cette technique ne nécessite l'utilisation que de faibles quantités d'agents d'imagerie (en comparaison à l'imagerie par résonance magnétique IRM).

L'imagerie de fluorescence a démontré son efficacité en complément des techniques d'imagerie non invasives actuellement utilisées en clinique (IRM, tomographie par émission de positrons TEP...). En effet, plusieurs études ont décrit l'utilité de la chirurgie assistée par fluorescence lors de la résection de tumeurs hépatiques ou ovariennes.

La principale limitation de cette technique est cependant la faible pénétration de la lumière dans les tissus ainsi que leur fluorescence intrinsèque qui interfère avec le signal de fluorescence émis par le fluorophore. La gamme de lumière proche-infrarouge (650-1100 nm) est la solution pour s'affranchir de cette situation. En plus de pénétrer plus profondément dans les tissus (jusqu'à 10-15 cm pour une sonde qui absorbe entre 700 et 800nm), la lumière proche infrarouge permet de s'affranchir de l'autofluorescence biologique. Autre avantage, les photons proche infrarouge diffusent moins que les photons visibles, permettant d'obtenir des images plus résolues.

En plus de posséder des longueurs d'ondes d'excitation et d'émission dans le proche infrarouge, la sonde fluorescente idéale devra posséder un bon rendement quantique (défini par le rapport entre le nombre de photons émis et le nombre de photons absorbés), un coefficient d'extinction molaire élevé ainsi qu'une bonne résistance au photoblanchiment.

Actuellement le nombre de rapporteurs fluorescents/luminescents efficaces pour des applications d'imagerie biologique dans le proche infrarouge est relativement limité. Il s'agit pour la plupart de fluorophores organiques et de quantum dots.

Les fluorophores organiques les plus utilisés pour la fluorescence *in vivo* appartiennent aux familles des cyanines, des squaraines ou des BODIPYs. L'utilisation de squaraines et des BODIPYs reste toutefois limitée par leur faible solubilité dans l'eau.

Les cyanines en revanche sont plus largement répandues avec l'exemple du vert d'indocyanine (ICG) couramment utilisé dans le monde médical notamment pour des angiographies (ophtalmologiques mais aussi cardiaques et hépatiques).
Le principal inconvénient des fluophores organiques est leur sensibilité générale au photoblanchiment qui peut devenir une réelle limitation en cas d'expositions longues et/ou répétées.

Les nano-cristaux semi-conducteurs appelés quantum dots (ou boîte quantique) quant à eux résistent au photoblanchiment, possèdent des coefficients d'extinction molaire et des rendements quantiques élevés. Leurs longueur d'ondes d'émission sont contrôlées par la taille de ces nano-objets et couvrent la gamme de lumière allant du visible jusqu'au proche infrarouge. L'inconvénient majeur qui a freiné l'engouement pour les quantum dots est leur toxicité, induite par la libération de métaux lourds (type cadmium ou sélénium) lors de leur dégradation *in cellulo* et *in vivo*.

Les complexes à base de lanthanides luminescents dans le proche infrarouge semblent être une bonne alternative aux composés précédemment décrits. En effet, les lanthanides possèdent des propriétés uniques qui les rendent très attractifs pour le monde de l'imagerie biologique. Ils possèdent des bandes d'émission étroites qui ne se recouvrent pas et dont les longueurs d'onde ne varient pas en fonction des conditions expérimentales (pH, température, solvant...). Ils résistent également au photoblanchiment et ont des temps de vie de luminescence long (de quelques nanosecondes à plusieurs millisecondes) comparés aux fluorophores organiques (de quelques picosecondes à la nanoseconde). Cette propriété offre la possibilité de séparer le signal d'émission spécifique du lanthanide du bruit de fond d'autofluorescence biologique par discrimination temporelle.
Cependant, les lanthanides libres ont de faibles coefficients d'extinction de par les transitions $f \rightarrow f$ interdites par les lois de Laporte et ne peuvent pas être directement excités. Pour pallier à cela, une antenne (ou chromophore) va sensibiliser le cation lanthanide par ce qu'on appelle" l'effet antenne". Lorsqu'elle est placée suffisamment près du lanthanide, l'antenne va transférer l'énergie des photons absorbés vers le lanthanide qui pourra alors émettre sa longueur d'onde spécifique. En plus de sensibiliser le lanthanide, l'antenne a pour rôle de le protéger contre les vibrations -OH, -NH, et -CH qui désactivent l'émission de signal et diminuent les temps de vie de luminescence.
A l'heure actuelle, le design d'antennes efficaces pour sensibiliser les cations lanthanides (et particulièrement ceux émettant dans le proche infrarouge) représente un réel défi pour les

chimistes. En revanche, même si de nombreuses molécules à base de lanthanides émettant dans le proche infrarouge sont décrites, un seul exemple rapporte leur utilisation pour de l'imagerie en cellules, et ce en imagerie bi-photonique. A notre connaissance, aucun exemple de rapporteur luminescent à base de lanthanide n'a été décrit pour des applications en imagerie mono-photonique cellulaire ou petit animal.

Le travail présenté dans ce manuscrit propose une stratégie consistant à densifier le nombre de chromophores et de lanthanides par unité de volume pour augmenter la sensibilité de détection et s'affranchir de leur faible rendement quantique dans le proche infrarouge.
Pour cela, les réseaux métallo organiques (MOFs) et les dendrimères polyaminoamide (PAMAM), deux familles de nanoparticules chimiquement très différentes, ont été choisis pour incorporer un grand nombre de lanthanides et de chromophore dans leur structure.
Le but principal de ce travail de thèse a été d'établir la preuve de principe de l'utilité des MOFs et dérivés de dendrimères PAMAM en tant que rapporteurs luminescents dans le proche infrarouge *in cellulo* et *in vivo*.

Le manuscrit s'articule autour de trois parties principales:
- Dans la première partie, une introduction bibliographique centrée sur l'utilisation des MOFs pour des applications biologiques sera suivie par la présentation des résultats de caractérisation du nano-Yb-PVDC-3 montrant sa capacité à être observé dans le proche infrarouge (à travers l'émission de l'YB^{3+}) dans des cellules HeLa et NIH 3T3.
- La seconde partie sera dans un premier temps consacrée à dresser l'état de l'art des applications biomédicales des dendrimères PAMAM, puis la caractérisation et l'étude des comportements en milieu biologique des dendrimères luminescents Ln-G3P-NH2 et Ln-G3P-NB seront présentées. Pour la première fois, il a été possible de détecter le signal de l'Yb^{3+} *in vivo*.
- La dernière partie sera consacrée à la description d'un phénomène inattendu observé sous exposition à la lumière bleue de cellules vivantes après incubation avec les dendrimères luminescents. De nombreuses expériences réalisées *in cellulo* et *in vitro* ont permis d'établir et/ou de rejeter des hypothèses afin d'expliquer ce phénomène complexe observé dans les cellules.

Pour terminer, les deux systèmes, qui se sont avérés efficaces, seront comparés avec leurs avantages et inconvénients respectifs afin de proposer d'éventuelles applications en fonctions de leurs spécificités.

2-Metal-Organic Frameworks

The work presented here has been realized in collaboration with Kristy Gogick, Tao Li and Professor Nathaniel Rosi (Department of Chemistry, University of Pittsburgh) for MOFs synthesis and characterization of crystals. The results presented here have been published to *PNAS* under the title: "Lanthanide near-infrared imaging in living cells with Yb^{3+} nano Metal Organic Frameworks". (see page 155)

2.1-Introduction

2.1.1-Metal-Organic Frameworks

Metal-Organic Frameworks (MOFs) were described for the first time in 1995 by Omar Yaghi (Yaghi 1995).

MOFs are crystalline and rigid compounds composed of metal ions or clusters coordinated to organic ligands that form a wide variety of 1-, 2-, or 3- dimensional porous structures. (Kitagawa, Kitaura *et al*. 2004; Ferey 2008). A broad variety of structures can be synthesized in a one pot synthesis by altering different reaction parameters (Scheme 2.1).

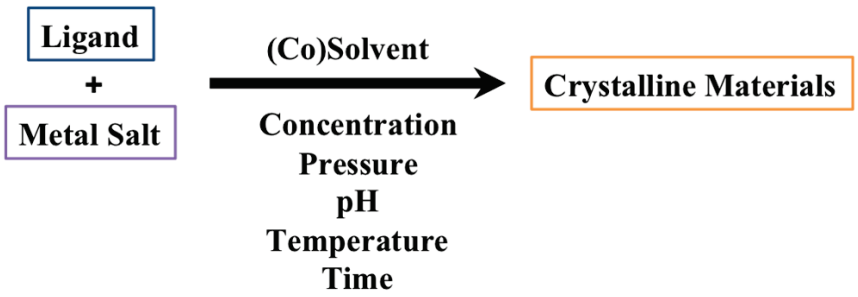

Scheme 2.1. Scheme of general MOFs synthesis

One of the special properties of these materials, its porosity, has attracted the interest of the scientific community and has helped to develop an important field of science and research due to the impact for some important applications such as gas storage, nonlinearoptics, chemical sensing, catalysis, or as described more recently for drug delivery (Oh and Mirkin 2005; Rowsell and Yaghi 2005; Horcajada, Serre *et al*. 2006; Lee, Farha *et al*. 2009).

The pore size, the network topology and the surface areas can be tuned in a controlled way to adjust the MOFs to the expected properties.

One main limitation of classical MOFs for biological applications is their submicrometric size. Their miniaturization has become a real challenge to obtain nanometric nanoparticles more compatible with biological applications (more specifically for their cellular internalization). The goal is to design nano-MOFs with well-defined and uniform sizes to disperse them in aqueous solvent in order to obtain or improve their biocompatibility without losing their initial properties. (Carne, Carbonell *et al*. 2011)

Two major strategies have been described for the miniaturizationof MOFs:
- The controlled precipitation of self-assembled supramolecular metal-organic polymers once they are formed by the use of microwaves, ultrasounds or temperature. (Ni and Masel 2006; Son, Kim et al. 2008; Horcajada, Chalati *et al*. 2010)

- The confinement of the self-assembly at specific locations (for example into droplets on the basis of nanoemulsion techniques) (Vaucher, Li *et al.* 2000).

2.1.2-Biological applications

The use of MOFs for biomedical purpose is attractive for numerous reasons such as the swell-controlled structure (crystallinity) and the large possibilities offered by the porosity.
First, their high porosity allows numerous possibilities by loading of biological molecules, including therapeutic agent especially anticancer drugs, biogases (nitric oxide), or imaging agents (Gd^{3+}) (McKinlay, Morris *et al.* 2010). Several methods have been developed for the incorporation of molecules of interest into MOFs structures. It can be a direct incorporation during the synthesis or a post synthesis reaction in order to fix the relevant agents (Scheme 2.2).

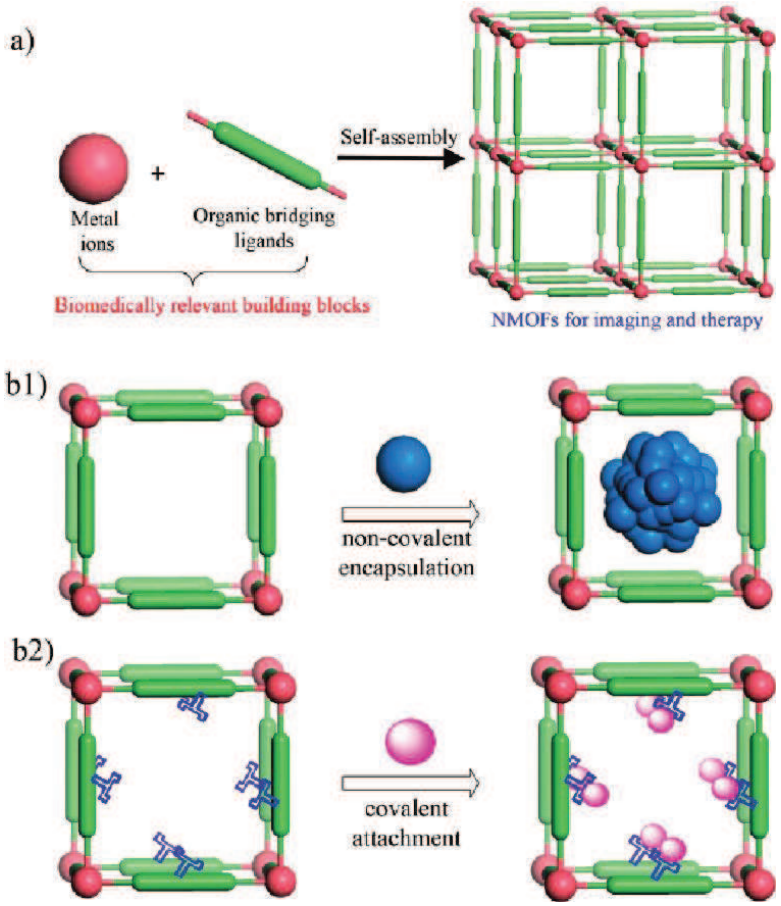

Scheme 2.2.Different strategies for incorporating relevant agents into nanoMOFs.(a) Direct incorporation of biomedically relevant metal connecting points or bridging ligands (b1). Postsynthesis incorporation via covalent attachment (b2). (Della Rocca, Liu *et al.* 2011)

A combination of these two techniques can also be used for the development of theranostic nanoparticles by combination of therapeutic molecules and imaging agents in the same MOF. Secondly and mostly important, the structure, composition, particle size and degradation of MOFs can be modulated in order to control the time-release of the incorporated molecule ranging from few days to several weeks (Low, Benin *et al*. 2009; Horcajada, Chalati *et al.* 2010). This strategy allows the use of those rigid-crystalline structures as potential nanovectors for delivering therapeutic agents.

Another appealing strategy is to synthesize MOFs that are biologically active by themselves. The MOFs components can be degraded and released in the body. In this area, the biodegradability became the most important factor to take into account with respect to the porosity. Several reports describe biocompatible ligands being used in frameworks: nucleotide (adenine (An, Geib *et al.* 2009), fumarate (Murray, Dinca *et al*. 2010)) and amino acid

(histidine (Horcajada, Serre *et al*. 2006),tyrosine, proline (Ingleson, Bacsa *et al*. 2007), aspartate (Anokhina, Go *et al*. 2006; Vaidhyanathan, Bradshaw *et al*. 2006)), based MOFs.

The first groups of MOFs that have been investigated as potential nanovectors for drug delivery was the MIL (Materials of Institut Lavoisier) family developed by Férey and coworkers (Ferey, Mellot-Draznieks *et al.* 2005). They are built from carboxylic acidic ligands and trivalent metal centers. The Férey group has studied different MOFs from MIL family for storage and release of ibuprofen and showed a complete drug release after three weeks. The long delivery time was attributed to the flexibility of the studied MOFs (MIL-53) and to the strong drug-framework interaction (Horcajada, Serre *et al.* 2008).

2.1.3-MOFs and lanthanide for imaging

In the same way that MOFs are studied as drug carrier, they present an interest for biological imaging as MRI or fluorescent/luminescent reporters. As of today, there are only very few reports of MOFs as biological imaging agents.

Lin and co-workers have demonstrated the effectiveness of Gd^{3+} containing MOFs for magnetic resonance imaging (MRI) (Rieter, Taylor *et al.* 2006; Rieter, Taylor *et al.* 2007; Taylor, Jin *et al.* 2008; Taylor, Rieter *et al.* 2008). They described the synthesis of known MOFs build from carboxylate linkers and lanthanide cations (Gd^{3+}, Eu^{3+} and Tb^{3+}). By selecting lanthanide as the metal nodes, they showed that nano-MOFs could be used as potential imaging agents. Gd^{3+} based nano-MOFs have very high relaxivity parameters. The doping of the Gd^{3+} nano-MOFs with 5% of Eu^{3+} or 5% of Tb^{3+}allows new nanoparticles with high relaxivity and luminescence properties specific to the coordinated lanthanide. (Figure 2.1).

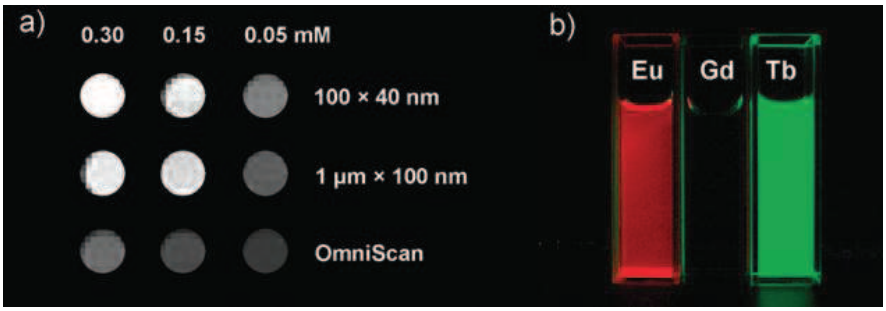

Figure 2.1. (a) T1-weighted MR images of suspensions of$Gd_2(BDC)_3(H_2O)_4$ nano-MOFs in water containing 0.1% xanthan gum.(b) Luminescence images of ethanolic suspensions of $Gd_2(BDC)_3(H_2O)_4$nano-MOFs doped with 5 mol% Eu^{3+} or Tb^{3+}. Adapted from (Rieter, Taylor *et al.* 2006)

Bünzli, Mallah and co-workers have reported water soluble nano-MOFs based on Tb^{3+} luminescence with a typical size below 10 nm with potential applications as biological reporter (Kerbellec 2008).

A new application of lanthanide based MOFs was described by White *et al*. with the creation of luminescent barcoded system. This system is based on multiple NIR emitted lanthanide included in the crystalline structure of the MOF material (Figure 2.2) (White, Chengelis *et al*. 2009).

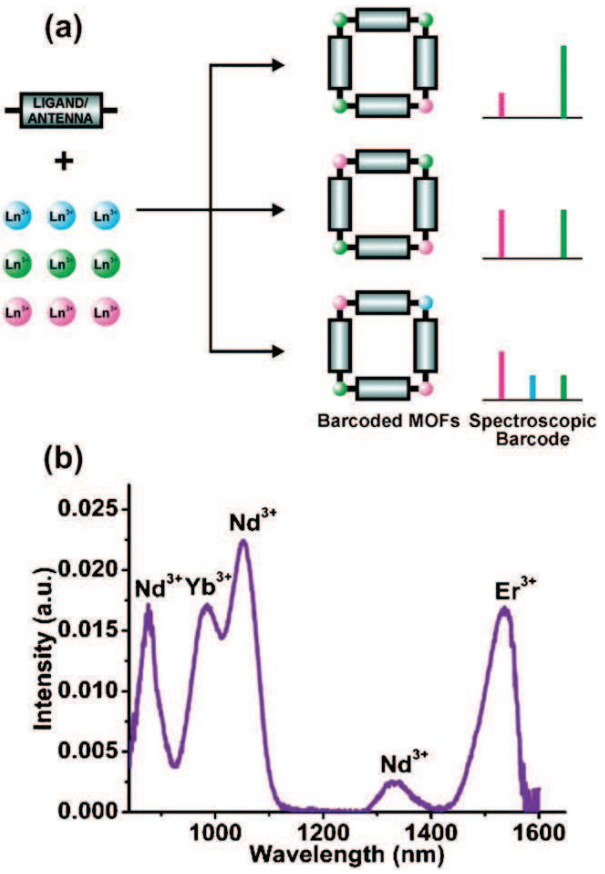

Figure 2.2. 1 (a) Schematic representation to design photoluminescent barcoded systems based onthe use of multiple NIR-emitting Ln^{3+}ions in a single MOF structure. (b) Nd^{3+}, Yb^{3+} andEr^{3+} emission from$[(Nd_{0.09}Er_{0.55}Yb_{0.36})_2(pvdc)_3(H_2O)_{2_6}DMF_{_8.5}H_2O$.

The different lanthanide (Yb^{3+} and Er^{3+}) are excited by the same chromophore and their relative emission intensities are linearly correlated to the ratio of each of these lanthanides present in the MOF. This interesting approach has potential applications for multiplexed detection in biological systems with the help of an appropriate set of optical filters due to the sharp, non-overlapping emission bands of lanthanide cations.

Guo et al., have reported a microporous NIR luminescent MOFs based on Yb^{3+} suitable for sensing of organic solvent (MOF-1). The NIR emission of MOF-1 is significantly dependent of the nature of the solvent with a strong emission intensity in DMF and a low signal in acetone. However, the authors did not report any possibility to obtain NIR emission in water which is a significant limitation for the sensing of biological substrates. (Guo, Xu *et al.* 2011)

2.1.5-MOFs Yb-PVDC-1 and Yb-PVDC-2

White et al. of the Petoud group previously reported Yb^{3+}-PVDC NIR-emitting lanthanide MOFs which exhibit tunable photophysical properties as bulk materials.(White, Chengelis *et al*. 2009).

These MOFs, Yb-PVDC-1 and Yb-PVDC-2, are constructed from4,4'-[(2,5-dimethoxy-1,4-phenylene)di-2,1-ethenediyl]bis-benzoic acid (H_2-PVDC), (Figure 2.3).

This ligand was chosen because of its strong absorptivity in the visible range and its ability to sensitize several NIR emitting lanthanides such as Yb^{3+} and its length could promote the formation of large, accessible pores within the MOF structure.

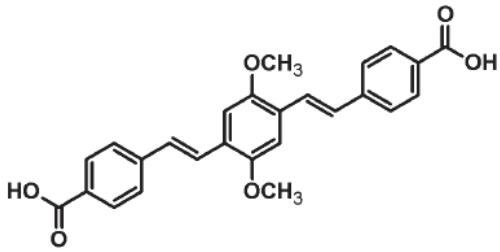

Figure 2.3. H_2-PVDC ligand for the sensitization of NIR lanthanide in Yb-PVDC MOFs.

Usually, lanthanides were incorporated in the MOFs pores after the synthesis. This allow to the lanthanide to be constrained in space, which can provide effective protection of lanthanides from solvent vibrations even while in solution.

MOFs allow the tuning of the distance and angles between the sensitizers with respect to each other within the structure, which could lead to the control of the spectroscopic properties of the resulting compounds to achieve a goals such as the shift of the excitation wavelenghts towards lower energies.

Additionally, similar to lanthanide doped nanoparticles, MOFs are polymetallic species with a high density of lanthanide cations, a desirable feature to maximize the number of photons per unit volume for a high detection sensitivity.

Two strategies are possible to incorporate lanthanide cations in the MOFs (Scheme 2.3). They can be incorporated into the pores (as for therapeutics molecules), or they can be directly incorporate into the MOFs structure. In this case, the pores stay available for therapeutic molecules incorporation and theranostics applications.

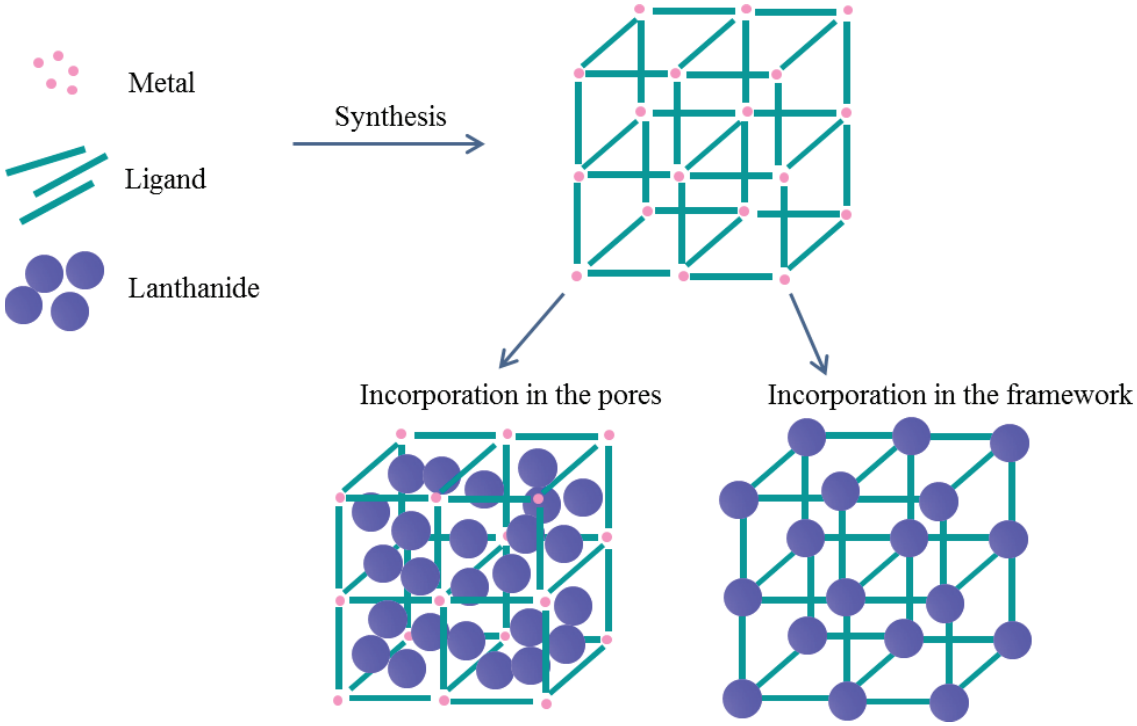

Scheme 2.3. The two strategies to incorporate lanthanide cations in MOFs.

With the synthesis of Yb-PVDC-1 and Yb-PVDC-2, *White et al*., have demonstrated the efficiency of NIR-emitting lanthanide sensitization by the antenna effect (Figure 2.4) in a MOF where lanthanides are part of the crystalline framework.

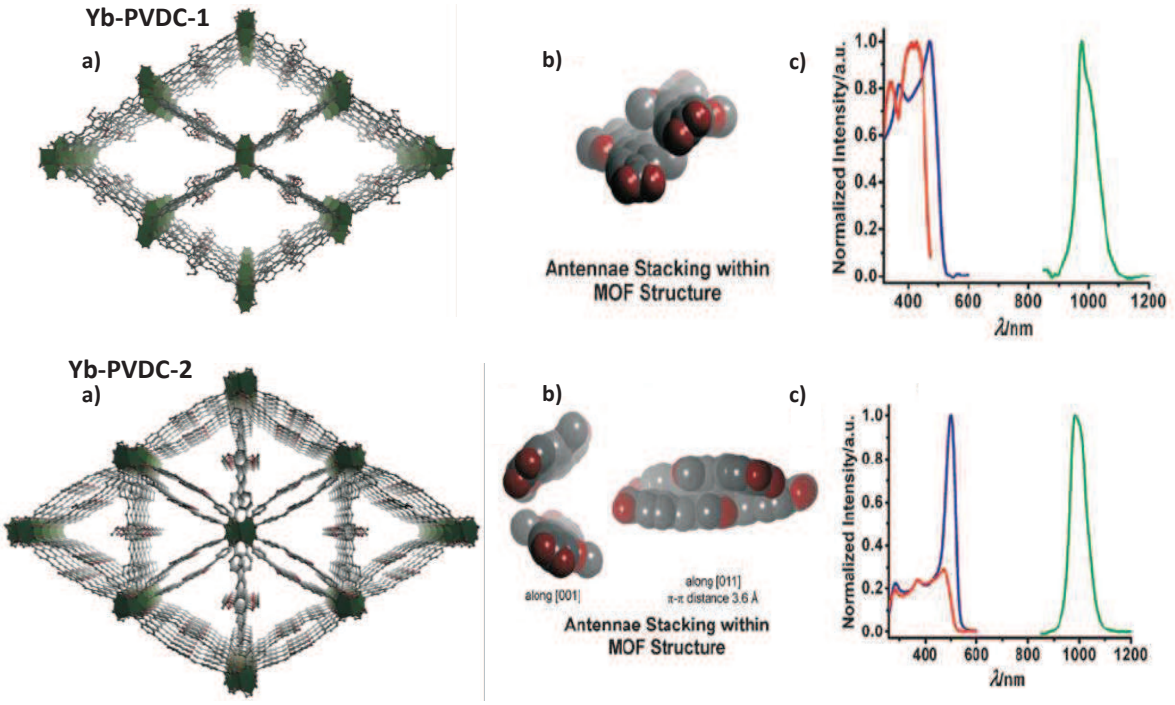

Figure 2.4.Structure and spectral data for Yb-PVDC-1 (top) and Yb-PVDC-2 (bottom). (a) projection view of the framework viewed along the *a* crystallographic direction; (b) ligand stacking motif (C, grey; O, red, Yb^{3+}, dark) and (c) luminescence data comparing the excitation profiles of Yb-PVDC molecular complex (red: λ_{em}=980 nm) to Yb-PVDC-1, Yb-PVDC-2 (blue; λ_{em}=980 nm) and displaying the Yb^{3+} emission (green; λ_{ex}=470nm) upon excitation of Yb-PVDC-1, Yb-PVDC-2. Adapted from (White, Chengelis *et al.* 2009)

To take advantage of the PVDC ligand/sensitizer in a novel type of luminescent MOF whose size is compatible with biological systems (and more specifically with cells), the synthetic conditions used to generate Yb-PVDC-2 were modified and a third type of crystalline framework was created in the bulk phase, Yb-PVDC-3. From this step, using a reverse microemulsion synthesis (Rieter, Taylor *et al.* 2006; Rieter, Taylor *et al*. 2007; Taylor, Rieter *et al.* 2008), a nanoscale version of the same Yb-PVDC-3MOF was created. As a proof-of-principle, a series of experiments demonstrated here, for the first time, the ability of this novel type of nanoMOFs to enter HeLa and NIH 3T3 living cells and to operate as a NIR imaging agents.

2.2-Materials and methods

2.2.1-Synthesis of Yb-PVDC-3 and nano-Yb-PVDC-3

The synthesis of Yb-PVDC-3 and nano-Yb-PVDC-3 were realized in the Department of Pittsburgh by Kristy Gogick. Details of the synthesis are described in the appendix 1.

2.3.2.2-X-ray powder diffraction

These measurements were realized at the University of Pittsburgh by Kristy Gogick and Tao Li.

X-ray powder diffraction patterns for the bulk material were collected using a Bruker AXS D8 Discover powder diffractometer at 40 kV, 40 mA for Cu Kα, (λ = 1.5406 Å) with a scan speed of either 0.20 sec/step or 0.50 sec/step and a step size of 0.02018°. X-ray powder diffraction patterns for the nanoMOFs were collected using a Philips PW1830 diffractometer at 40 kV, 40 mA for Cu Kα, (λ = 1.54056 Å) with a scan speed of 0.50 sec/step and a step size of 0.020°.

2.2.3-Scanning electron microscopy

Samples were coated with palladium for 60 seconds prior analysis with a Philips XL 30 SEM. ImageJ 1.47f software was used to determine the particle dimensions and OriginPro 8.6 software was used to process experimental data.

2.2.4-Photophysical characterization

UV/Visible absorption spectra were recorded using a Perkin-Elmer Lambda 9 spectrophotometer.

Excitation and emission spectra were measured using a Jobin Yvon–Horiba Fluorolog 3-22 spectrofluorimeter equipped with a R928 Hamamatsu detector for visible detection and with an Electro-Optical Systems, Inc. DSS-IGA020L detector for the NIR domain. An integrating sphere developed by Frédéric Gumy and Prof. Jean-Claude G. Bünzli (Laboratory of Lanthanide Supramolecular Chemistry, École Polytechnique Féderale de Lausanne (EPFL), BCH 1402, CH-1015 Lausanne, Switzerland) as an accessory to the Fluorolog 3-22

spectrofluorimeter (Patent pending) using quartz tube sample holders was used for determination of quantum yield and commercialized and manufactured by GMP (Renens Switzerland).(Aebischer, Gumy *et al*. 2009) Spectra were corrected for variations in lamp intensity over the spectra range, excitation monochromator response and emission monochromator and detector responses.

Relative quantum yields were measured with the Fluorolog 3-22 set-up described above using ytterbium tropolonate ($[Yb(trop)_4]^-$) in DMSO (Φ_{Yb} = 1.9(±0.1) x 10^{-3}) as a reference (Zhang, Badger *et al*. 2005).

Using the Fluorolog 3-22 set-up described above emission spectra (λ_{ex} = 355 nm) were collected every thirty minutes for a photobleaching study. The samples were exposed to white light from the xenon lamp of the Fluorolog 3-22 in between collection of emission spectra.

2.2.5-Luminescence lifetimes

Luminescence lifetimes were measured using a Nd:YAG Continuum Powerlite 8010 or a Quantel YG980 laser (354 nm, 3rd harmonic) as the excitation source. Emission was collected at a right angle to the excitation beam, and wavelengths were selected by a Spectral Products CM 110 1/8 meter monochromator. The signal was monitored by a Hamamatsu R316-02 photomultiplier tube and collected on a 500 MHz band pass digital oscilloscope (Tektronix TDS 754D). Signals from >1000 flashes were collected and averaged. Three decay curves were collected for each sample and the data were analyzed using OriginPro 8.6 software using exponential fitting modes.

2.2.6-Cell Culture

HeLa (Human Epithelial Ovarian Carcinoma) and NIH 3T3 (Mouse Embryonic Fibroblast) cell lines obtained from ATCC (Molsheim, France) were grown at 37 °C in a 5% CO_2 humidified atmosphere. Every 3-4 days, 5x10^5 cells were seeded into 25 cm^2 plastic flask.Cells were respectively cultivated in Mimimum Essential Medium (MEM) and in Dulbecco's-MEM (DMEM) supplemented with 10% fetal bovine serum (FBS) and for HeLa cells 1% L-glutamine, 1% penicillin/streptomycin, and with 1% of a 100x non-essential amino acid solution. The presence of mycoplasma was checked using "MycoAlert Detection kit" (Lonza) and only certified mycoplasma-free cells were used for experiments.

2.2.7-Alamar Blue assay

For the cytotoxicity test, $1x10^4$ cells per well were seeded in a 96 well microplate. After 24 hours of cell attachment, cells were treated with increasing concentrations of nano-Yb-PVDC-3 diluted for 24 hours at 37 °C. The cytotoxicity was evaluated with the Alamar Blue assay (Invitrogen, Courtaboeuf, France). Alamar Blue was added to the medium (10% v/v) and its fluorescence (λ_{ex} = 530 nm, λ_{em} = 590 nm) was measured after 4 hours at 37 °C with a microplate reader (Victor 3V, Perkin-Elmer, Courtaboeuf, France). This assay compares fluorescence of untreated cells with fluorescence of cells after incubation with nano-Yb-PVDC-3.

2.2.8-Stability in cell lysate

The emission of nano-Yb-PVDC-3 was followed during 6 hours in cell lysate. For this, $1x10^6$ cells (HeLa and NIH 3T3) were collected. After centrifugation, the pellets were re-suspended in water and cell membranes were lysed using a syringe 25G for a mechanic lyse. The lysate were centrifuged again to exclude cell membrane fragments. Nano-Yb-PVDC-3 was diluted in the supernatant and the emission spectra were measured using the Fluorolog 3-22.

2.2.9-Inductively Coupled Plasma (ICP) for cellular uptake quantification

To quantify the concentration of Yb^{3+} in cells, $1x10^6$ cells were seeded in a 6 well microplate. After 24 hours of attachment, the cells were incubated with 20, 30, 40 mg/L of nano-Yb-PVDC-3 for 24 hours at 37 °C. Cells were trypsinated and centrifuged for 5 minutes at 1500 rpm. Pellets were re-suspended in nitric acid overnight before adding PBS (Phophate buffer saline) buffer to achieve a final concentration of 5% nitric acid. The measurements were taken on an ICP (Ultimate, Jobin Yvon, France) coupled with photomultiplier tube and High Dynamic Detection (HDD) system.

2.2.10-Confocal images by apotome

Confocal fluorescence imaging was realized with an Axio Observer Z1 fluorescence inverted microscope (Zeiss, Le Pecq, France) equipped with an ORCA-R2 high-resolution CCD

camera linked to a computer driving the acquisition software Axiovision (Zeiss). Confocality was obtained by Zeiss-ApoTome module of optical sectioning using structured illumination by grids oscillations. The Zeiss HXP-120 light source (metal halide) was used as excitation system and combined to a UV cube filter unit as follows: λ_{ex} = 365/12 nm, λ_{em} = 445/50 nm to observe phenylene emission. Optical sections were recorded at magnification 20 and 40 with Zeiss Plan-APOCHROMAT 20x/0.8 and 40x/1.4 objectives respectively.

2.2.11-NIR microscopy

NIR epifluorescence microscopy was realized on the same microscope as for confocal images except that it was equipped with an EMCCD Evolve 512 photometric camera. The Zeiss HXP 120 was combined to cube filters as follows: λ_{ex} = 365/12 nm, λ_{em} = 445/50 nm to observe phenylene emission and λ_{ex} = 377/50 nm, λ_{em} = Long Pass 770 nm to observe Yb^{3+} emission with 1 second of exposition.

2.2.12-Spectrale fluorescent microscopy

Cells were platted onto 25 mm round quartz coverslips and incubated 24 hours with 30 µg/mL nano-Yb-PVDC-3 before fixation with 4% PFA. Fluorescence spectra were recorded on Polypheme, the DUV inverted microspectrofluorimeter installed at DISCO beamline at Synchrotron SOLEIL(Saint Aubin, France) (Giuliani, Jamme *et al.* 2009). Excitation at 280 or 340 nm was provided by the continuous emission from the DISCO beamline bending magnet and focused on the sample using a 100x microscope objective (Zeiss).

One full fluorescence emission spectrum was recorded on each point of the image (typically 50x50 pixels) with an acquisition time of 10 seconds. A fluorescence intensity map was reconstructed in the spectral region of interest.

2.3-Results and discussion

2.3.1-Yb-PVDC-3 structure.

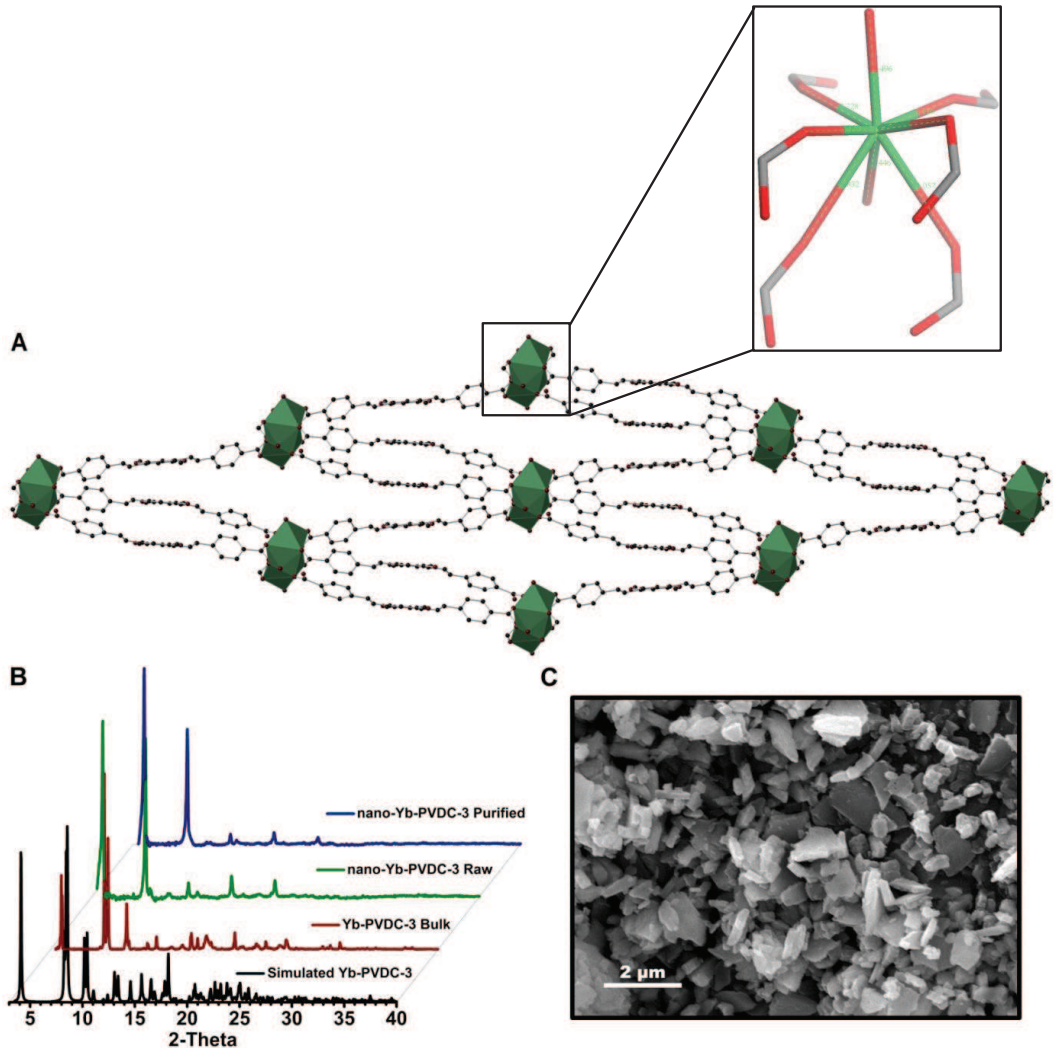

Figure 2.5. (A) Crystal structure of Yb-PVDC-3 viewed along crystallographic *a* axis. Yb^{3+} shown as polyhedral (C, gray; O, red; Yb^{3+}, green). (B) PXRD patterns for bulk and nano-Yb-PVDC-3. (C) SEM image of nano-Yb-PVDC-3; average dimensions (± standard deviation) are: 0.5(±0.3) µm (length), 316(±156) nm (width), 176(±52) nm (thick). Scale bar represents 2 µm.

Yb-PVDC-3 crystallizes in the low symmetry space group *P*-1 and exhibits infinite Yb-carboxylate secondary building units (SBUs) along the *a* crystallographic direction (appendix 3). The SBU consists of octa-coordinated Yb^{3+} with 6 carboxylates from 3 ligands and two oxygen atoms from two dimethylformamide molecules (Figure 2.5.A). The Yb-PVDC-3 nanoMOF is isostructural to the corresponding bulk material as evidenced by powder X-ray

diffraction (PXRD) pattern comparisons (Figure 2.5.B). Compared to the previously reported Yb-PVDC-1 and Yb-PVDC-2 (White, Chengelis *et al*. 2009), Yb-PVDC-3 has a lower symmetry and its structure is significantly more condensed, with 1-D channels along the *a* crystallographic direction measuring ~43× 9 Å (Yb^{3+}-Yb^{3+} center to center distances). The 1-D channels are very narrow: close contacts (e.g. 0.281, 0.637, and 0.706 Å) exist between the PVDC linkers lining opposite channel walls. Scanning electron microscopy (SEM) was used to study the size of nano-Yb-PVDC-3. The nanoMOFs exhibit a block-like morphology (Figure 2.6) having average dimensions of 0.5(±0.3) μm (length) by 316(±156) nm (width), by 176(±52) nm (thickness).

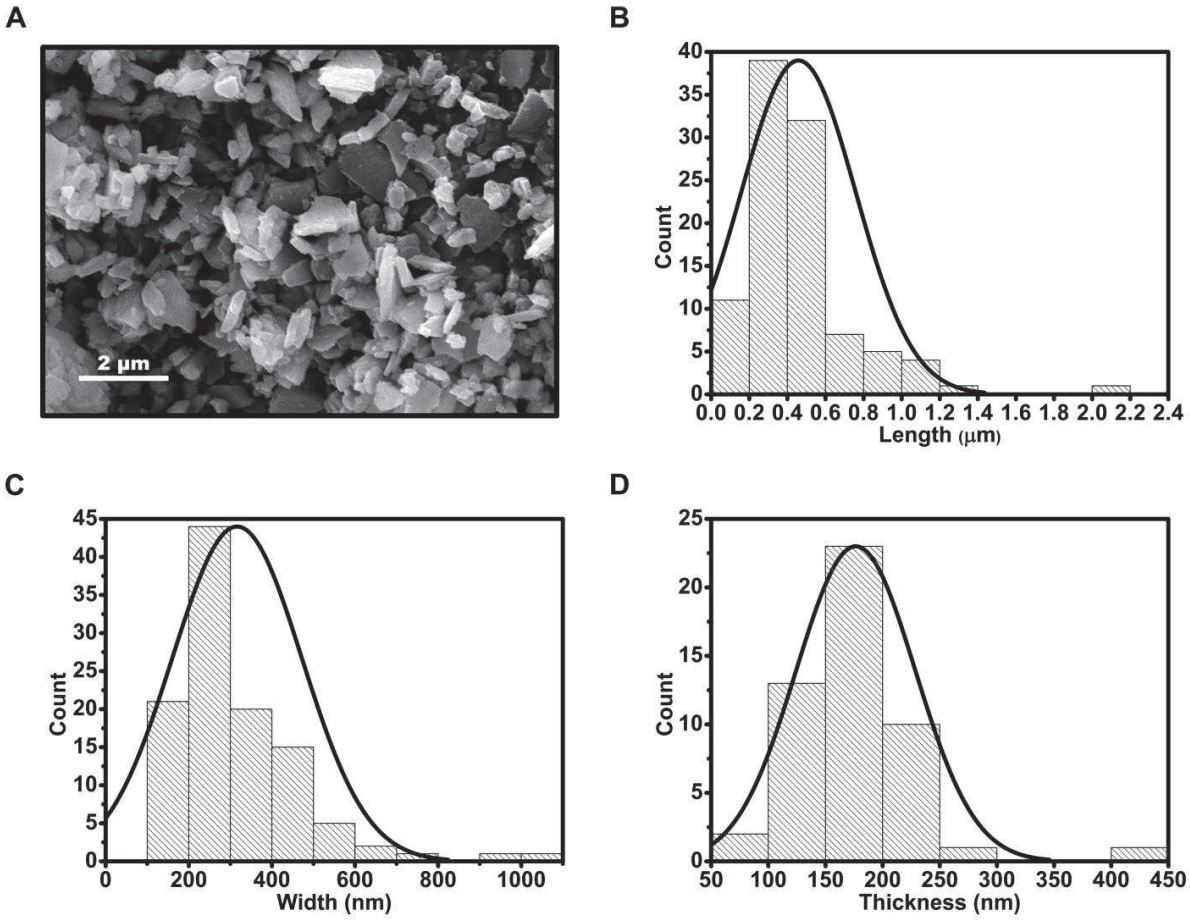

Figure 2.6. Size characterization of nano-Yb-PVDC-3.Representative SEM image (A) and histograms of length (B), width (C), and thickness (D) measurements.

2.3.2-Spectroscopic characterization of nano-Yb-PVDC-3.

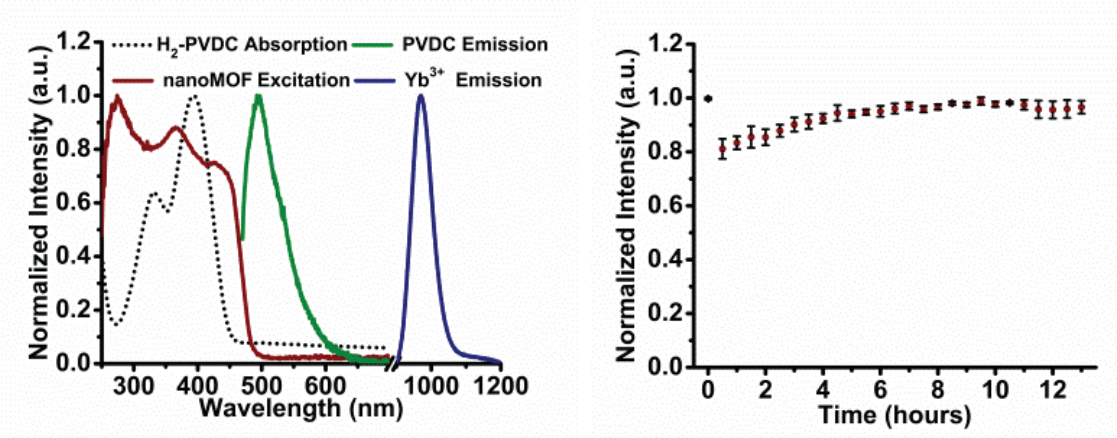

Figure 2.7. Spectroscopic characterization of nano-Yb-PVDC-3 in 0.1 M HEPES. Left: H_2-PVDC absorbance spectrum (black dotted line), nano-Yb-PVDC-3 excitation spectrum (red, λ_{em} = 980 nm), and emission spectra for both the ligand (green) and lanthanide (blue) obtained by exciting nano-Yb-PVDC-3 at 355 nm. Right: Photobleaching study monitoring the emission at 970 nm over a period of 13 hours. Error bars represent standard deviation based on three independent experiments.

Luminescence properties of the material were studied in water and in 0.1 M HEPES buffer (pH 7.3) (Figure 2.7). In both environments, nano-Yb-PVDC-3 exhibits Yb^{3+} luminescence centered at 970 nm upon excitation of the PVDC sensitizer. The overlap of the absorption spectrum of H_2-PVDC and the excitation spectrum of the MOF indicates that sensitization is occurring via the antennae effect. Since Yb^{3+} does not have accepting levels in the visible, the observed Yb^{3+} luminescence must result from the sensitization provided by PVDC located in sufficiently close proximity to the lanthanide cations. Quantum yields were recorded in order to quantify the efficiency of the energy transfer between the antenna and Yb^{3+} and the protection of the lanthanide cations against sources of non-radiative deactivation. Upon excitation at 450 nm, quantum yield values for the nano-Yb-PVDC-3 are $1.0(\pm0.3)\times10^{-4}$ in water and $5.2(\pm0.8)\times10^{-5}$ in 0.1 M HEPES. These values are relatively small in comparison to the best luminescent lanthanide compounds (Zhang, Badger *et al*. 2005; Comby, Imbert *et al.* 2006; Zhang and Petoud 2008; Eliseeva and Bunzli 2010), but the approach of utilizing a MOF system to maximize the number of chromophores and lanthanide cations per unit volume is expected to reduce this limitation.

Table 2.1. Relative quantum yields (Φ) and luminescent lifetimes (τ_x) of Yb^{3+} centered emission at 980 nm

	Solvent*	Φ_{Yb}†	τ_1‡ (μs)	τ_2‡ (μs)
nano-Yb-PVDC-3	H_2O	$1.0(\pm0.3)x10^{-4}$	7.01 (±0.07)	1.51 (±0.01)
	0.1 M HEPES	$5.2(\pm0.8)x10^{-5}$	4.6 (±0.1)	1.04 (±0.02)

*nanoMOFs as a crystalline solid under solvent. †λ_{ex} = 450 nm. ‡λ_{ex} = 354 nm.

Luminescence lifetime experimental data (Table 2.1) were best fit with a bi-exponential decay curve, indicating that the Yb^{3+} cations are present within two distinct environments. From the crystal structure obtained from X-Ray diffraction all Yb^{3+} ions present in the MOF have a coordination number of eight (octa-coordinate) and the different environments observed from the luminescence lifetimes are attributed to the Yb^{3+} present in the interior of the nanoMOF and the Yb^{3+}located on the edges/faces of the crystallites (exterior). Exterior $Yb^{3+}$are more susceptible to non-radiative deactivations and will have shorter lifetime values.

Ideally, reagents for bioanalytical applications and for imaging should emit a constant number of photons over time and their signals should not be affected by species and parameters other than the amount of targeted analyte. A common limitation for organic fluorophores is their tendency to photobleach when exposed to light. Photobleaching test experiments were performed by exposing a suspension of nano-Yb-PVDC-3 in 0.1 M HEPES (pH =7.3) to light over a period of 13 hours. Results showed that the signal does not significantly change over an extended period of time (Figure 2.7) as strong, indication that the material is stable in these conditions and usable over this extended period of time.

2.3.3-Stability studies.

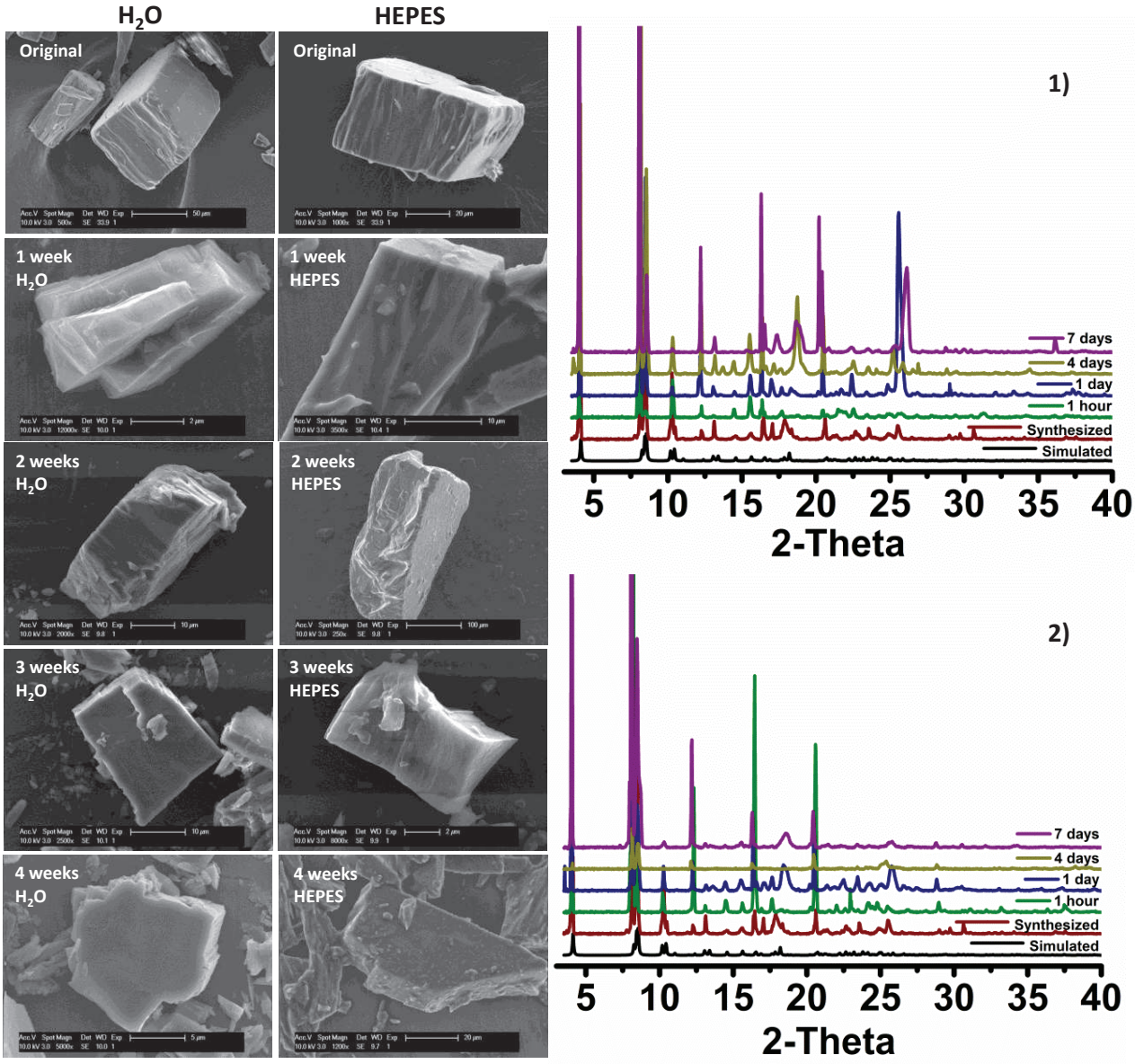

Figure 2.8. SEM images over a period of seven days for Yb-PVDC-3 soaked in H_2O or 0.1M HEPES (left) and Powder X-ray diffraction patterns over a period of seven days for Yb-PVDC-3 soaked in H_2O (top) or 0.1M HEPES (bottom). These measurements were performed at the University of Pittsburgh.

We rigorously evaluated the stability of Yb-PVDC-3 and nano-Yb-PVDC-3 in various conditions including water, 0.1 M HEPES buffer, and cellular media. First, samples of Yb-PVDC-3 were soaked in water or 0.1 M HEPES (pH =7.3), and cellular media. First, samples of Yb-PVDC-3were soaked in water or 0.1 M HEPES. At different time points, SEM images were collected to visualize bulk structure and PXRD patterns were obtained to confirm the retention of crystallinity (Figure 2.8). In general, SEM images indicate that the crystals remain intact after soaking in water or HEPES for up to 4 weeks; however, crystallite

fragmentation occurs during this time, and consequently the average crystallite size decreases. Notably, the faces of the crystallites remain smooth, and no significant pitting was observed on the crystal surfaces. Powder X-ray diffraction patterns of crystallites collected after soaking in either water or HEPES buffer for different time intervals suggest retention of crystallinity.

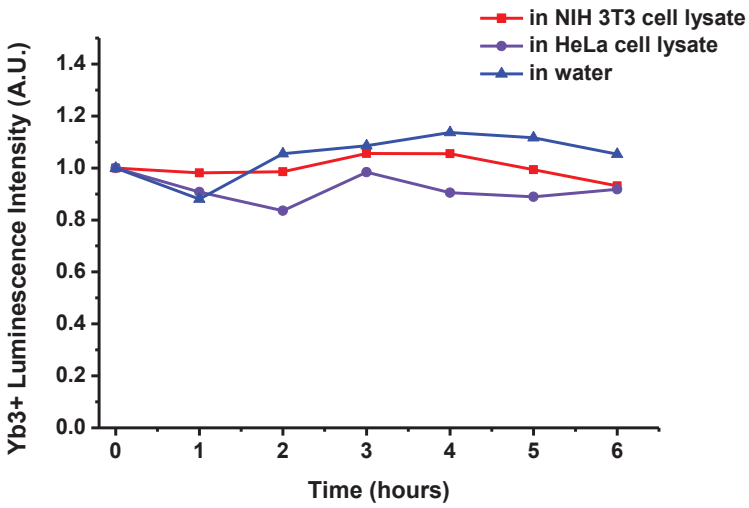

Figure 2.9. Spectroscopic evaluation of the nano-Yb-PVDC-3 stability in cell lysate. Emission intensity values correspond to the maxima of Yb^{3+} emission (970 nm) after dilution of nano-Yb-PVDC-3 at 30 µg/mL in water, HeLa cell lysate, or NIH 3T3 cell lysate.

We emphasize that to preserve the luminescence properties of the NIR emitting reagent and to prevent the release of free lanthanide cations in cellular media, the nano-Yb-PVDC-3 must remain intact. Therefore, crystallite stability was quantitatively evaluated in cellular media by monitoring the Yb^{3+} emission signal upon excitation of the antenna. The signal of the lanthanide cations can only be generated if the antenna effect is present which can be only obtained if the antenna is located at sufficiently close proximity to the lanthanide. Therefore, if the MOF dissociates via hydrolysis of the Yb-carboxylate bonds, one should expect a significant decrease in the luminescence. Signal arising from Yb^{3+} was measured at regular time intervals after dilution of nano-Yb-PVDC-3 in cell lysate (HeLa or NIH 3T3 cells) and in water as a control. Intensities of the emission bands compared to initial intensity (recorded upon the monitoring the Yb^{3+} band at 970 nm) are reported in Figure 2.9. The total emission intensity remains constant over time which suggests that the nano-Yb-PVDC-3 structure is not significantly modified by enzymes or other cellular components. Indeed the constant total intensity of Yb^{3+} emission signal is a quantitative indication that the nanoMOFs measured retain their integrity in this challenging environment. Therefore, we expect that nano-Yb-

PVDC-3 will be stable inside of the cell and should not interfere significantly with physiological cell metabolism.

2.3.4-Nano-Yb-PVDC-3 cytotoxicity.

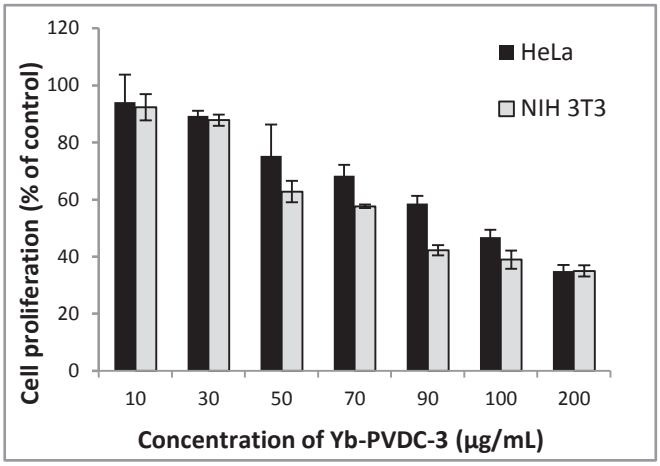

Figure 2.10. Cellular viability by Alamar Blue assay on HeLa and NIH 3T3 cells after 24h of incubation with increasing concentrations of nano-Yb-PVDC-3.

A principal aim of this study is to test nano-Yb-PVDC-3 in cells as NIR imaging agents. Human cancer (HeLa) and mouse (NIH 3T3) cells were chosen as representative cell lines. The nano-Yb-PVDC-3 cytotoxicity was first evaluated for both cells lines using the Alamar Blue assay. The cell proliferation test presented in Figure 2.10 indicated a similar effect on the two cell lines after 24 hours of incubation. The compound is found to have relatively low toxicity for concentrations up to 50 µg/mL. Working concentration was chosen on the criterion of 90% of cellular viability (30 µg/mL).

2.3.5-Cellular uptake.

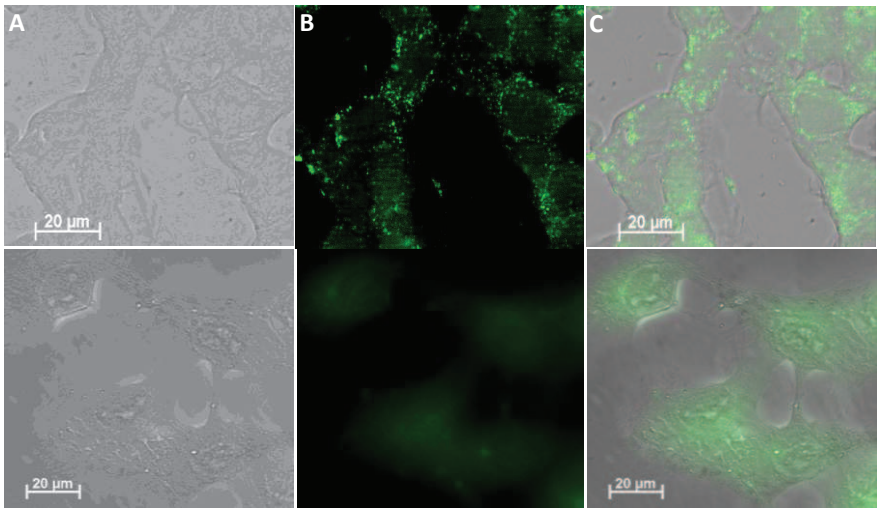

Figure 2.11. Cellular uptake of nano-Yb-PVDC-3.Confocal microscopy of NIH 3T3 cells after incubation with nano-Yb-PVDC-3 at 30 µg/mL (top) and untreated cells (bottom). (A) Brightfield, (B) H_2-PVDC emission (λ_{ex} = 365/12 nm, λ_{em} = 445/50 nm), and (C) Merge.

Internalization of nano-Yb-PVDC-3 by the cells was confirmed with confocal microscopy and inductively coupled plasma (ICP) spectrometry experiments. Microscopy images in Figure 2.11 show that nano-Yb-PVDC-3 is internalized by cells. Optical slices of 1 µm (less than cell thickness) were obtained for NIH 3T3 cells after incubation with nano-Yb-PVDC-3 at 30 µg/mL. Despite the fact that untreated cells generate autofluorescence at these wavelengths (λ_{ex} = 365 nm, λ_{em} = 445/50 nm), we could unambiguously detect the chromophore signal inside the cells. This fluorescence signal is located specifically in the cytoplasm (and not in the nucleus).

Table 2.2. Determination of Cellular Uptake by ICP

Sample	Concentration of nano-Yb-PVDC-3 in Cell Media (μg/mL)	Theoretical Concentration of Yb^{3+} in Cell Media (μg/mL)	Concentration of Yb^{3+} in $1x10^6$ cells (μg/mL)
HeLa Cells	0	0	0.000±0.002
	20	4.06	0.113±0.003
	30	6.09	0.213±0.003
	40	8.12	0.270±0.003
NIH 3T3 Cells	0	0	0.000±0.002
	20	4.06	0.466±0.010
	30	6.09	0.996±0.020
	40	8.12	1.130±0.003

To confirm results obtained from confocal microscopy, the quantity of nano-Yb-PVDC-3 associated with $1x10^6$ cells was measured by ICP (Table 2.2). More specifically, the amount of Yb^{3+} in cells was measured after 24 hours of incubation of HeLa and NIH 3T3 cells with nano-Yb-PVDC-3. ICP results confirm the presence of nano-Yb-PVDC-3 in the cells. For both cell lines, the Yb^{3+} amount in cells increases with the amount of nano-Yb-PVDC-3 present in cellular incubation medium. No saturation of cellular uptake has been observed at these concentrations. The uptake is more important in NIH 3T3 than in HeLa cells. The mechanism of cell uptake has not been analyzed at this time and is currently under investigation.

2.3.6-Spectral microscopy.

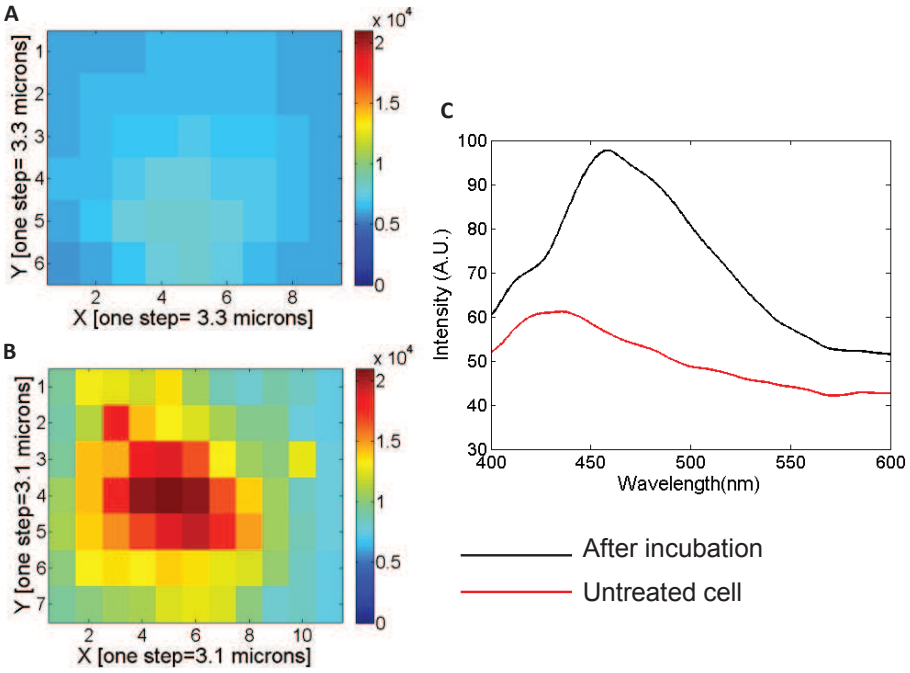

Figure 2.12. Spectral microscopy of nano-Yb-PVDC-3 in the visible region. The fluorescence intensity map of untreated NIH 3T3 cells (A) and after incubation with nano-Yb-PVDC-3 (B) (λ_{ex}= 340 nm- λ_{em}=390-650 nm). Spectra (C) correspond to the mean of intensity of each map.

Several cellular compounds are excited by UV light and emit in the visible such as tryptophan (λ_{ex} = 275 nm, λ_{em} = 335 nm), collagen (λ_{ex} = 335 nm, λ_{em} = 405 nm), and NAD(P)H (λ_{ex} = 340nm, λ_{em} = 460 nm) (Wagnieres, Star *et al*. 1998). To fully confirm that the detected signal observed with confocal microscopy is arising from PVDC emission, we conducted spectral fluorescence microscopy analysis on cells after 24 hours of incubation with nano-Yb-PVDC-3. At each individual point of the image (step size = 3µm), an emission spectrum was recorded. The intensity value averaged between 400 and 600 nm was used to create an intensity map of the cell (Figure 2.12). This spectral fluorescence microscopy experiment permits the discrimination of nano-Yb-PVDC-3 emission from cellular autofluorescence. The signal obtained from untreated cells can be attributed to cellular autofluorescence with a maximum of the emission band located at 420 nm. Spectra obtained from treated cells result from the overlay of autofluorescence emission and PVDC emission signals (λ_{em} = 455 nm). This result is a third confirmation that the nanoMOF is able to enter incubated cells.

2.3.7-Near-infrared epifluorescence microscopy.

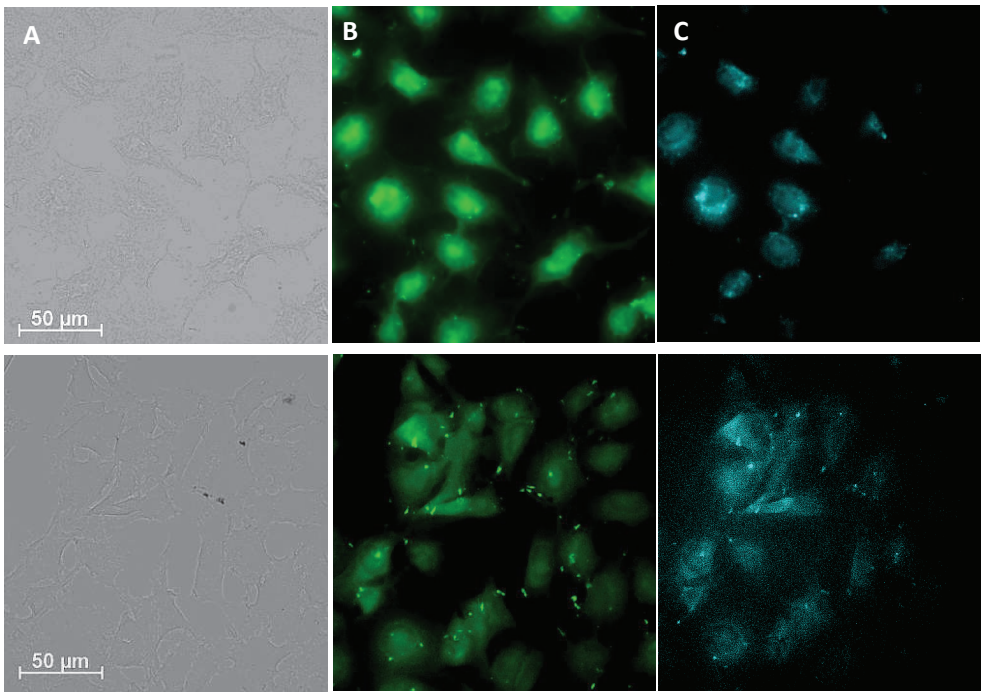

Figure 2.13. Visible and NIR microscopy images of nano-Yb-PVDC-3 in HeLa cells (top) and NIH 3T3 (bottom) (A) Brightfield, (B) H_2-PVDC emission (λ_{ex} = 377/50 nm, λ_{em} = 445/50 nm) and (C) Yb^{3+} emission (λ_{ex} = 377/50 nm, λ_{em} = Long Pass770 nm).

The ability to use nano-Yb-PVDC-3 as a NIR lanthanide-based imaging agent was tested in a NIR microscopy experimental setup. HeLa and NIH 3T3 cells were incubated with 30 µg/mL of nano-Yb-PVDC-3 for 24 hours. Visible chromophore PVDC and NIR Yb^{3+} emission signal were both observed by epifluorescence microscopy (Figure 2.13). In the NIR microscopy mode, the specific Yb^{3+} emission signal was collected with a satisfying sensitivity (exposition time 1s) as the result of a high signal to noise ratio. In parallel, switching to visible detection mode, the specific fluorescence arising from the PVDC was observed in addition to the cellular autofluorescence, and the resulting images were used as a comparison. The difference observed between the PVDC and Yb^{3+} emission signal results from the discrimination of the NIR signal from the autofluorescence arising from the biological material.

The images presented in Figure 2.13 are the first report of NIR microscopy experiments obtained with a lanthanide compound in living cells using a conventional excitation source.

2.4-Conclusion

In this chapter, was described the synthesis, photophysical properties, cytotoxicity and ability to enter living cell of nano-Yb-PVDC-3. The ability of this new nanoMOF to operate as a lanthanide-based NIR imaging agent in cells has also been tested and demonstrated.

The overlap of the excitation spectrum of nano-Yb-PVDC-3 with the absorbance spectrum of H_2-PVDC demonstrates that the Yb^{3+} is sensitized through the "antenna effect," provided by the electronic structure of the phenylene group where the sensitizers embedded in the MOF are excited and transfer energy to the accepting levels of the Yb^{3+} cations.

The nanoscale material was shown to be luminescent in water andin HEPES buffer. The nanoMOF quantum yield is low in water, likely due to a quenching process as the energy level of the -OH overtone vibration being so close to that of Yb^{3+}. It further decreases when the nanoMOF is placed in HEPES, likely due to the increase in number of moieties with -OH vibrations per unit volume in solution. The low quantum yield value does not prevent nano-Yb-PVDC-3 to operate as imaging agent in cells because of the large number of sensitizers and the polymetallic design.

The energy transfer is conserved after 24 hours of incubation in cellular media, proving the integrity of nano-Yb-PVDC-3 inside of the cells. This outstanding stability combined with cytotoxicity results are promising for using nano-Yb-PVDC-3 as a biological probe for *in vivo* applications.

This structure which is able to incorporate a large number of lanthanide sensitizers (PVDC) and a large number of NIR emitting lanthanide cations on a single MOF nanoparticle, was used to validate the efficacy of the strategy to increase the number of emitted NIR photons per unit volumeto obtain a satisfactory sensitivity to allow the first report of NIR microscopy based on lanthanide using a single photon excitation in living cells.

Results have shown that nano-Yb-PVDC-3 is not highly uptaken by cells. This is probably due to the relatively large size of crystals (of 0.5(±0.3) µm of length; 316(±156) nm of width and 176(±52) nm of thickness). As perspective of this work, we hypothesize that improvement of the miniaturization and of the homogeneity of nano-Yb-PVDC-3 batches will also improve cellular uptake.

The actual important size of nano-Yb-PVDC-3could be a limiting factor for applications in living cells /organism but not for *ex vivo* applications. The results have demonstrated the sufficient brightness in the NIR and its efficacy to be observed by microscopy. We can also consider using nano-Yb-PVDC-3 for the specific staining of histological slices. Indeed, for

this specific application, detection sensitivity is often limited by autofluorescence due to the presence of fixer (parrafin, OCT). By using the special advantages of NIR emitting lanthanide cations, such limitations can be overcome. The autofluorescence will be probably less important or non-existent in the NIR, and for non-ambiguous results, time resolved microscopycan be used to observe only Yb^{3+} emission signal after the media background thanks to lanthanide long lifetime.

References

- Aebischer, A., F. Gumy, *et al*. (2009). "Intrinsic quantum yields and radiative lifetimes of lanthanide tris(dipicolinates)." Physical Chemistry Chemical Physics**11**(9): 1346-1353.
- An, J., S. J. Geib, *et al*. (2009). "Cation-triggered drug release from a porous zinc-adeninate metal-organic framework." J Am Chem Soc**131**(24): 8376-8377.
- Anokhina, E. V., Y. B. Go, *et al*. (2006). "Chiral three-dimensional microporous nickel aspartate with extended Ni-O-Ni bonding." J Am Chem Soc**128**(30): 9957-9962.
- Carne, A., C. Carbonell, *et al*. (2011). "Nanoscale metal-organic materials." Chem Soc Rev**40**(1): 291-305.
- Comby, S., D. Imbert, *et al*. (2006). "Stable 8-hydroxyquinolinate-based podates as efficient sensitizers of lanthanide near-infrared luminescence." Inorg Chem**45**(2): 732-743.
- Della Rocca, J., D. Liu, *et al*. (2011). "Nanoscale metal-organic frameworks for biomedical imaging and drug delivery." Acc Chem Res**44**(10): 957-968.
- Eliseeva, S. V. and J. C. Bunzli (2010). "Lanthanide luminescence for functional materials and bio-sciences." Chem Soc Rev**39**(1): 189-227.
- Ferey, G. (2008). "Hybrid porous solids: past, present, future." Chem Soc Rev**37**(1): 191-214.
- Ferey, G., C. Mellot-Draznieks, *et al*. (2005). "A chromium terephthalate-based solid with unusually large pore volumes and surface area." Science**309**(5743): 2040-2042.
- Giuliani, A., F. Jamme, *et al*. (2009). "DISCO: a low-energy multipurpose beamline at synchrotron SOLEIL." Journal of Synchrotron Radiation**16**(6): 835-841.
- Guo, Z., H. Xu, *et al*. (2011). "A robust near infrared luminescent ytterbium metal-organic framework for sensing of small molecules." Chem Commun (Camb)**47**(19): 5551-5553.
- Horcajada, P., T. Chalati, *et al*. (2010). "Porous metal-organic-framework nanoscale carriers as a potential platform for drug delivery and imaging." Nat Mater**9**(2): 172-178.
- Horcajada, P., C. Serre, *et al*. (2008). "Flexible porous metal-organic frameworks for a controlled drug delivery." J Am Chem Soc**130**(21): 6774-6780.
- Horcajada, P., C. Serre, *et al*. (2006). "Metal-organic frameworks as efficient materials for drug delivery." Angew Chem Int Ed Engl**45**(36): 5974-5978.
- Ingleson, M. J., J. Bacsa, *et a*l. (2007). "Homochiral H-bonded proline based metal organic frameworks." Chem Commun (Camb)(29): 3036-3038.
- Kerbellec, N. C., L. Daiguebonne, *et al*. (2008). "Luminescent coordination nanoparticles." New Journal Of Chemistry **32**: 584-587.
- Kitagawa, S., R. Kitaura, *et al*. (2004). "Functional porous coordination polymers." Angew Chem Int Ed Engl**43**(18): 2334-2375.

- Lee, J., O. K. Farha, *et al*. (2009). "Metal-organic framework materials as catalysts." Chem Soc Rev**38**(5): 1450-1459.
- Low, J. J., A. I. Benin, *et al*. (2009). "Virtual high throughput screening confirmed experimentally: porous coordination polymer hydration." J Am Chem Soc**131**(43): 15834-15842.
- McKinlay, A. C., R. E. Morris, *et al*. (2010). "BioMOFs: metal-organic frameworks for biological and medical applications." Angew Chem Int Ed Engl**49**(36): 6260-6266.
- Murray, L. J., M. Dinca, *et al*. (2010). "Highly-selective and reversible O2 binding in Cr3(1,3,5-benzenetricarboxylate)2." J Am Chem Soc**132**(23): 7856-7857.
- Ni, Z. and R. I. Masel (2006). "Rapid production of metal-organic frameworks via microwave-assisted solvothermal synthesis." J Am Chem Soc**128**(38): 12394-12395.
- Oh, M. and C. A. Mirkin (2005). "Chemically tailorable colloidal particles from infinite coordination polymers." Nature**438**(7068): 651-654.
- Rieter, W. J., K. M. Taylor, *et al*. (2006). "Nanoscale metal-organic frameworks as potential multimodal contrast enhancing agents." J Am Chem Soc**128**(28): 9024-9025.
- Rieter, W. J., K. M. Taylor, *et al*. (2007). "Surface modification and functionalization of nanoscale metal-organic frameworks for controlled release and luminescence sensing." J Am Chem Soc**129**(32): 9852-9853.
- Rieter, W. J., K. M. L. Taylor, *et al*. (2006). "Nanoscale metal−organic frameworks as potential multimodal contrast enhancing agents." J Am Chem Soc**128**(28): 9024-9025.
- Rowsell, J. L. and O. M. Yaghi (2005). "Strategies for hydrogen storage in metal--organic frameworks." Angew Chem Int Ed Engl**44**(30): 4670-4679.
- Son, W. J., J. Kim, *et al.* (2008). "Sonochemical synthesis of MOF-5." Chem Commun (Camb)(47): 6336-6338.
- Taylor, K. M., A. Jin, *et al*. (2008). "Surfactant-assisted synthesis of nanoscale gadolinium metal-organic frameworks for potential multimodal imaging." Angew Chem Int Ed Engl**47**(40): 7722-7725.
- Taylor, K. M., W. J. Rieter, *et al*. (2008). "Manganese-based nanoscale metal-organic frameworks for magnetic resonance imaging." J Am Chem Soc**130**(44): 14358-14359.
- Taylor, K. M. L., W. J. Rieter, *et al*. (2008). "Manganese-based nanoscale metal−organic frameworks for magnetic resonance imaging." J Am Chem Soc**130**(44): 14358-14359.
- Vaidhyanathan, R., D. Bradshaw, *et al*. (2006). "A family of nanoporous materials based on an amino acid backbone." Angew Chem Int Ed Engl**45**(39): 6495-6499.
- Vaucher, S., M. Li, *et al*. (2000). "Synthesis of Prussian Blue Nanoparticles and Nanocrystal Superlattices in Reverse Microemulsions." Angew Chem Int Ed Engl **39**(10): 1793-1796.
- Wagnieres, G. A., W. M. Star, *et al*. (1998). "In vivo fluorescence spectroscopy and imaging for oncological applications." Photochem Photobiol**68**(5): 603-632.

- White, K. A., D. A. Chengelis, *et al*. (2009). "Near-infrared luminescent lanthanide MOF barcodes." J Am Chem Soc**131**(50): 18069-18071.
- White, K. A., D. A. Chengelis, *et al.* (2009). "Near-infrared emitting ytterbium metal-organic frameworks with tunable excitation properties." Chem Commun (Camb)(30): 4506-4508.
- Yaghi, O. M. L., H. (1995). "Hydrothermal Synthesis of a Metal-Organic Framework Containing Large Rectangular Channels." J. Am. Chem.Soc **117**(41): 10401-10402.
- Zhang, J., P. D. Badger, *et al*. (2005). "Sensitization of Near-Infrared-Emitting Lanthanide Cations in Solution by Tropolonate Ligands." Angew Chem Int Ed Engl**44**(17): 2508-2512.
- Zhang, J. and S. Petoud (2008). "Azulene-moiety-based ligand for the efficient sensitization of four near-infrared luminescent lanthanide cations: Nd3+, Er3+, Tm3+, and Yb3+." Chemistry**14**(4): 1264-1272.

Résumé Français

Le travail présenté dans ce chapitre porte sur la caractérisation de nouveaux réseaux métallo organiques nano (nano-MOFs) à base de lanthanides luminescents pour des applications en imagerie biologique.

Les MOFs sont des composés cristallins formés d'ions, ou de groupes d'ions métalliques coordinés. Ces nanoparticules rigides et poreuses suscitent un intérêt grandissant pour de nombreuses applications comme le stockage de gaz, les piles à combustibles, la catalyse et beaucoup plus récemment, la délivrance de molécules thérapeutiques et l'imagerie.

La structure parfaitement définie des MOFs ainsi que le contrôle de la taille des pores offrent de nombreuses possibilités pour le transport de molécules d'intérêts telles que des molécules thérapeutiques, des biogazs (monoxyde d'azote), ou des agents de contrastes (Gd^{3+}).

Quelques exemples de la littérature rapportent l'utilisation de nano-MOFs à base de lanthanides (Gd^{3+}, Eu^{3+}, Tb^{3+}) incorporés dans les pores pour des applications en imagerie biologique. Le travail rapporté ici se situe dans la continuité d'une étude menée par notre groupe de recherche qui a développé des nouveaux MOFs à base d'Yb^{3+} directement incorporés dans la structure métallo-organique (Yb-PVDC-1 et -2). La stratégie développée ici vise à augmenter la sensibilité de détection en augmentant la densité de chromophore et de lanthanides par unité de volume. Le ligand choisi pour former la structure de ces MOFs, le dicarboxylate de phenylènevinylène (PVDC), sensibilise parfaitement les cations Yb^{3+}. A partir de ces résultats, la synthèse a été modifiée afin de miniaturiser ces MOFs et de les rendre plus compatible pour des applications biologiques, donnant le nano-Yb-PVDC-3.

La structure cristalline du nano-Yb-PVDC-3 a été observée par diffraction de rayons X en poudre ainsi que par microscopie électronique à balayage. Les cristaux présentent une taille d'environ 500 nm de long, 316 nm de large et 176 nm d'épaisseur, ce qui reste relativement gros pour des applications *in cellulo* par exemple.

D'un point de vue photophysique, le chromophore PVDC, qui absorbe à 355nm et atteint son maximum d'émission à 490 nm, sensibilise l'Yb^{3+} (λ_{em}: 980nm). Les rendements quantiques mesurés dans l'eau et dans l'HEPES 0.1M sont respectivement de $1{,}0(\pm0{,}3).10^{-4}$ et $5{,}2(\pm0{,}8).10^{-5}$. Ces faibles valeurs vont être compensées par l'approche qui vise à maximiser le nombre de photons émis par unité de volume en incorporant un grand nombre de chromophores et de lanthanide par nanoparticule. Les nano-MOFs Yb-PVDC-3 possèdent deux temps de vie de luminescence correspondant aux cations Yb^{3+} situés à l'intérieur (temps

de vie le plus longs) et à ceux situés à l'extérieur (temps de vie le plus courts) de la structure cristalline, qui se trouvent dans deux environnements distincts.

Le nano-Yb-PVDC-3 a montré une bonne résistance au photoblanchiment, une conservation de la structure cristalline après 4 semaines dans l'eau et dans l'HEPES 0.1M ainsi qu'une stabilité du transfert d'énergie au lanthanide dans un lysat cellulaire au cours du temps.

Ces composés sont capables de rentrer dans les cellules après 24h d'incubation avec une dose de 30 µg/ml (non toxique pour les lignées cellulaires HeLa et NIH 3T3 testées). Des coupes optiques d'1 µm réalisées dans le volume de la cellule ont montré l'internalisation du nano-MOF avec un signal d'émission localisé au niveau du cytoplasme. Une limitation expérimentale nous a contraints à observer le signal émis par le chromophore à des longueurs d'onde où l'autofluorescence est très présente. Cependant la microscopie spectrale a bien révélé la présence du spectre d'émission du chromophore dans le cytoplasme. Ces résultats associés à des valeurs d'ICP confirmant la présence d'Yb^{3+} dans les cellules après 24h d'incubation confirment la capacité des nano-Yb-PVDC-3 à être internalisés par les cellules.

Le signal d'émission de l'Yb^{3+} a été observé par microscopie à épifluorescence sur des cellules HeLa et NIH 3T3 après 24h d'incubation. Les images obtenues sont plus résolues et affranchies du bruit de fond d'autofluorescence, permettant de localiser le signal de luminescence sans ambigüité.

La preuve de principe de l'efficacité des nano-MOFs Yb-PVDC-3 en tant qu'agents d'imagerie proche infrarouge a été établie ici. Pour la première fois, il a été possible d'observer le signal d'émission d'un composé à base de lanthanide luminescent dans le proche infrarouge dans des cellules. La stratégie visant à augmenter le nombre de photons émis par unité de volume s'avère efficace pour s'affranchir des rendements quantiques très faibles dans le proche infrarouge.

La taille actuellement importante des cristaux peut être limitante pour des applications *in cellulo*/*in vivo*, cependant elle n'est pas incompatible avec des applications *ex vivo* (type marquage histologique).

3-Luminescent lanthanide-based polyamidoamine dendrimers

The work presented here has been realized in collaboration with Dr. Hyounsoo Hu (Stéphane Petoud Research Group, Department of Chemistry, University of Pittsburgh) for the polyamidoamine (PAMAM) dendrimer synthesis and Dr. Svetlana Eliseeva (Stephane Petoud Research Group, CBM-CNRS Orléans) for quantum yield and life time measurements.

3.1-Introduction

3.1.1- The origin of dendrimers

Dendritic architecture is one of the most common topologies on the planet. This pattern can be found in abiotic (erosion fractal, snow crystals) as well as in biological systems from micrometric scale (neurons) to the meter scale (trees) via millimetric and centimetric scale (fungi, vascular network) (Figure 3.1).

The reasons for such mimicry of dendritic architecture at all dimensional length scale remain unsolved. However, it appears that dendritic topology have matured over the past years to optimize their unique interfacial properties.

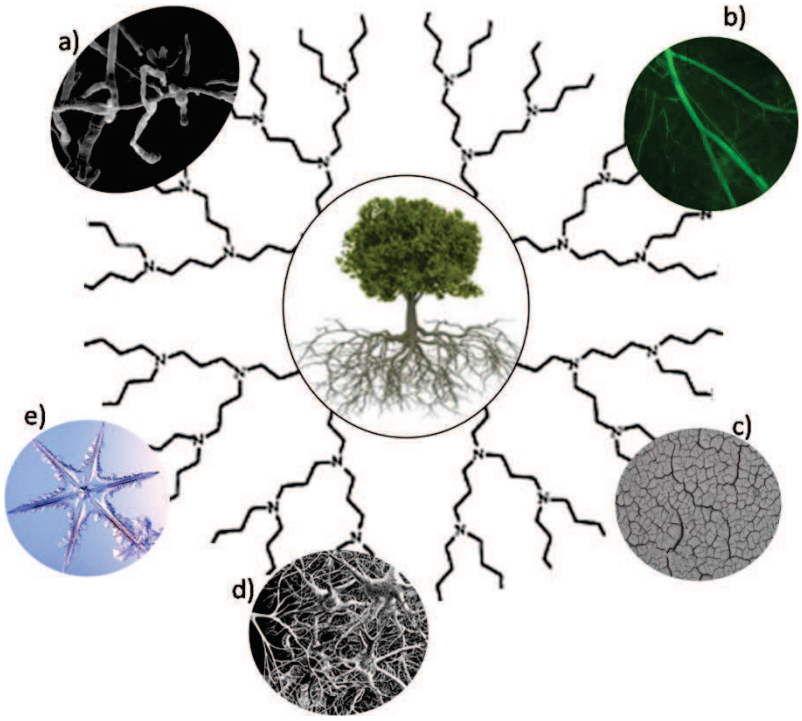

Figure 3.1. Dendritic topologies as found in the abiotic and biological world: (a) mycelium of *Aspergillus niger*; (b) a vascular network; (c) a soil fractal erosion; (d) network of neurons; (e) snow crystal.

Chemists have always researched and found inspiration in the nature located around them. From a chemistry point of view, dendritic architecture represents the ideal low polydispersity macromolecules with a regular tridimensional structure.

From an historical point of view, the concept of repetitive growth branched molecules were described for the first time by Vögtle and collaborators in 1978 (Buhleier E. 1978).

Denkewalter *et al.*, patented the synthesis of macromolecules formed from at least of 4 layers of L-lysin (which will be called " polylysin dendrimers" later on) (Denkewalter R G., Kolc, J. Lukasavage, W. J. U.S. Pat. 4,-289,872, Sept. 15, 1981).

Only in 1985, Donald Tomalia proposed the name "dendrimer" inspired from the greek*dendros* that translates to "tree" and *meros* to "part" (Tomalia 1985).

Dendrimers are described as polymeric hyperbranched macromolecules composed of repetitive sequences of monomers starting from a multifunctional core. This particular dendritic structure branching result in a semi-globular to globular well define structure with a low polydispersity compared to linear polymer.

Since the nineties, the field has developed with an exponential number of publications indifferent application fields (materials, catalysis, biotechnology and nanomedecine) (Astruc, Boisselier *et al*. 2010).

3.1.2- General structure

Dendrimers are composed of three main domains: i) the central core; ii) the branches formed with monomers repetition attached on a unit junction point; iii) the terminal functional groups at the dendrimer periphery wich will play a key role in physicochemical properties (Caminade, Laurent *et al*. 2005). (Figure 3.2).

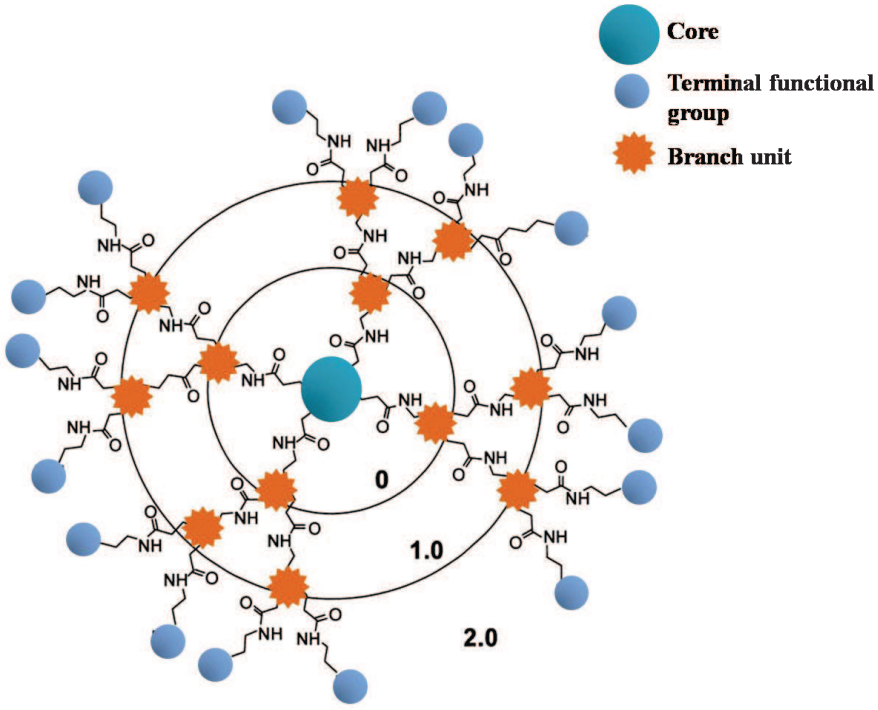

Figure 3.2. Scheme of a second generation PAMAM dendrimer structure.

The series of concentric monomer layers attached on the unit junction point define a "generation" and allows the well-defined dendrimer structure with radial geometry.

The core is often mentioned as G0 dendrimer. At each repeated unit, the generation increase to give a G1, G2 dendrimer (Figure 3.2).

The particular growth of the dendrimer result in the presence of internal cavities that can be exploited for encapsulation of small molecules to form "dendritic box"(Jansen, de Brabander-van den Berg *et al*. 1994).

Several families of dendrimers have been developed and the third most studied structure for biological/biomedical applications are depicted on the Figure 3.3: polyaminoamide (PAMAM, commercially available, Starbust™), polypropylenemine (PPI, also called DAB commercially available Astramol®) and PEG-polyester dendron a dendritic hybrid, especially attractive for drug delivery applications (Ihre, Padilla De Jesus *et al.* 2002) .

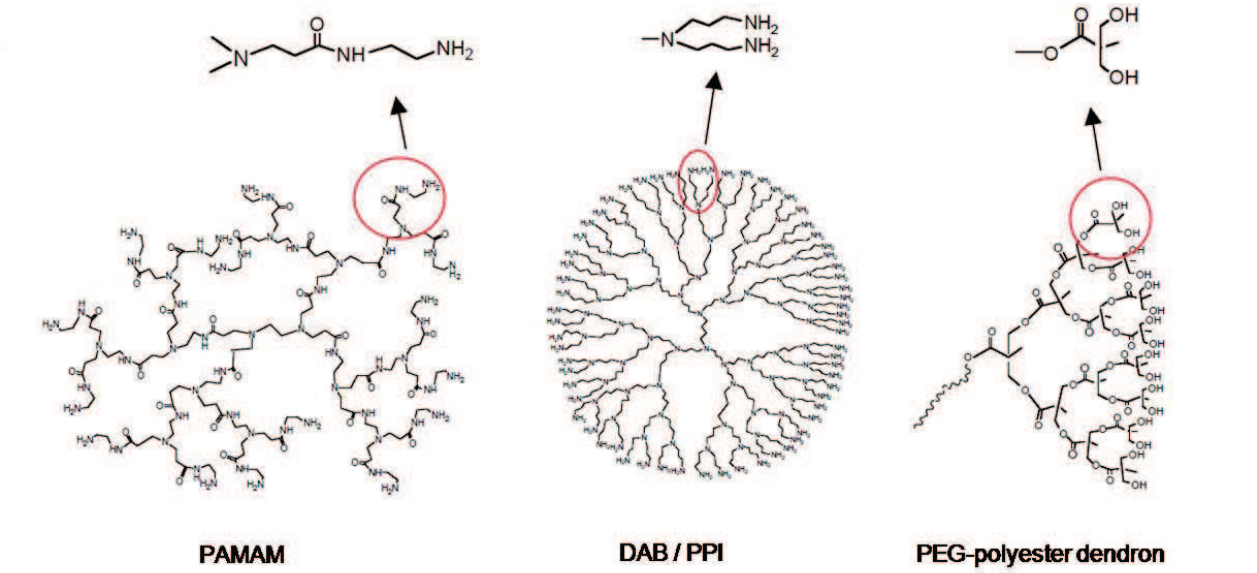

Figure 3.3. Three main families of dendrimers used for biological applications: PAMAM (polyaminoamide), DAB (diaminobutane) or PPI (polypropylenemine), PEG-polyester dendron. Adapted from (Duncan and Izzo 2005)

The present work will focus only on PAMAM family which was the first complete dendrimer family to be synthetized, characterized and commercialized. This is also the most common structure used for biological applications and we have used this family of dendrimer for work presented here. Next paragraphs will described a non exhaustive state of the art on PAMAM dendrimer and their biological applications.

3.1.3- PAMAM dendrimers in biology

3.1.3.1-PAMAM dendrimers as artificial proteins

Because of the globular structure and biomimetic properties, PAMAM dendrimers are often compared to artificial proteins (Weyermann, Gisselbrecht *et al.* 1999; Hecht and Frechet 2001; Svenson and Tomalia 2005). Furthermore, sizes of PAMAM can be compared with those of proteins. (Figure 3.4).

For example, insulin, cytochrome C and hemoglobin are in the same range of size than PAMAM dendrimers of generations 3, 4 and 5 respectively.

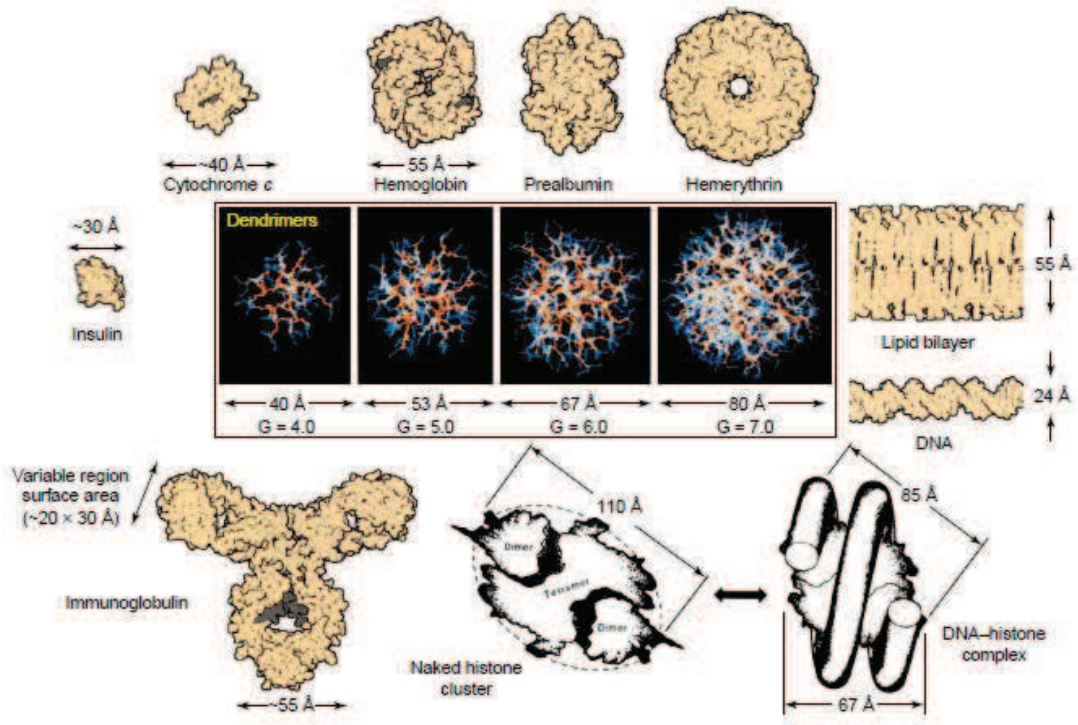

Figure 3.4. Comparison beween PAMAM dendrimer and proteins, lipid-bilayer membrane, DNA to illustrate the mimicry between dendrimer and proteins size.Adapted from (Esfand and Tomalia 2001)

Despite their similarities, PAMAM dendrimers and globular proteins have fundamental differences. Proteins possess tertiary and quaternary structures resulting from complex folding of sequenced linear structures. They are highly sensitive to denaturing conditions such as temperature, pH, solvent etc. The structure of folded proteins is highly dense with an unpredictable heterogeneous surface motif (Esfand and Tomalia 2001).

In contrast, dendrimers are robust, less flexible due to the covalent bounds, with an homogeneous surface.

Due to their properties and the possibility to easily diversified the structure of dendrimers, this family of macromolecule have been used in numerous biological applications.

3.1.3.2-Toxicity and biocompatibility

Prior using a new compound for biomedical applications, it has to be tested as being non-toxic, non-immunogen (for vaccine), able to cross relevant biological barriers (such as blood vessels, cellular membranes), possess long enough in blood retention time to generate its activity. Its metabolization and kidney elimination have also to be evaluated.

The toxicity of dendrimers seems to be directly correlated with the generation of dendrimers and consequently to the positive charges at their surfaces (El-Sayed, Ginski *et al.* 2002).

Cationic PAMAM dendrimers have shown some level of toxicity *in vitro* (Duncan and Izzo 2005). They induced hemolysis (Malik, Wiwattanapatapee *et al*. 2000) by destabilization of cellular membrane due to electrostatic interactions between negatively charged cellular membrane and positively charged dendrimer surface.

Anionic and PEGylated dendrimers showed lower cytotoxicity than the corresponding PAMAM-NH_2. Modification of the surface of PAMAM dendrimers with biocompatible terminal groups (like PEG) has been demonstrated as efficient for the creation of a less toxic macromolecule.

Nevertheless, even if PAMAM dendrimers appear to be toxic *in cellulo*, Roberts *et al*. have demonstrated that they seem to be non-toxic *in vivo* even when high generations (G5) and high concentrations (10 mg/kg injected) are injected, independent of the nature of surface groups (Roberts, Bhalgat *et al.* 1996).

Malik *et al*., have studied the biodistribution of G3 and G4 ^{125}I-labelled PAMAM dendrimers after intravenous injection to Wistar rats (Malik, Wiwattanapatapee *et al*. 2000). Cationic dendrimers demonstrated a rapid clearance so that only less than 2% of the injected dose are remaining in the blood after 1h. Anionic dendrimers showed longer circulation time (20 to 40% of the injected dose remaining after 1h). In both cases, a high liver accumulation was observed 1h after injection (30 to 90% of the injected dose).

In summary, PAMAM dendrimers are versatile macromolecules and their relevant properties and behavior *in vivo* can be easily adapted through the modification of the surface groups.

3.1.3.1-Biological applications

3.1.3.1.1-PAMAM dendrimer for gene transfer

Amino-terminated PAMAM dendrimer have been reported as non-viral gene transfer agents enhancing the transfection of DNA by endocytosis and transport to the nucleus (Bielinska, Chen *et al*. 1999; Eichman, Bielinska *et al*. 2000). Synthetic vector systems including polylysines, cationic liposomes, cationic polymers and dendrimers have been shown to self-assemble with plasmid DNA expression vectors through electrostatic interactions.

Negatively charged phosphate groups of the nucleic acid interact with primary amino groups on the dendrimer surface.

The number of primary amino surface groups increases with the generation number (i.e. 4 surface groups for G0; 8 for G1, 32 for G3, 128 for G5...). In turn, cationic character of the dendrimer increases with the generation (G5 or above) leading to higher DNA condensation.

The figure 3.5 depicts a schematic representation of dendrimer-oligonucleotide pathway used for gene delivery.

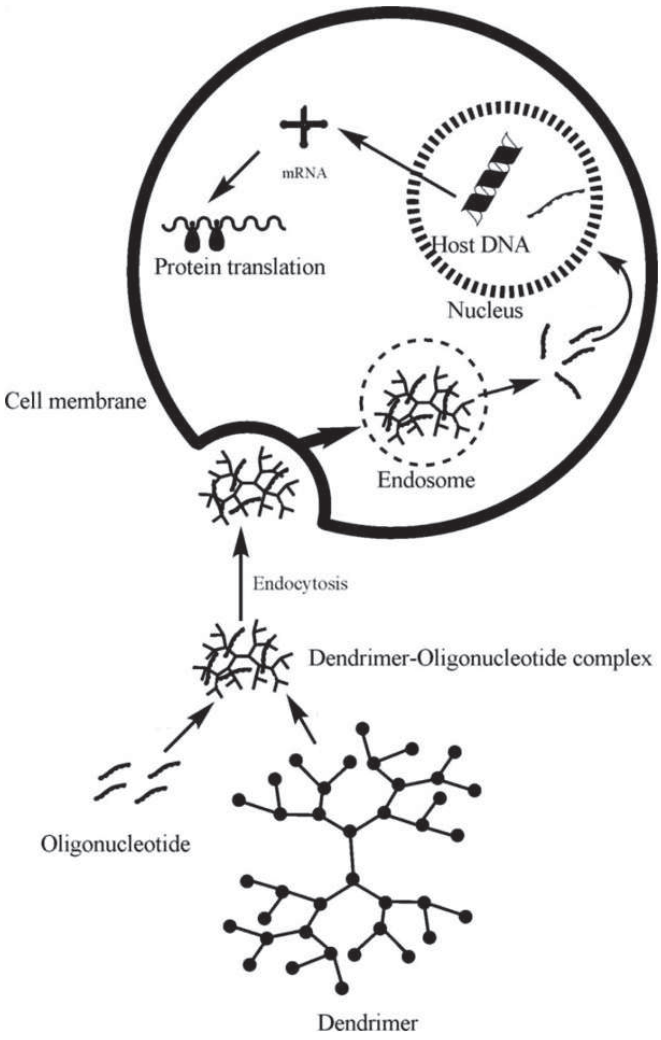

Figure 3.5. Schematic representation of dendrimer-oligonucleotide complex pathway into cell for gene transfer (Tekade, Kumar *et al.* 2009).

Positively charged surface of dendrimer-DNA complex interacts with the negatively charged cell membrane. The complex enters cells via an endocytosis pathway. Cationic polymers have a buffer capacity due to their protonable amine groups (Haensler and Szoka 1993). Indeed, primary amines in the end of the branches of PAMAM dendrimers have a pKa value in a range comprised between 7 and 9 (and comprised between between 3 and 6 inside for the tertiary amines located in the core of the PAMAM). In the presence of the acidic pH of endosomes-lysosome, the protonation of dendrimers surface groups can disturb the organelle membrane and can promote DNA and/or complex release (Kleinman 2000). Molecular and cellular mechanisms of the translocation to the nucleus have not been rationalized at this time.

3.1.3.1.2-PAMAM dendrimer for drug delivery

In addition to DNA, dendrimers have been used to carry a broad variety of small molecules. Two techniques can be considered for dendrimer-based drug delivery: the candidate molecules can be covalently conjugated to the dendrimer surface groups to form a macromolecular prodrug, or the drug can be non-covalently encapsulated in the interior of the dendrimer (Figure 3.6).

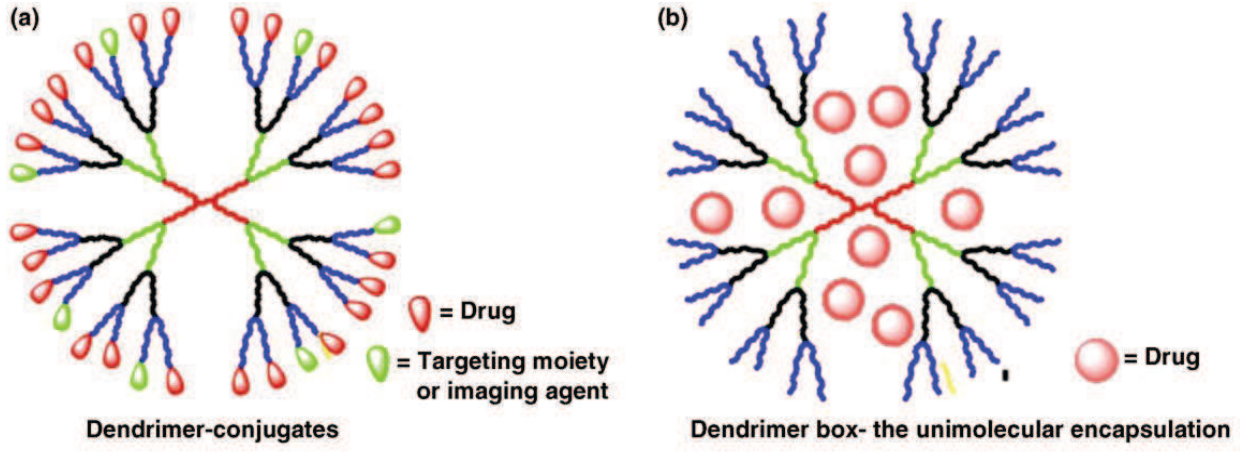

Figure 3.6. Two different strategies for drug delivery with the help of dendrimers. a) conjugation of drug on the dendrimer surface, b) drug encapsulation inside of dendritic cavities. adapted from (Esfand and Tomalia 2001).

Hydrophobic anticancer drugs were encapsulated inside of dendrimers (doxorubicin, methotrexate, cisplatin, paclitaxel) to obtain higher therapeutic effect with the possibility to bring several drug molecules per dendrimer. The major current limitation is a lack of controlled drug release kinetics (as it is lasting during several hours). For this reason, drug-encapsulated dendrimer may be best utilized via intratumoral injection (Svenson and Tomalia 2005).

The release of drugs molecules from PAMAM depends on the generation, on the surface functionality, on the ionic strength, on the pH conditions and solvent.

Techniques used on dendrimer-drug conjugate technique seem to be more advantageous than drug-encapsulation. Indeed, numerous therapeutic molecules can be attached to dendrimer and their release is partially controlled by the nature of the linkages (i.e. pH sensitive linkage between the drug and the dendrimer) (Wolinsky and Grinstaff 2008).

3.1.3.1.3-PAMAM dendrimers for imagery

Dendrimeric imaging agents were essentially developed for MRI and fluorescence imaging with the main advantages to conjugate a high number of small contrast agent molecules per dendrimer.

Gadolinium paramagnetic contrast agents (Gd(III)-DTPA and Gd(III)-DOTA) have been coordinated with dendrimers for contrast enhancement, improved clearance characteristics and potential targeting (Wiener, Brechbiel *et al*. 1994).

Kobayshi and Brechbiel have reported (Figure 3.7) that dendrimer-based MRI agents exhibit size-dependent, organ specific passive targeting. PAMAM dendrimers can also accumulate in solid tumors by enhanced permeability and retention (EPR) effect. Tumor vasculature has excessive leakage, with large pore, compared with healthy vasculature. Nanoscale therapeutic or imaging agents are well known to accumulatein the leaky pores of tumors.

With similar imaging properties, the generation of dendrimer-MRI contrast agents can be adapted to target a specific organ(Greish 2007).

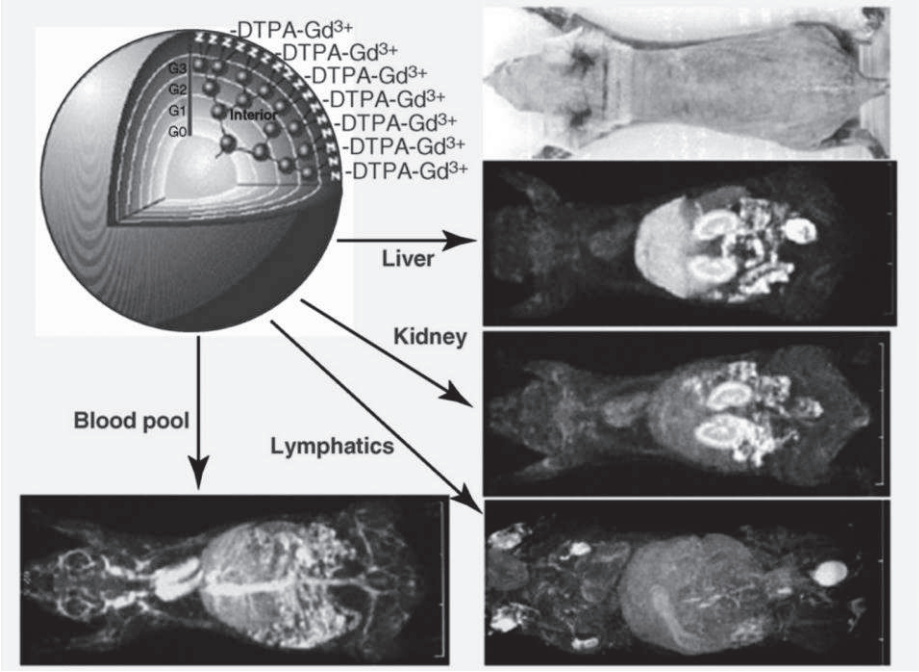

Figure 3.7. Nanosized-selective PAMAM dendrimer-based MRI contrast agents as a function of dendrimer generation and organ specificity. (Kobayashi and Brechbiel 2003)

Several fluorescent PAMAM dendrimers have been described in the literature. Usually dendrimer-drug conjugates are functionalized with an organic dye like FITC, Cy5 or

Rhodamine B (Backer, Gaynutdinov *et al.* 2005; Sarin, Kanevsky *et al.* 2008). Such assemblies are very useful to follow therapeutic and/or targeting efficiency of the probe. However, examples of optical imaging using PAMAM dendrimers are quite scarce (Kitchens, Kolhatkar *et al.* 2006; Saovapakhiran, D'Emanuele *et al.* 2009).

An interesting multimodal dendrimer agent have been reported by Kobayashi *et al.*,,in 2007(Kobayashi, Koyama *et al.* 2007). Radioisotope (^{111}In) and Alexa Fluor (660, 680,700 and 750) dyes have been attached to the generation 2 PAMAM dendrimer to be used as multimodal γ-ray and multicolor optical imaging agents. The figure 3.8 presents results obtained on athymic mice after intracutaneous injection of the different labeled-dendrimers.

.

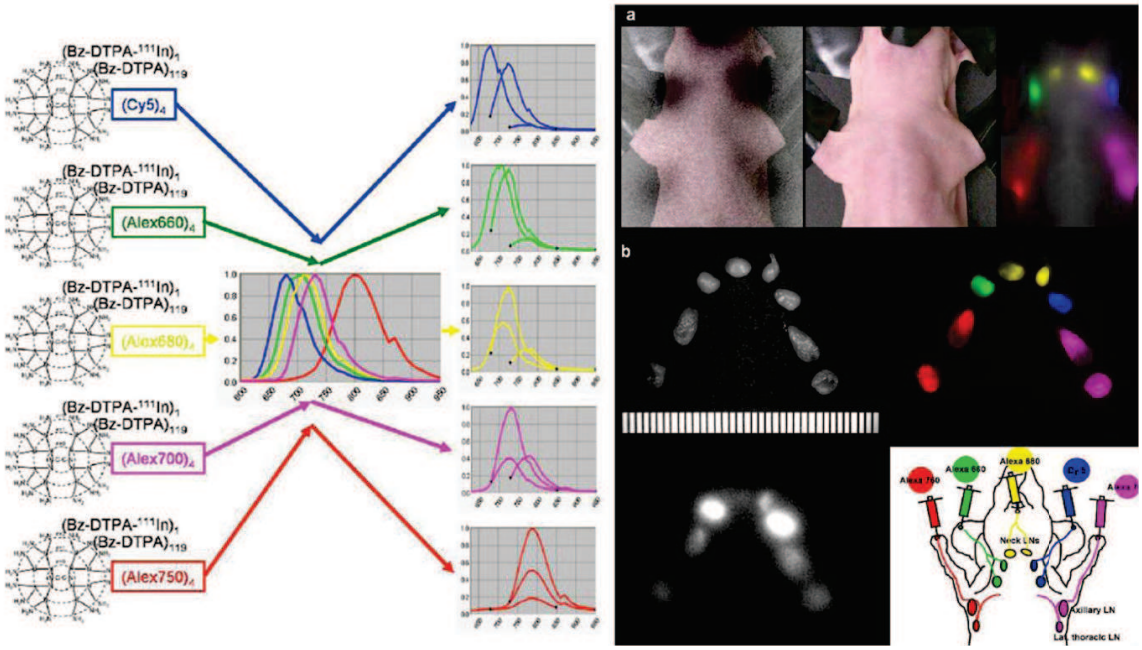

Figure 3.8. Multimodal dendrimer agents for *in vivo* imaging. Left: emission spectra of the 5 different nanoprobes. Right: a) *in vivo* multi-excitation spectral fluorescence after intracutaneous injection; b) *ex vivo* fluorescence and PET images of the corresponding implants. Adapted from (Kobayashi, Koyama *et al.* 2007)

Several dendrimers based on visible and NIR emitting lanthanides were described but no *in vivo* imaging applications have been described so far.

Lanthanide-based-dendrimers were previously reported by our group for *in vivo* tumor optical imaging (Alcala, Kwan *et al.* 2011; Alcala, Shade *et al.* 2011). Generation 3 PAMAM dendrimers were modified by addition of 1,8-napthalimide derivatives groups on the surface

of the 32 dendrimer branches. This allowed the sensitization of 8 Eu^{3+}. The combination of unique spectroscopic properties of lanthanide ions with a large number of chromophores attached to the PAMAM dendrimer allowed to enhance the emission intensity and *in vivo* detection sensitivity.

Other lanthanide-based-dendrimers were described for visible and NIR emission without cellular or animal fluorescence applications (Vögtle 2001; Vicinelli, Ceroni *et al.* 2002; vicinelli 2002; Qiong-Qiong Chen 2006; Branchi, Ceroni *et al.* 2010; Pillai, Ceroni *et al.* 2013)

As a major next step, the present work describes the characterization of new luminescent lanthanides imaging agents derived from generation 3 PAMAM dendrimer for NIR imaging. Their physical and photophysical properties were studied, as well as their *in cellulo* behavior. Preliminary *in vivo* study demonstrated that the developed luminescent dendrimers as promising reporters for NIR *in vivo* imaging.

3.2-Materials and methods

3.2.1-Dendrimer synthesis

The synthesis of G3P-NH_2 and G3P-NB were realized in the group (located in the Department of Chemistry of the University of Pittsburgh) by Dr. Hyounsoo Hu. The details of the synthesis are reported in the appendix 4.

3.2.2-Lanthanide coordination

The lanthanide-dendrimer complexes (Ln-G3P-NH_2 and Ln-G3P-NB, Ln = Eu^{3+}, Yb^{3+}, Nd^{3+}) were synthesized by addition of 8 equivalents of lanthanide nitrate salt (Eu^{3+}, Yb^{3+}, Nd^{3+}) to one equivalent of dendrimer ligand in DMSO. After 7 days under stirring at room temperature, the lanthanide complexes were purified by dialysis in DMSO using the same membrane of corresponding dendrimer (appendix 4).

3.2.3-Spectrofluorimetry measurement

UV/Vis absorption spectra were recorded using a Perkin–Elmer Lambda 9 spectrophotometer. Excitation and emission spectra were measured using a Jobin Yvon–Horiba Fluorolog 3-22 spectrofluorimeter equipped with a xenon lamp 450 W, a R928 Hamamatsu detector for visible emission (sensitivity range 250-850 nm), H10330-45 Hamamatsu detector (sensitivity range 900-1450 nm) or a solid-state DSS-IGA 020L detector (sensitivity range 800-1500 nm) for NIR emission.

Spectra were corrected for variations of the lamp intensity over the spectral range, an excitation and emission monochromators as well as detector responses.

For quantum yields measurements, report to chapter 2.

3.2.4-Scanning electron microscopy

Ln-G3P-NH_2 and Ln-G3P-NB were diluted to 1 µM concentration in ethanol. The samples were coated with carbon prior to analysis by scanning electron microscopy (FEG SEM, Hitachi S4200) in the Center of electron microscopy at the University of Orléans, France.

3.2.5-Luminescence lifetime

Luminescence lifetimes were measured Quantel YG980 laser (355 nm, 3^{rd} harmonic) as the excitation source. Emission was collected at a right angle to the excitation beam, and wavelengths were selected by a Spectral Products CM 110 1/8 meter an iHR320 (Horiba Jobin-Yvon) monochromators. The signal was monitored by H10330-75 photomultiplier tubes and collected on a 500 MHz band pass digital oscilloscope (Tektronix TDS 754C). Three decay curves were collected for each sample and the data were analyzed using OriginPro 8.6 software using exponential fitting modes.

3.2.6-Cell culture

HeLa (Human Epithelial Ovarian Carcinoma), NIH 3T3 (Mouse Embryonic Fibroblast) and 4T1 (Mouse mammary carcinoma) cell lines obtained from ATCC (Molsheim, France) were grown at 37 °C in a 5% CO_2 humidified atmosphere. Every 3-4 days, $5x10^5$ cells were seeded into 25 cm^2 plastic flask.Cells were respectively cultivated in Mimimum Essential Medium

(MEM), in Dulbecco's-MEM (DMEM) and Roswell Park Memorial Institute *medium (*RPMI) supplemented with 10% fetal bovine serum (FBS), 1% penicillin/streptomycin and for HeLa cells 1% L-glutamine, and with 1% of a 100x non-essential amino acid solution. The presence of mycoplasma was checked using "MycoAlert Detection kit" (Lonza) and only certified mycoplasma-free cells were used for experiments.

3.2.7-cytotoxicity evaluation

For the cytotoxicity test, 1.10^4 cells (HeLa, NIH 3T3 or 4T1) per well were seeded in a 96 wells microplate. After 24h of cell attachment, the cells were treated with increasing concentrations of dendrimers diluted for 24h at 37°C. The cytotoxicity was evaluated with the Alamar Blue assay (Invitrogen, Courtaboeuf, France). Alamar Blue was added to the medium (10% v/v) and its fluorescence (excitation 530 nm; emission 590 nm) was measured after 4h at 37°C with a microplate reader (Victor 3V, Perkin-Elmer, Courtaboeuf, France). This assay compares the fluorescence of untreated cells with the fluorescence of cells after incubation with dendrimers.

3.2.8-Visible and near-infrared microscopy

HeLa cells were incubated in 8 well Lab Tek Chamber coverglass (Nunc, Dutsher S.A., Brumath, France) with 1µM of Yb/Nd-G3P-NB and Yb/Nd-G3P-NH_2. After 24h at 37°C, the cell culture medium was changed and replaced by Opti-MEM medium exempt of phenol red. NIR epifluorescence microscopy was realized with an Axio Observer Z1 fluorescence inverted microscope (Zeiss, Le Pecq, France) equipped with an EMCCD Evolve 512 photometric camera linked to a computer driving the acquisition software Axiovision (Zeiss). The inverted microscope was equipped with a Zeiss immersion Plan Apochromat 63x (Numerical Aperture (NA)=1.4) objective. The Zeiss HXP-120 light source (metal halide) was used as excitation system and combined to a UV cube filter unit as follows: λ_{ex} = 470/40 nm, λ_{em} = 525/50 nm to observe 1,8 naphthalimide emission with 10 ms of acquisition time. And λ_{ex} = 414/60 nm, λ_{em} = Long Pass filter at 805 nm to observe Yb^{3+} and Nd^{3+} NIR emission with 500 ms of acquisition time.

3.2.9-Flow cytometry

$1.5x10^5$ cells were seeded in a 24 wells microplate. After 24h of cell attachment, cells were incubated with increasing concentrations of Opti-MEM diluted dendrimers (from 0.5 to 2µM). After 24h of incubation at 37°C, cells were washed, trypsinated, centrifugated during 10 minutes (1500 rpm at 4°C). The pellet were re-suspended in 400µL of PBS and their fluorescence was detected using a FACS-LSR flow cytometer (BD Biosciences) using an excitation laser at 488 nm and emission filter 530/28 nm and analyzed using CellQuest software (BD Biosciences).

Concerning the endocytosis pathway, cells were pre-incubated for 30 minutes at 37°C with inhibitor of endocytosis: wortmannin 100nM (macropynocytosis pathway), sucrose 100nM (clathrin dependent pathway) or fillipin III (caveolae pathway). After that, cells were incubated for 24h at 37°C with 1µM of Eu-G3P-NB before FACs analysis.

3.2.10-Confocal microscopy

HeLa cells were seeded in 4-well Lab Tek Chamber coverglass. After 24h of attachment, cells were incubated with 1µM of Eu^{3+} complexed dendrimers and were observed in real-time with confocal laser scanning microscopy (CLSM). CLSM experiments were performed using a Zeiss Axiovert 200M microscope coupled with a Zeiss LSM 510 scanning device (Carl Zeiss Co. Ltd., Iena, Germany). The inverted microscope was equipped with a immersion Plan-Apochromat 63× objective (N A = 1.4). Images were recorded with Carl Zeiss's LSM Image Browser software. The 1,8 naphthalimide chromophore was excited with a 488 nm laser and the emission wavelength was selected using the Meta mode between 499 and 550 nm.

3.2.11-Immunocytochemistry assay

The cellular localization of Eu-G3P-NB dendrimer was studied by immunocytochemistry.

HeLa cells were seeded in a 8-well Lab Tek Chamber coverglass. After 24h of incubation with 1µM of Eu-G3P-NB, cells were incubated with different specific organelle label-dyes. The mitochondria were labeled after incubation with 0.5µM of Mitotracker-Red® (Invitrogen, Saint Aubin, France) during 20 min at 37°C.The endoplasmic reticulum was labeled after 30

minutes of incubation with 1µM of ER Red Tracker® (Invitrogen). Lysosomes were labeled after 2h of incubation with 1µM of LysoTracker-Red®. After the different labeling, cells were washed with PBS and fixed with PFA (paraformaldehyde) 4% .

Golgi apparatus was labeled after fixation with PFA 4%. The cells were permeabilized with PBS-Triton X-100 1% during 15 minutes at room temperature. After washing, cells were incubated during 2h in the presence of 1µg/mL of anti Golgin_97 Antibody (Invitrogen). After washing with PBS-BSA 1%, the cells were incubated with 100 µg/mL of Alexa Fluor 568 antimouse antibody during 2h.

The different labeled cells were observed by confocal microscopy with the follow parameters: Mitotracker-Red®: excitation with 543 nm laser - λ_{em}: 563-628 nm, Anti Golgin97/AlexaFluor 568 excitation with 543 nm laser - λ_{em}: 555-660 nm, ER Red Tracker® excitation with 543 nm laser - λ_{em}: 553-660 nm, Lysotracker-Red® excitation with 543 nm laser - λ_{em}: 553-628 nm.

3.2.12-*In vivo* dendrimer-matrigel plug assay

8 to 10-weeks old females Balb/C mice (Charles River Laboratories, L'Arbresle, France) were used for the studies. 4T1 cells were incubated during 24h with 1µM of Yb-G3P-NB. After washing, $1x10^6$ labels cells were added in 200 µL of Matrigel™ diluted 2 times in saline and subcutaneously injected on anesthetized shaved mice. 24h after injection, the mice were observed with fluorescence macroscopy. A Nikon AZ100 Multizoom equipped with an EMCCD Evolve 512 photometric camera and driven by the NIS Element BR software was chosen. Acquisitions were done through the skinof sacrificed mice. The objectives was an Nikon AZ 100 Apo 0.5x (NA=0.05). For fluorescence imaging, the epifluorescence illumination system used an Intensilight HGFIE HG, pre-centered fiber illuminator (130 W mercurylamp). Fluorescence channels were selected with the help of filter (Semrock, Rochester, New York, USA) combinations for chromophore emission: λ_{ex} 482/35 nm, λ_{em} 536/40 nm; for Yb^{3+} emission: λ_{ex} 417/60 nm, λ_{em} LP805 nm. Acquisition times were respectively of 100 ms and 1 s.

3.2.13-*In vivo* toxicity

7 weeks old females Balb/C mice (Charles Rivers, France) were used for the toxicity studies. Mice were divided into 3 groups: 3 mice for control which received DMSO diluted in saline

solution, 5 mice for short term toxicity and 5 mice for the long term analysis. The short term group received one IV (intravenous injection) injection of 100 µL at 10 µM of Yb-G3P-NB diluted in saline. The long term group received 3 IV injections (1 per week) of 100 µL at 10 µM of Yb-G3P-NB. Mice were weighed daily and their behavior was observed. After one month the mice were sacrificed by inhalation of CO_2 and lung, liver and kidney were harvested and fixed in PFA 4% at 4°C. Histological examinations were performed at Novaxia (St Laurent-Nouan - France).

Histological sections, mounted on glass slides, were submitted to the study pathologist. The sections, cut at approximately 4 microns were stained with hematoxylin and eosin. Each slide was inspected microscopically by a pathologist to search for any evidence of damage such as adhesions, necrosis, cellular infiltration, or hypervascularity.

3.3-Results and discussion

3.3.1-Luminescents dendrimers functionalized with 1,8-naphthalimide derivatives.

3.3.1.1-Ln-G3P-NH_2/NB dendrimers structure

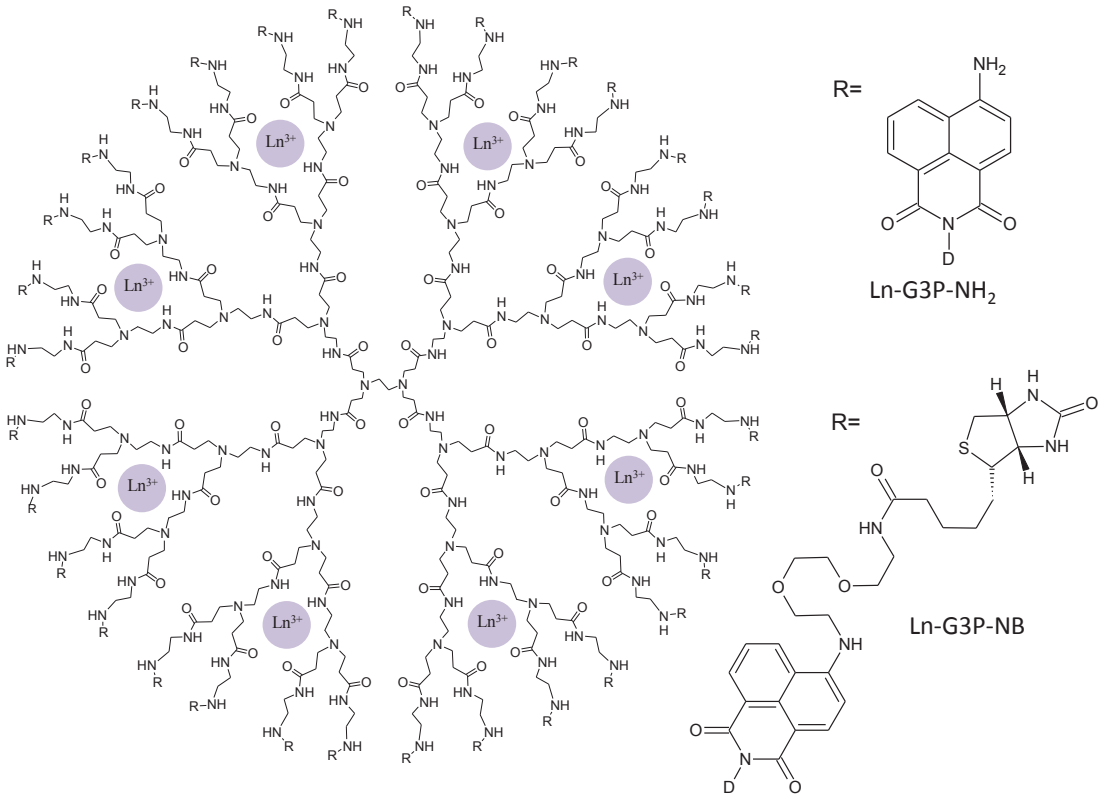

Figure 3.9. Structures of the two generation-3 dendrimer complexes discussed in this chapter

Two types of generation 3 PAMAM dendrimers functionalized with derivatives of 1,8-napthalimide chromophore at the periphery were studied here: G3P-NH_2 (4-amino-1,8-naphthalimide) and G3P-NB (biotinylated 4-amino-1,8-naphthalimide). In both cases, all 32 terminal amino groups of the generation 3 PAMAM were coupled with 1,8-naphthalimide derivatives, thus G3P-NH_2 and G3P-NB contain 32 chromophores (Figure 3.9). The biotinylation of the dendrimer when going from G3P- NH_2 to G3P-NB allowed to improve water solubility and also to anticipate the vectorisation through biotin-streptavidin-antibody coordination.

It has been demonstrated that generation 3 PAMAM dendrimers are able to incorporate 8 lanthanide cations inside their branches (Cross, Lauz *et al*. 2004) . To obtain lanthanide-based dendrimers, Ln-G3P-NH_2 and Ln-G3P-NB (Ln = Eu^{3+}, Nd^{3+} and Yb^{3+}), the corresponding dendrimer was treated with 8 equivalents of lanthanide nitrate followed by dialysis purification. Consequently, due to the specific structure of the synthesized dendrimers it is possible to combine within one molecule 8 lanthanide cations and 32 chromophoric groups which can act as antenna.

3.3.1.2-Characterization

3.3.1.2.1- Photophysical properties

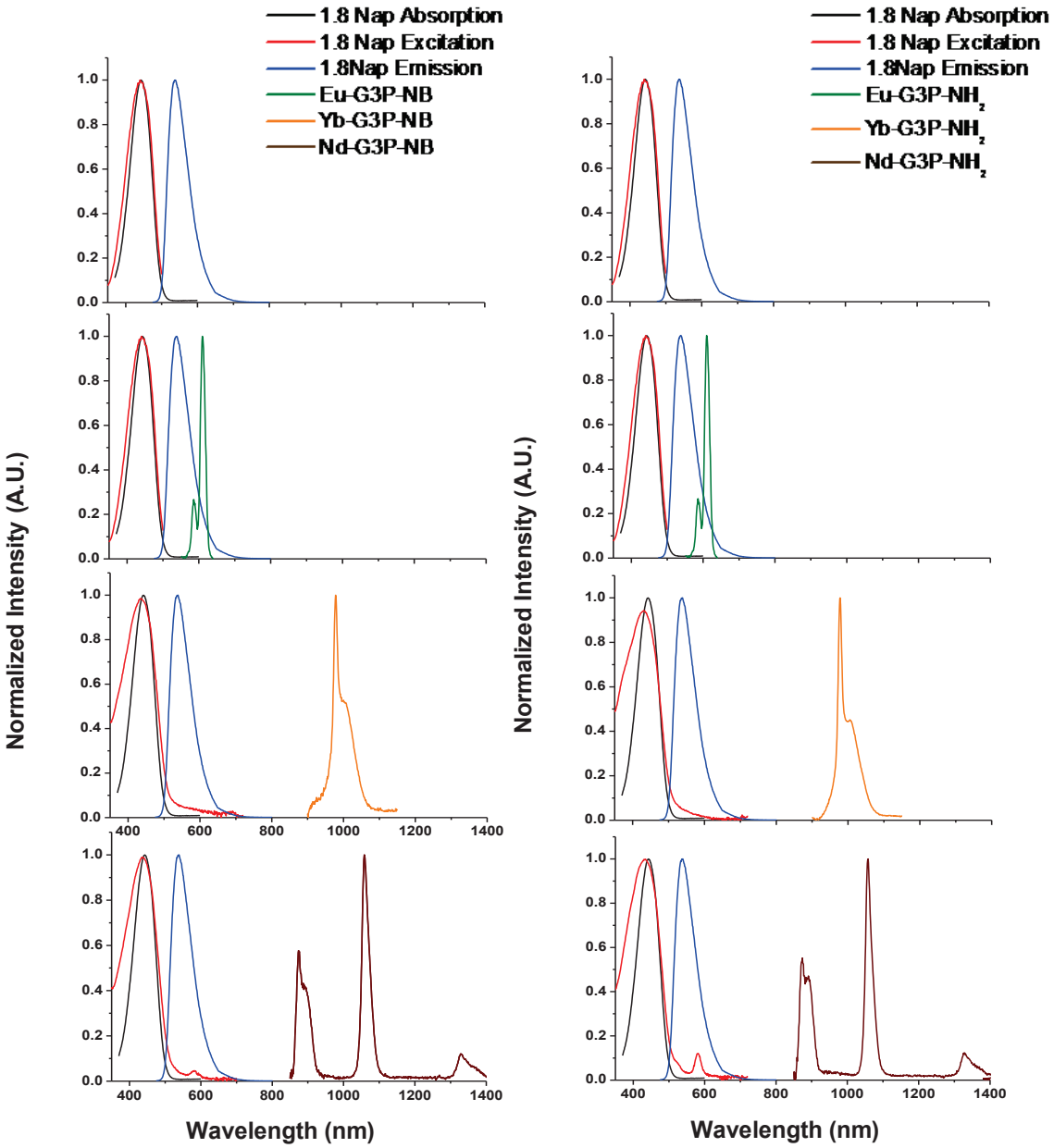

Figure 3.10. Absorption, excitation (λ_{em} = 540 nm for 1,8-naphthalimide-centered emission in the visible, for lanthanide-centered emission in the NIR λ_{em} = 980 nm for Ln = Yb and λ_{em} = 1060 nm for Ln = Nd) and emission spectra (λ_{ex} = 440 nm) of Ln-G3P-NB (left) and Ln-G3P-NH_2 (right). Lanthanide-centered emission spectra of Ln-G3P-NB and Ln-G3P-NH_2 (Ln = Yb, Nd) are given after substraction of the residual chromophore emission (Appendix 6).

Absorption spectra of G3P-NH_2/Ln-G3P-NH_2 and G3P-NB/Ln-G3P-NB are similar and exhibit intense bands (ε ~$3.7 \cdot 10^5$ M^{-1} cm^{-1}) in the range of 350-510 nm centered at 440 nm due to $\pi^* \leftarrow \pi$ transitions within 1,8-naphthalimide moieties. Upon excitation at 440 nm, all dendrimers exhibit broad-band green emission centered at 540 nm (Figure 3.10), the tail of this band is extending further in the NIR range and a weak emission could be detected up to 1300 nm (appendix 6 and 7). In addition to chromophore-centered emission Yb- and Nd-containing dendrimers exhibit characteristic sharp-band emission in the NIR range due to $^2F_{5/2} \rightarrow {}^2F_{7/2}$ and $^2F_{3/2} \rightarrow {}^4I_J$($J$ = 9/2-13/2) transitions, respectively. The overlap of the absorption and the excitation spectra of Yb-G3P-NB/NH_2 and Nd-G3P-NB/NH_2 dendrimers while monitoring lanthanide emission at 980 and 1060 nm, respectively, indicates that sensitization of lanthanides is occurring through the 1,8-naphthalimide chromophores. In case of Eu-G3P-NB and Eu-G3P-NH_2, due to an overlap of the chromophore and Eu-centered emission characteristic sharp bands centered at 614 nm could be detected only upon application of a delay of 50 μs after flash. Thus, depending on the nature of the lanthanide ion incorporated inside the PAMAM dendrimer one can tune emission from visible to NIR range.

Table 3.1. Quantum yields (λ_{ex}:440 nm) and luminescence lifetimes (λ_{ex}:355 nm) of Ln-G3P-NH_2 and Ln-G3P-NB dendrimer in DMSO (15 μM, 298 K).[a]

Dendrimer	Quantum yield (%)[b]	Lifetime (μs)[c]
Eu-G3P-NB	36(1)	730(20)
Yb-G3P-NB	$0.76(1)\times10^{-3}$	6.43(1)
Nd-G3P-NB	$0.25(1)\times10^{-3}$	1.42(2)
Eu-G3P-NH_2	16(1)	560(20)
Yb-G3P-NH_2	$3.2(1)\times10^{-3}$	6.98(4)
Nd-G3P-NH_2	$1.7(1)\times10^{-3}$	1.35(1)

[a] 2σ values between parentheses. [b]Quantum yields of lanthanide-centered emission in the NIR range in case of Yb- and Nd-containing dendrimers, and chromophore-centered emission in the visible for Eu-G3P-NB/NH_2. [c]

Quantum yields and luminescence lifetimes were recorded in DMSO for all dendrimers under study (Table 3.1). Quantum yields values for the Eu^{3+} dendrimers complexes have been obtained by adding the 1,8-naphthalimide and Eu^{3+} emissions. Eu-G3P-NH_2 has a quantum yield of 16% and Eu-G3P-NB a value of 36%.

The quantum yields recorded for NIR emitting lanthanide-based dendrimers are relatively small (of the order of 10^{-3}%) in comparison with the best luminescent compounds (Zhang, Badger *et al*. 2005; Comby, Imbert *et al.* 2006; Eliseeva and Bunzli 2010).

However, the strategy to maximize the number of chromophores and thus luminescence efficiency defined as $\varepsilon \times Q$ (in the order of 370), and lanthanide cations in the dendrimer to increase detection sensitivity is expected to reduce this limitation in this NIR range.

Luminescence decay curves (Table 3.1) were best fitted by a mono-exponential function, indicating that 8 lanthanide cations inside dendrimer branches are in the same coordination environments. Moreover, similarities of luminescence lifetime values for Ln-G3P-NH_2 and Ln-G3P-NB indicate that coordination environments provided by generation 3 PAMAM dendrimers for a given lanthanide cation is independent on the nature of the periphery group.

3.3.1.22- Size measurements

Dendrimer complex sizes were evaluated by SEM. The size of Ln-G3P-NH_2 is comprised between 30 and 35 nm in diameter (Figure 3.11). The size of Ln-G3P-NB, is larger, being comprised bewteen 45 and 55 nm. Classical generation-3 of PAMAM dendrimer are described to have a size of 3 nm of diameter (Svenson and Tomalia 2005). However, 32 chromophoric groups have been added to the PAMAM structure as well as 32 biotin for the Ln-G3P-NB groups. In respect to size, the dendrimer presented here can be compared with higher generation PAMAM dendrimers.

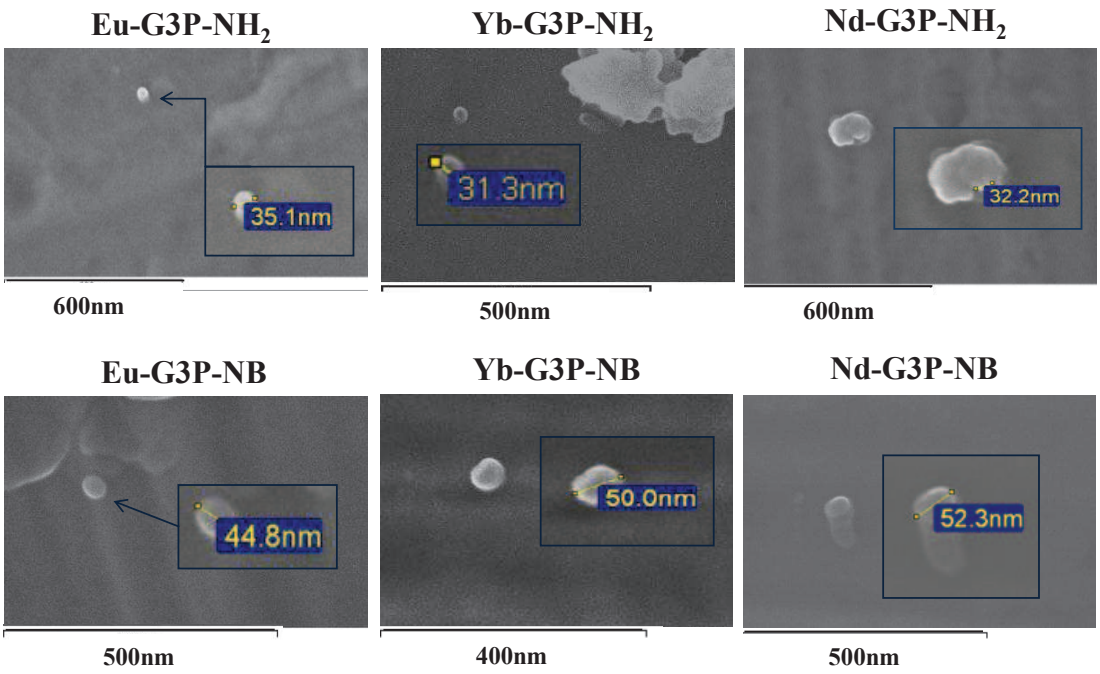

Figure 3.11. SEM microscopy images of Ln-G3P-NH_2 (top) and Ln-G3P-NB (bottom) dendrimer complexes formed with three different lanthanide cations.

3.3.1.3-Cellular studies

3.3.1.3.1-Cytoxicity

Free lanthanide cations can be toxic for organism by accumulation in bones, liver and spleen (being uptaken by phagocytic cells).

The toxicity induced by lanthanide and earth rare element is in general due to their chemical form which is very close to the Ca^{2+} form. Earth rare elements act as Ca^{2+} antagonist *in vitro* and can replace Ca^{2+} from cells or biomolecules *in vivo*. (Hirano and Suzuki 1996)

For these reasons, it is important to ensure that lanthanides ions coordinated in the luminescent macromolecules can not be released as free metal during the time of the experiment and will not induce toxicity by competition with Ca^{2+}. More recently, some contrast agents used for MRI have been found as being responsible for Nephrogenic Systemic Fibrosis (NSF).

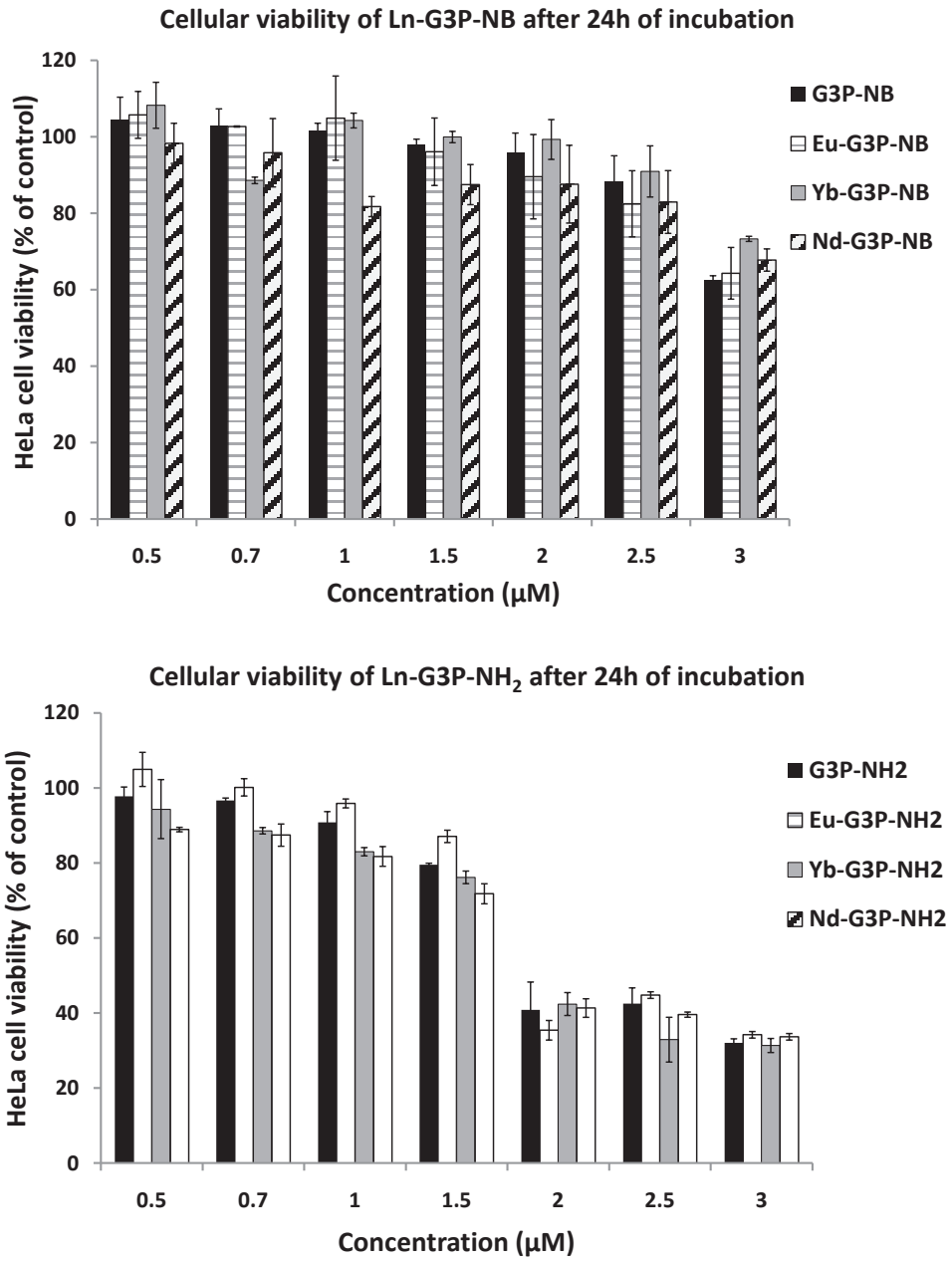

Figure 3.12. Results of the evaluation of dendrimerscytotoxicity measured on lanthanide complexes formed with Ln-G3P-NB (top) and Ln-G3P-NH_2 (bottom) ligands on HeLa cells after 24h of incubation.

The cytotoxicity of dendrimers was evaluated with the help of the Alamar Blue assay. The first indication given by the figure 3.12 an importance of sufficient water solubility has been demonstrated for dendrimer complexes is that the complexes formed with Ln-G3P-NB are less cytotoxic than those formed with Ln-G3P-NH_2 up to concentration of 1.5 µM. This result

can be explained by the lower solubility and the tendency of Ln- G3P-NH_2 to aggregate in aqueous solution (as described in the part 3.3.1.3.3.2- Cellular localization).

Results depicted in the figure 3.12 indicate also that there is no influence of the nature of the complexed lanthanide on dendrimer toxicity which is not surprising as all lanthanide cations have similar chemical reactivities. Cytotoxicities of the different studied dendrimers are independent on the nature of the lanthanide cations.

The low cytotoxicity values recorded in this study suggest that there is no significant liberation of free lanthanide during the incubation time. The dendrimer complexes are relatively inert system. The kinetic of complexed formation is relatively long (one week under stirring at room temperature) and previous experiments have shown that the kinetic of complexes dissociation has similar duration (appendix 8). The lanthanide cations stay coordinated within the dendrimer branches and will not dissociate in the cell culture media during the 24h of incubation time. They do not induce a strong cytotoxicity on HeLa cells.

Dendrimers can be used at a concentration of 1 µM on cells for 24h of incubation which is a sufficient amount to observe a good NIR emission signal in optical imaging without triggering any significant cytotoxicity.

3.3.1.3.2-Visible and NIR microscopy

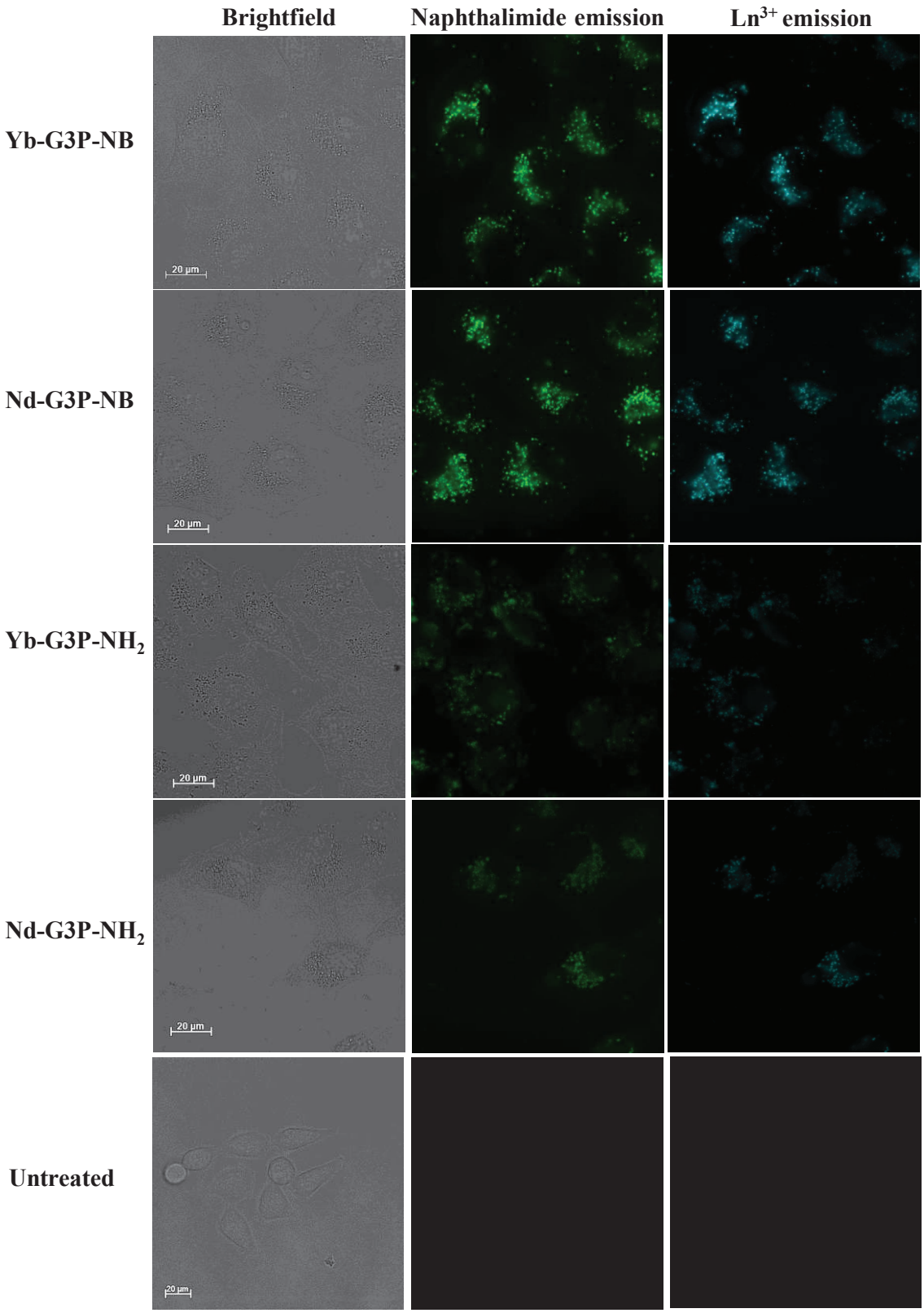

Figure 3.13. Visible and near-infrared epifluorescence microscopy images of HeLa cells after 24h of incubation with 1 µM of Yb/Nb-G3P-NB or Yb/Nd-G3P-NH_2. (left) Brightfield. (green) chromophore

emission (λ_{ex}: 470/40 nm - λ_{em}: 525/50 nm - 10 ms acquisition time). (blue) Yb^{3+} or Nd^{3+} near-infrared emission λ_{ex}: 417/60 nm - λ_{em}: LP805 nm - 500 ms acquisition time).

Visible and near-infrared epifluorescence microscopy experiments were realized on Hela cells after 24h of incubation with Yb/Nd-G3P-NH_2 and Yb/Nd-G3P-NB (Figure 3.13).

Ln-G3P-NB provides a strong emission signal which allows to obtain visible and near-infrared microscopy images with short acquisition time: 10 ms for the naphthalimide emission and 500 ms for corresponding Ln^{3+} emission (Nd^{3+} and Yb^{3+}). For the same acquisition time, the emitted signal arising from the naphthalimide groups or from the lanthanide cations in the Ln-G3P-NH_2 complexes formed with all the three lanthanide cations (Eu^{3+}, Nd^{3+} and Yb^{3+}) were systematically lower in intensity suggesting that amino dendrimer complexes are less uptaken by cells than the corresponding biotin one.

Even if the concentration of Ln-G3P-NH_2 dendrimers complexes is lower in cells, the emission signal and detection sensitivity can by improved by increasing the acquisition time. However, it is important to know that when the visible signal is monitored, the autofluorescence signal will also increase and that the obtain images with longer exposition time will likely not provide a better information. In the near-infrared domain, the autofluorescence background is minimal or absent and the signal/noise ratio will be enhanced for improved detection sensitivity.

The excitation wavelength used for the chromophore is 488 nm, which can generate some damage to cells if long and repeated acquisitions are used.

In view of these results, both systems are promising candidates for microscopy imaging experiments. At equal concentration and incubation time, the biotin dendrimer will provide more photons and therefore higher detection sensitivity.

3.3.1.3.3- Cellular uptake

Due to instrumental limitations, it was not possible to detect Yb^{3+} or Nd^{3+} near-infrared emission signal for cellular uptake evaluation. The commercially available flow cytometers and confocal microscopes that we have access are not equipped for the signal detection of luminescent species possessing an emission wavelength larger than 800 nm. For this reason, all confocal microscopy cellular studies were done with Eu^{3+} complexed dendrimer (detection a combination of 4-amino-1,8-naphthalimide and Eu^{3+} emission signal). For the cytometry

analyses, the chromophore of the dendrimer complexes was detected between 502 and 558 nm.

3.3.1.3.3.1- Flow cytometry

The cellular uptake was quantified by flow cytometry. HeLa cells were incubated with different concentration of Eu/Nd-G3P-NB and Eu/Nd-G3P-NH_2 during 24h before analysis by flow cytometry.

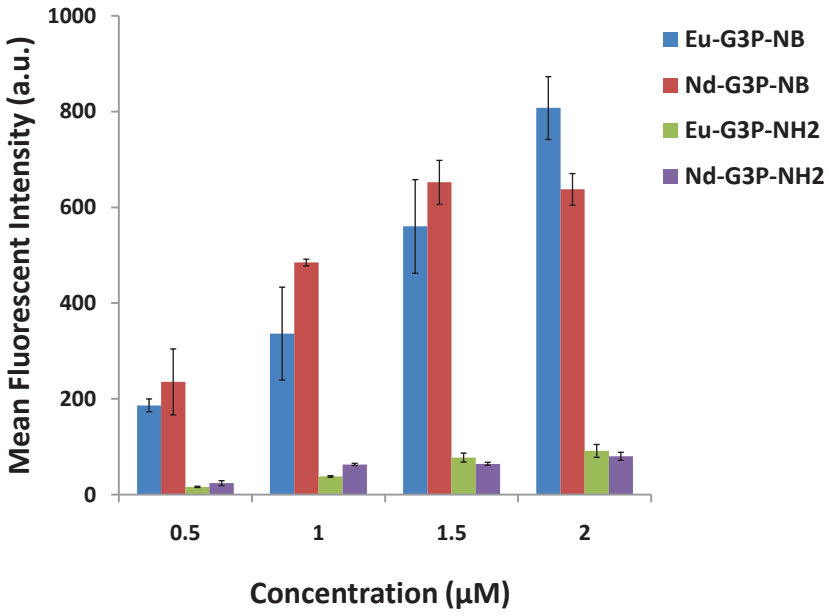

Figure 3.14. Results of the evaluation of cellular uptake by flow cytometry. HeLa cells were analyzed after 24h of incubation with increasing concentration of Eu/Nd-G3P-NB and Eu/Nd-G3P-NH_2. λ_{ex}: 488 nm- λ_{em}: 530/56 nm.

As previously observed from the cytotoxicity experiments, there is no significant influence of the nature of complexed lanthanide on cellular uptake. (Figure 3.14).

Flow cytometry quantification allowed to determine that biotin dendrimer complexes are uptaken by a factor comprised between 7 and 8 more than amino dendrimer complexes.

These results explain the lower intensities of the emission signal for the amino dendrimer complexes in the NIR epifluorescence microscopy experiments.

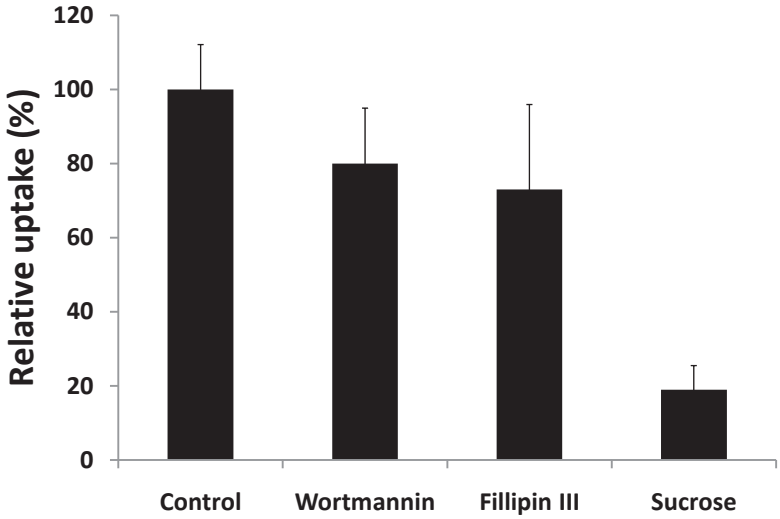

Figure 3.15. Relative cellular uptake of Eu-G3P-NB 1 µM after treatment with different concentrations of endocytosis inhibitors: wortmannin 100nM, fillipin1µg/ml and sucrose 100nM.

Endocytosis pathways were studied after treatment of cells with different inhibitors. The wortmannin (which blocks PI-3 kinase and by this way macropinocytosis), fillipin (which perturbs caveolae and sequesters choloesterol) and sucrose which inhibits clathrin mediated endocytosis) (Wang, Rothberg *et al*. 1993; Pless and Wellner 1996; Orlandi and Fishman 1998). The relative uptake of Eu-G3P-NB dendrimer by HeLa cells after such treatment is reported in the figure 3.15. The cellular uptake is clearly decreased after inhibition by clathrin mediated endocytosis indicating that dendrimer are mostly uptaken by this pathway.

3.3.1.3.3.2- Cellular localization

In parallel to the flow cytometry measurements, the cellular uptake was evaluated qualitatively with the help of confocal microscopy. HeLa cells were observed after 24h of incubation with 1µM of Eu-G3P-NH_2 and Eu-G3P-NB dendrimers. These experiments indicated a peri-nuclear localization of the dendrimers. (Figure 3.16)

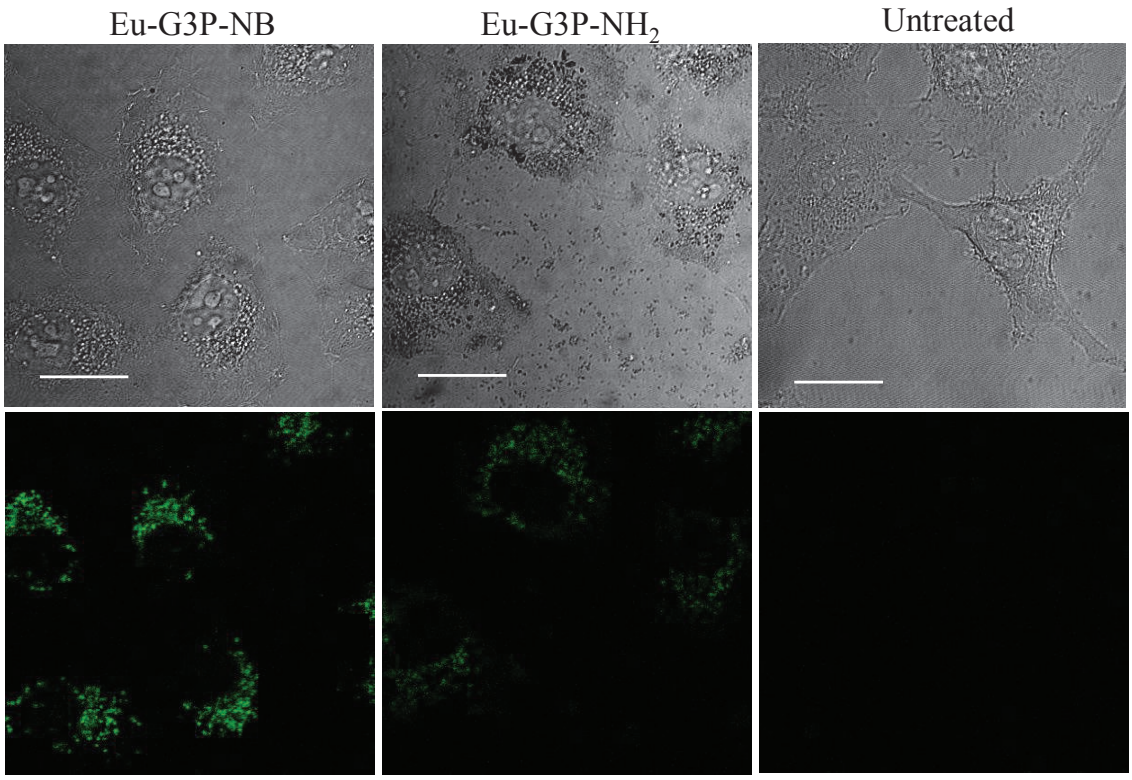

Figure 3.16. Images obtained from confocal microscopy measurements on HeLa cells after 24h of incubation with Eu-G3P-NB and Eu-G3P-NH_2 dendrimers (1 µM). (Left) Eu-G3P-NB, (middle) Eu-G3P-NH_2, (right) and untreated cells. (Top) Brightfield, (bottom) dendrimers fluorescent signal (λ_{ex}: 488 nm - λ_{em}: 499-550 nm). Scale bar: 20 µm.

Confocal microscopy is a third confirmation that Ln-G3P-NH_2 dendrimers are less uptaken by cells than Ln-G3P-NB. We can clearly observe many aggregates of Eu-G3P-NH_2 on the brightfield image. Effectively, Ln-G3P-NH_2 dendrimers are not water soluble enough to permit a good cellular uptake.

Even if the quantity of amino (Ln-G3P-NH_2) and biotin (Ln-G3P-NB) dendrimers is significantly different inside of the cells, the localization remains the same.

Immunocytochemistry on different cellular organelles (Figure 3.17) show a preferential co-localization with lysosomes. Lysosomal localization of PAMAM dendrimers is described in the literature (Saovapakhiran, D'Emanuele *et al.* 2009). The modification of the initial structure of PAMAM dendrimer by attachment of the chromophores and complexation with lanthanide did not change the cellular behavior of dendrimers.

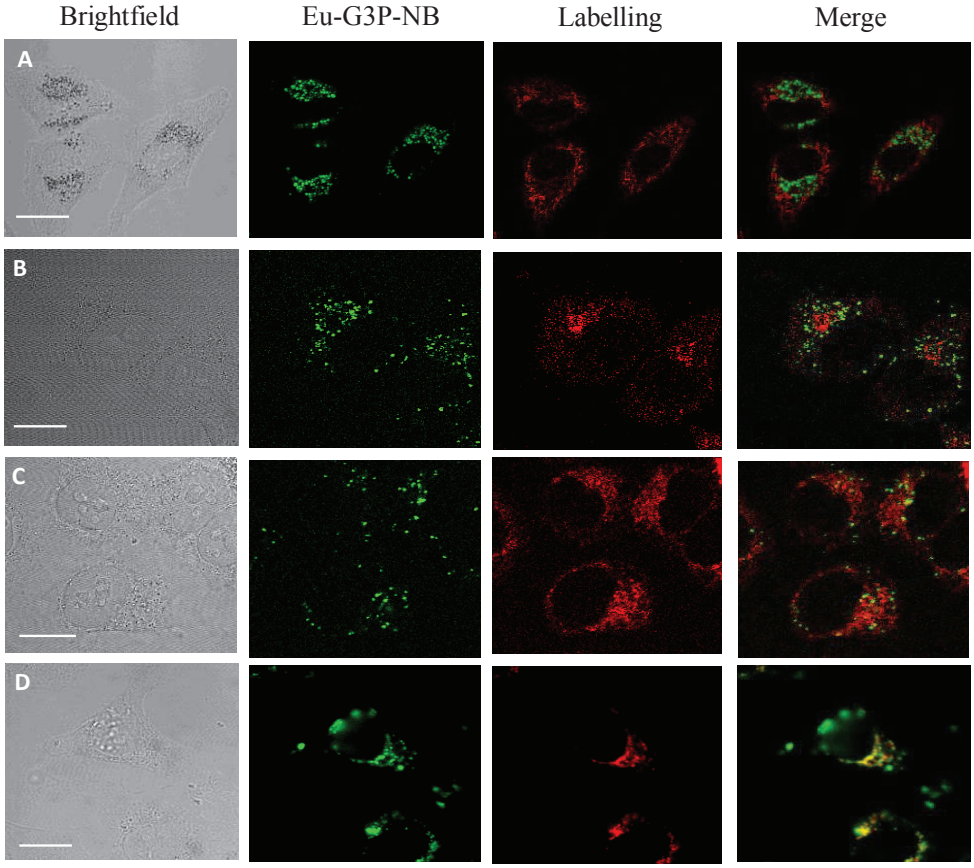

Figure3.17. Immunocytochemistry of HeLa cells after 24h of incubation with Eu-G3P-NB (1 µM). Left column: brightfield. Green: Eu-G3P-NB (λ_{ex}: 488 nm - λ_{em}: 499-531 nm), Red: labels tracker. Right column: merge. (line A) Mitochondria labelling with Mitotracker Red (λ_{ex}: 543 nm - λ_{em}: 563-628nm), (B) Golgi Apparatus labelling with Golgin97/AlexaFluor 568 (λ_{ex}: 543 nm - λ_{em}: 555-660 nm), (C) Endoplasmic Reticulum labelling with ER Red Tracker (λ_{ex}: 543 nm - λ_{em}: 553-660 nm), (D) Lysozome labelling with Lysotracker Red (λ_{ex}: 543 nm - λ_{em}: 553-628 nm). Scale bar: 20 µm.

Acidic pH of lysosomes (between 3.5 and 5) doesn't influence the emission intensity of Eu-G3P-NB (Appendix 5).

3.3.1.4-*In vivo* studies

3.3.1.4.1- Ability of *in vivo* imaging

Cells were labelled by Yb-G3P-NB dendrimer complexes to establish the proof of principle of the NIR luminescent reporters to be used *in vivo*. The excitation wavelength that is used for the excitation of the dendrimer complexes (417/60 nm) is not well optimized to cross important depths of tissues due to their important absorption at these wavelengths. The breast

tumor model (mammary carcinoma) is well adapted for this study because of its subcutaneous localization. To mimic the presence of a tumor, 4T1 cells (which were previously treated with 1µM of Yb-G3P-NB during 24h) were injected subcutaneously on a Balb/C mouse in a matrigel plug. The day after injection, the shaved mouse was observed under the macroscope (Figure 3.18).

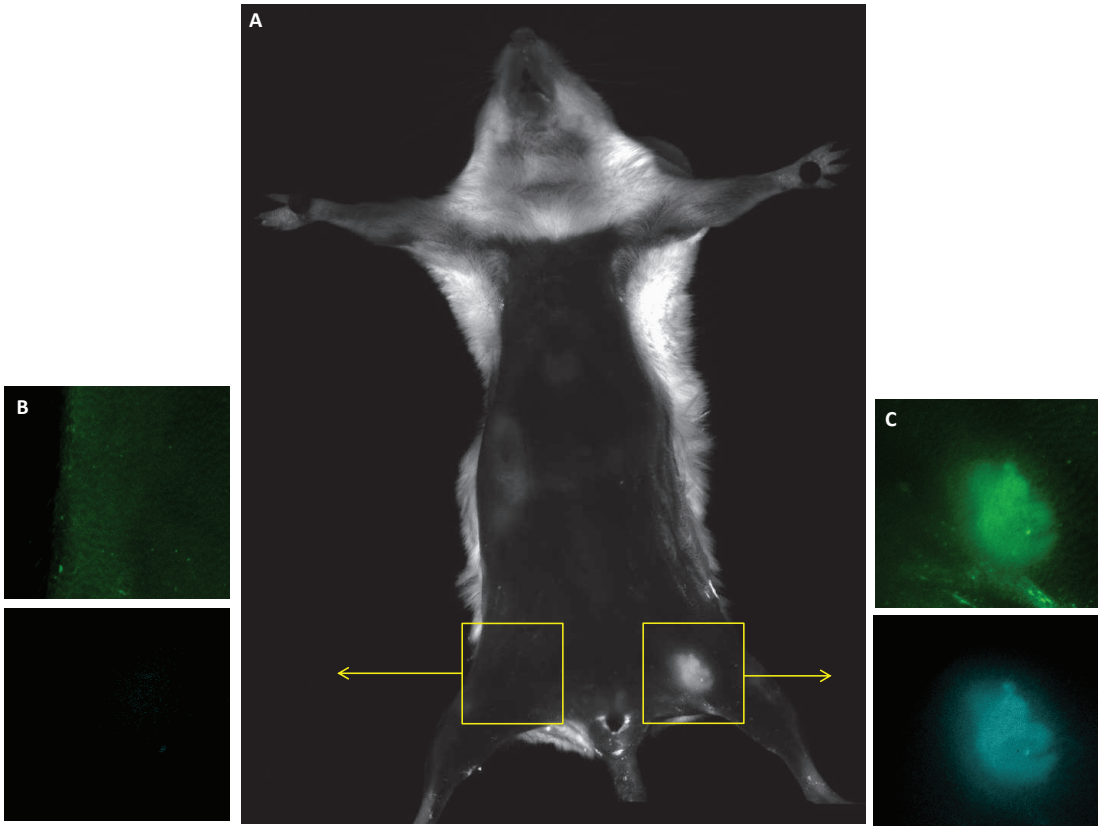

Figure 3.18: Image of untreated 4T1 cells (B) and after 24h of incubation with 1 µM of Yb-G3P-NB (C) subcutaneously injected on Balb/C mouse. The dendrimer luminescence was observed under 417/60 nm excitation. (A) Whole mouse shaved, λ_{em}: 536/40 nm. (green), λ_{em}: 536/40 nm (naphthalimide emission) – 100 ms acquisition time, (blue) λ_{em}: LP805 nm (Yb^{3+} emission) – 1 s acquisition time.

We can easily observe the fluorescence of the 1,8-naphthalimide chromophore in the visible and the Yb^{3+} emission in the NIR. Acquisition time are surprisingly short even in the NIR (1 s). Pictures obtained by the monitoring of the NIR emission of the dendrimer indicate a better sensitivity of detection in comparison to the signal arising from visible emission of the chromophore. We can notice that the limit of the luminescent zone is better defined in the NIR.

These results are a major breakthrough in respect to biological *in vivo* imaging and lanthanide coordination chemistry and spectroscopy by demonstrating for the first time our ability to

observe NIR emitted lanthanide compound *in vivo* through the skin. This major result can be explained by the success of our strategy in designing polymetallic complexes with high number of lanthanide and antenna per unit volume. The dendrimer complexes are sufficiently stable to sustain the biological conditions and emit a sufficient number of photons to allow for a sensitive NIR detection.

3.3.1.4.2- Toxicity

The toxicity of the Yb-G3P-NB dendrimer complex was evaluated *in vivo* over short and long periods of time. For the short term evaluation, a group of Balb/C mice (n=5) received intravenously an injection of 100µL of Yb-G3P-NB (10 µM). Their weight was monitored daily during one month. For the long term toxicity, a group of Balb/C mice (n=5) received 3 intravenous injections (1 per week) of 100 µL of Yb-G3P-NB (10 µM). Their weight was monitored every day during one month. Initially, we had planned to monitor their weights evolution for 3 months to observe an eventual toxicity on the long term but as shown on the figure 3.19, no changes in the weights and behaviors of animals were observed. This is the reason why we decided not to continue the experiment more than one month after its beginning.

Control mice (n=3) received intravenous injection of saline solution).

All the mice were sacrificed by CO_2 inhalation. Livers, lungs and kidneys were removed for histological analysis.

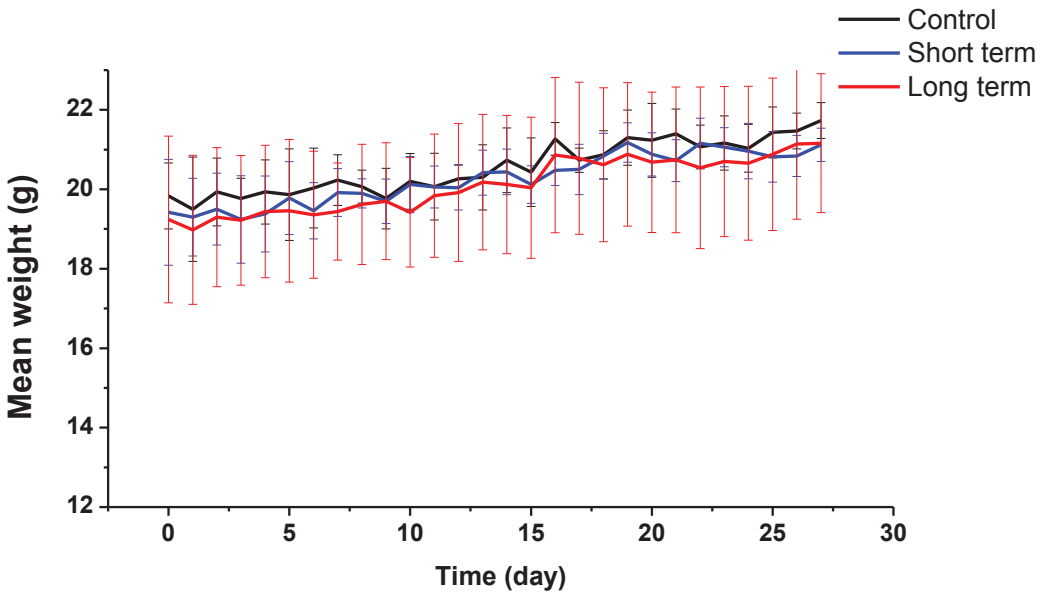

Figure 3.19. Plot showing results of the monitoring of the weight of Balb/C mice after intravenous injection of i) saline solutions (black), ii) solutions of Yb-G3P-NB (100 µL - 10 µM) for toxicity evaluation in the short term (blue) and in the long term (red).

Mice weight is an excellent indicator to measure a potential toxicity of the injected compounds as it directly reflects their state of health. It is not always straightforward to identify the signs of suffering in mice, but a decrease of weight loss is an unambiguous alert reflecting health troubles.

Intravenous injections of Yb-G3P-NB did not impact the weight evolution of mice compared to the control group of mice (Figure 3.19).

Animals were also observed daily and no significant behavior changes or suffering signs were noted.

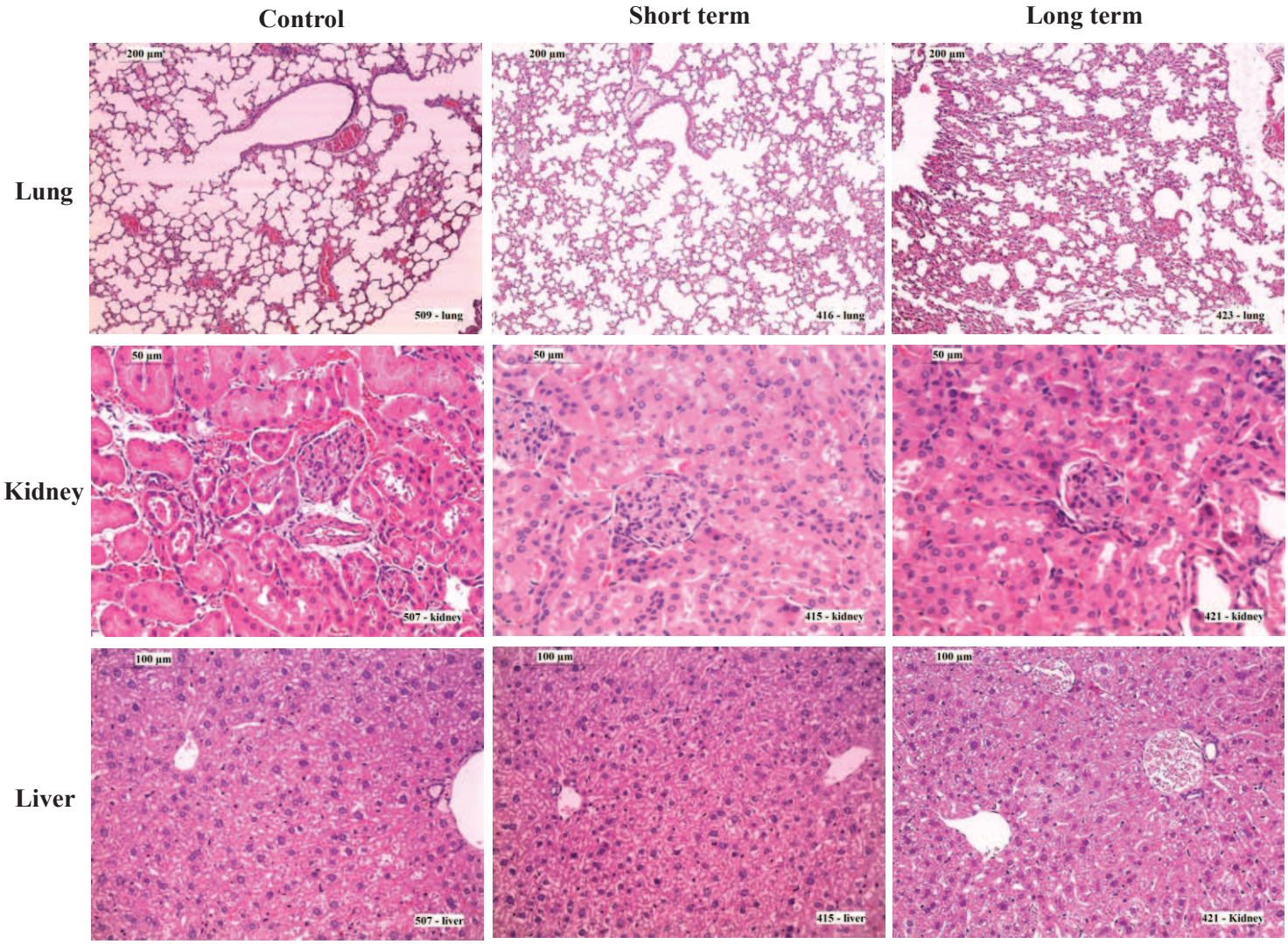

Figure 3.20. Histological specimens of mice tissues (lungs, kidneys and livers) collected from Balb/C mice sacrificed after 4 weeks, stained with hematoxylin and eosin showing normal histology. Mice received intravenous injection of saline solution (left column) and 100 µL of Yb-G3P-NB at 10 µM to evaluate short term (middle column) or long term toxicities (right column).

The pathologist from Novaxia society, who analyzed the slices, concluded that " one or three intravenous administrations of the test compound in mice did not induce, 1 month after administration, any microscopic effects on the lung, liver and kidneys"(Figure 3.20).

3.4-Conclusion

In this chapter, new lanthanide dendrimer complexes have been described for the first time to operate as NIR emitted reporters *in cellulo* and *in vivo*.

Ln-G3P-NH_2 and Ln-G3P-NB have both chemical structures that include the same 32 units of 4-amino-1,8-naphthalimide chromophores to sensitize Eu^{3+}, Yb^{3+} and Nd^{3+}. The only difference between them is that the first one is substituted with NH_2 groups in the end of dendrimer branches and the second one possesses biotin groups that increase water solubility and could facilitate targeting via biotin-streptavidin antibodies linkage.

These two families of dendrimer complexes present fairly comparable photophysical properties.

Despite its larger size (45 to 55 nm in diameter), lanthanide complexes formed with Ln-G3P-NB have demonstrated a better efficiency for cellular uptake than Ln-G3P-NH_2 through its higher biocompatibility. Complexes formed with Ln-G3P-NB have been shown to be less toxic. It is important for lanthanide based reporters to be sufficiently stable to prevent the release of any free metal to avoid cytotoxicity. This point is crucial to allow their use for diagnostic applications. All dendrimer complexes studied in this work have shown a good stability in different environments and particularly in biological media. Indeed, not shown data have demonstrated their ability to be observed by microscopy one week after the incubations of the cells. Incubated HeLa cells were followed by epifluorescence microscopy and dendrimer signal was still present after one week of cell divisions.

The good signal to noise ratio of the NIR emission signal arising from the Yb-G3P-NB complex placed subcutaneously in a living mouse is a major and unique advantage for future tumor diagnostic application.

Even if the excitation wavelength is not optimized at this time for the crossing of important depths of tissue *in vivo,* these results are very encouraging. With the design of our dendrimer complexes, chromophores can be modified or replaced without having the re-engineer the whole synthesis. We are currently working in developing chromophore that have a lower energy excitation wavelength for detection deeper in tissues.

We have demonstrated here that the low quantum yields of these NIR emitting lanthanide complexes are not a barrier that would prevent their observation *in vivo* through the skin with short acquisition time (1 s in the NIR). The efficiency of the strategy of generating a high density of photons per unit volume by the formation of polymetallic complexes to which are

attached a high number of lanthanide sensitizers is validated for the first time at the level of the whole animal.

Ln-G3P-NB appears to be not toxic for mice after intravenous injection of 100 mL of a 10 μM solution of dendrimer complexes. These results are highly promising for diagnostic purposes. Other important point will need to be studied to determine dendrimer efficiency as imaging agents for (tumor) diagnostic.

First the biodistribution of the dendrimer needs to be evaluated. Generally biodistribution studies of fluorescent compounds are realized by measuring the emission signal on the whole animal or *ex vivo* on isolated organs. These types of experiments will be realized in a similar ways with our dendrimer complexes and, in addition, will be associated to ICP measurements aiming at the quantification of Yb^{3+} concentration in each organs collected at different times after injection. ICP is a more sensitive technique to evaluate the presence of dendrimer complexes in organs (through determination of the Yb^{3+} concentration) than fluorescence microscopy. These experiments will allow to determine the lower limit of detection of the dendrimer complexes through fluorescence macroscopy.

Secondly, dendrimer clearance is a significant advantage for dendrimer efficiency. To be efficient as a target reporter, luminescent dendrimer complexes must remain for long enough in the blood circulation to interact and concentrate at the targeted location. If the compound is eliminated too fast, an insufficient amount of luminescent compound will remain in the biological system to ensure accurate and sensitive detection. The clearance can also be evaluated by ICP after blood and urine collection at different times after intravenous injection (experiments in progress).

A series of experiments have demonstrated that the behavior of dendrimers is not influenced by the presence and the nature of coordinated lanthanides. This point constitute an advantage: the system is flexible and it is possible to adapt the emission wavelength by the choice of the lanthanide cation to the experimental needs. It is possible to direct Ln-G3P-NB towards a specific target using the biotin-streptavidin-antibody link. This design allows to direct our luminescent dendrimer complexes to a broad variety of targets available through the blood circulation. Indeed, the size of the complex dendrimer-streptavidin-antibody will be important and may ultimately limit the cellular uptake. Nevertheless, it is good to keep in mind that in order to image tumor cells, the fixation of the dendrimer complex fixation on a tumor cells receptors is sufficient for their recognition and localization.

This point overrides the size limitation for in vivo applications. With the goal of intracellular target, the flexibility of the design allows the modification of the periphery of dendrimers can by chemical modification to improve the size/efficiency ratio.

References

- Alcala, M. A., S. Y. Kwan, *et al*. (2011). "Luminescence targeting and imaging using a nanoscale generation 3 dendrimer in an in vivo colorectal metastatic rat model." Nanomedicine**7**(3): 249-258.

- Alcala, M. A., C. M. Shade, *et al*. (2011). "Preferential accumulation within tumors and in vivo imaging by functionalized luminescent dendrimer lanthanide complexes." Biomaterials**32**(35): 9343-9352.

- Astruc, D., E. Boisselier, *et al*. (2010). "Dendrimers designed for functions: from physical, photophysical, and supramolecular properties to applications in sensing, catalysis, molecular electronics, photonics, and nanomedicine." Chem Rev**110**(4): 1857-1959.

- Backer, M. V., T. I. Gaynutdinov, *et al*. (2005). "Vascular endothelial growth factor selectively targets boronated dendrimers to tumor vasculature." Mol Cancer Ther**4**(9): 1423-1429.

- Bielinska, A. U., C. Chen, *et al*. (1999). "DNA complexing with polyamidoamine dendrimers: implications for transfection." Bioconjug Chem**10**(5): 843-850.

- Branchi, B., P. Ceroni, *et al*. (2010). "A light-harvesting antenna resulting from the self-assembly of five luminescent components: a dendrimer, two clips, and two lanthanide ions." Chemistry**16**(20): 6048-6055.

- Buhleier E., W. W., Vögtle F. (1978). ""cascade" and "nonskid-chain-like" syntheses of molecular cavity topologies." Synthesis**78**: 155-158.

- Caminade, A. M., R. Laurent, *et al*. (2005). "Characterization of dendrimers." Adv Drug Deliv Rev**57**(15): 2130-2146.

- Comby, S., D. Imbert, *et al*. (2006). "Stable 8-hydroxyquinolinate-based podates as efficient sensitizers of lanthanide near-infrared luminescence." Inorg Chem**45**(2): 732-743.

- Cross, J. P., M. Lauz, *et al.* (2004). "Polymetallic lanthanide complexes with PAMAM-naphthalimide dendritic ligands: luminescent lanthanide complexes formed in solution." J Am Chem Soc**126**(50): 16278-16279.

- Duncan, R. and L. Izzo (2005). "Dendrimer biocompatibility and toxicity." Adv Drug Deliv Rev**57**(15): 2215-2237.
- Eichman, J. D., A. U. Bielinska, *et al.* (2000). "The use of PAMAM dendrimers in the efficient transfer of genetic material into cells." Pharm Sci Technolo Today**3**(7): 232-245.
El-Sayed, M., M. Ginski, *et al.* (2002). "Transepithelial transport of poly(amidoamine) dendrimers across Caco-2 cell monolayers." J Control Release**81**(3): 355-365.
- Eliseeva, S. V. and J. C. Bunzli (2010). "Lanthanide luminescence for functional materials and bio-sciences." Chem Soc Rev**39**(1): 189-227.
- Esfand, R. and D. A. Tomalia (2001). "Poly(amidoamine) (PAMAM) dendrimers: from biomimicry to drug delivery and biomedical applications." Drug Discov Today**6**(8): 427-436.
- Greish, K. (2007). "Enhanced permeability and retention of macromolecular drugs in solid tumors: a royal gate for targeted anticancer nanomedicines." J Drug Target**15**(7-8): 457-464.
- Haensler, J. and F. C. Szoka, Jr. (1993). "Polyamidoamine cascade polymers mediate efficient transfection of cells in culture." Bioconjug Chem**4**(5): 372-379.
- Hecht, S. and J. M. Frechet (2001). "Dendritic Encapsulation of Function: Applying Nature's Site Isolation Principle from Biomimetics to Materials Science." Angew Chem Int Ed Engl**40**(1): 74-91.
- Hirano, S. and K. T. Suzuki (1996). "Exposure, metabolism, and toxicity of rare earths and related compounds." Environ Health Perspect**104 Suppl 1**: 85-95.
- Ihre, H. R., O. L. Padilla De Jesus, *et al*. (2002). "Polyester dendritic systems for drug delivery applications: design, synthesis, and characterization." Bioconjug Chem**13**(3): 443-452.
- Jansen, J. F., E. M. de Brabander-van den Berg, *et al*. (1994). "Encapsulation of guest molecules into a dendritic box." Science**266**(5188): 1226-1229.
- Kitchens, K. M., R. B. Kolhatkar, *et al.* (2006). "Transport of poly(amidoamine) dendrimers across Caco-2 cell monolayers: Influence of size, charge and fluorescent labeling." Pharm Res**23**(12): 2818-2826.
- Kleinman, M. H. F., J. H. Tomalia, D. A. Turro, N. J. (2000). "Effect of protonation and PAMAM dendrimer size on the complexation and dynamic mobility of 2-Naphthol." J. Phys. Chem. B**104**: 11472-11479.
- Kobayashi, H. and M. W. Brechbiel (2003). "Dendrimer-based macromolecular MRI contrast agents: characteristics and application." Mol Imaging**2**(1): 1-10.

- Kobayashi, H., Y. Koyama, *et al.* (2007). "Multimodal nanoprobes for radionuclide and five-color near-infrared optical lymphatic imaging." ACS Nano**1**(4): 258-264.
- Malik, N., R. Wiwattanapatapee, *et al.* (2000). "Dendrimers: relationship between structure and biocompatibility in vitro, and preliminary studies on the biodistribution of 125I-labelled polyamidoamine dendrimers in vivo." J Control Release**65**(1-2): 133-148.
- Orlandi, P. A. and P. H. Fishman (1998). "Filipin-dependent inhibition of cholera toxin: evidence for toxin internalization and activation through caveolae-like domains." J Cell Biol**141**(4): 905-915.
- Pillai, Z. S., P. Ceroni, *et al*. (2013). "Dendrimers as Nd3+ ligands: effect of generation on the efficiency of the sensitized lanthanide emission." Chem Asian J**8**(4): 771-777.
- Pless, D. D. and R. B. Wellner (1996). "In vitro fusion of endocytic vesicles: effects of reagents that alter endosomal pH." J Cell Biochem**62**(1): 27-39.
- Qiong-Qiong Chen, L. L., Hong-Mei Chen, Shi-Ping Yang, Lian-Zhun Yang, Xi-Bin Yu (2006). "A polyamidoamine dendrimer with peripheral 1,8-naphthalimide groups capable of acting as a PET fluorescent sensor for the rare earth cations." Journal of Photochemistry and Photobiology A: Chemistry**180**(1-2).
- Roberts, J. C., M. K. Bhalgat, *et al.* (1996). "Preliminary biological evaluation of polyamidoamine (PAMAM) Starburst dendrimers." J Biomed Mater Res**30**(1): 53-65.
- Saovapakhiran, A., A. D'Emanuele, *et al*. (2009). "Surface modification of PAMAM dendrimers modulates the mechanism of cellular internalization." Bioconjug Chem**20**(4): 693-701.
- Sarin, H., A. S. Kanevsky, *et al*. (2008). "Effective transvascular delivery of nanoparticles across the blood-brain tumor barrier into malignant glioma cells." J Transl Med**6**: 80.
- Song, H. Y., M. H. Ngai, *et al*. (2009). "Practical synthesis of maleimides and coumarin-linked probes for protein and antibody labelling via reduction of native disulfides." Org Biomol Chem**7**(17): 3400-3406.
- Svenson, S. and D. A. Tomalia (2005). "Dendrimers in biomedical applications--reflections on the field." Adv Drug Deliv Rev**57**(15): 2106-2129.
- Tekade, R. K., P. V. Kumar, *et al.* (2009). "Dendrimers in oncology: an expanding horizon." Chem Rev**109**(1): 49-87.
- Tomalia, D.A., H. Dewald, *et al*. (1985). "A new class of polymers: Starbust-Dendritic Macromolecules." Polymer Journal **17**: 117-132.

- Vicinelli, V., P. Ceroni, *et al.* (2002). "Luminescent lanthanide ions hosted in a fluorescent polylysin dendrimer. Antenna-like sensitization of visible and near-infrared emission." J Am Chem Soc**124**(22): 6461-6468.
- Vicinelli, V. C., P. Maestri, *et al.* (2002). "Luminescent lanthanide ions hosted in a fluorescent Polylysin dendrimer. Antenna-like sensitization of visible and near-infrared emission." J. Am. Chem.Soc**124**: 6461-6468.
- Vögtle, F. G., M. Vicinelli, V. *et al.* (2001). "A Dendritic Antenna for Near-Infrared Emission of Nd3+ Ions." Chem phys chem**2**(12): 769-773.
- Wang, L. H., K. G. Rothberg, *et al*. (1993). "Mis-assembly of clathrin lattices on endosomes reveals a regulatory switch for coated pit formation." J Cell Biol**123**(5): 1107-1117.
- Weyermann, P., J. P. Gisselbrecht, *et al.* (1999). "Dendritic Iron Porphyrins with Tethered Axial Ligands: New Model Compounds for Cytochromes." Angew Chem Int Ed Engl**38**(21): 3215-3219.
- Wiener, E. C., M. W. Brechbiel, *et al*. (1994). "Dendrimer-based metal chelates: a new class of magnetic resonance imaging contrast agents." Magn Reson Med**31**(1): 1-8.
- Wolinsky, J. B. and M. W. Grinstaff (2008). "Therapeutic and diagnostic applications of dendrimers for cancer treatment." Adv Drug Deliv Rev**60**(9): 1037-1055.
- Zhang, J., P. D. Badger, *et al.* (2005). "Sensitization of near-infrared-emitting lanthanide cations in solution by tropolonate ligands." Angew Chem Int Ed Engl**44**(17): 2508-2512.

Résumé Français

Le travail présenté dans ce chapitre porte sur la caractérisation photophysique de nouveaux complexes luminescents dérivés de dendrimères PAMAM ainsi que sur l'étude de leur comportement au niveau cellulaire.

Les dendrimères sont décrits comme étant des macromolécules polymériques constituées de séquences répétitives de monomères à partir d'un cœur multifonctionnel.

D'un point de vue historique, le concept de molécules branchées à croissance répétitive a été décrit pour la première fois en 1978 par Vögtle, mais c'est seulement en 1985, avec Tomalia, qu'apparait le terme de "dendrimère". La croissance particulière des dendrimères permet la formation de cavités internes qui peuvent être exploitées pour l'encapsulation de petites molécules.

Plusieurs familles de dendrimères ont été développées mais nous allons nous focaliser sur la famille des polyamidoamine (PAMAM) qui est actuellement la plus utilisée pour des applications en biologie (transfert de gènes, délivrance de molécules thérapeutiques, imagerie, etc.).

Deux types de dendrimères luminescents ont été développés dans le groupe à partir de dendrimères PAMAM de génération 3. 32 chromophores dérivés du1,8-naphthalimide ont été ajoutés à la périphérie des branches: le 4-amino-1,8-naphthalimide pour le dendrimère G3P-NH_2 et le 4-amino-1,8-naphthalimide biotinilé pour le dendrimère G3P-NB. L'ajout de la biotine a permis d'augmenter la solubilité du dendrimère dans l'eau ainsi que d'anticiper leur vectorisation par le biais d'un couplage biotine-streptavidine-anticorps.

Il a été montré que ces ligands chromophore-dendrimères sont capables d'incorporer et de sensibiliser 8 cations lanthanides (Eu^{3+}, Nd^{3+}ou Yb^{3+}). Les dendrimères Ln-G3P-NH_2 et Ln-G3P-NB possèdent les mêmes caractéristiques photophysiques avec une longueur d'onde d'excitation centrée autour de 440 nm et une longueur d'onde d'émission à 614, 980 ou 1064 nm en fonction du lanthanide complexé. Les rendements quantiques sont faibles dans le proche infrarouge (de l'ordre de 10^{-3}) mais compensés par le grand nombre de chromophores et de lanthanides par dendrimère qui augmentent le nombre de photons émis par unité de volume.

La microscopie électronique a permis d'observer des tailles respectives de 30 à 35 nm et 45 à 55 nm pour les dendrimères Ln-G3P-NH_2 et Ln-G3P-NB.

Lorsqu'ils sont libres, les lanthanides sont toxiques pour l'organisme. Il est donc crucial de s'assurer que les composés développés n'induisent pas de toxicité par relargage de cations de lanthanide. Les dendrimères Ln-G3P-NH_2 et Ln-G3P-NB ne sont pas toxiques aux doses utilisées en microscopie. Des images de microscopie à épifluorescence ont montré le signal d'émission des dendrimères Yb/Nd-G3P-NH_2 etYb/Nd-G3P-NB dans des cellules Hela. Cependant, les dendrimères Ln-G3P-NH2 ont tendance à s'agréger et sont moins internalisés par les cellules (confirmé par microscopie confocale et cytométrie en flux). Les dendrimères sont localisés préférentiellement dans les lysosomes et sont internalisés principalement par voie d'endocytose clathrine dépendante.

Pour la première fois, il a été possible d'imager l'émission proche infrarouge de l'Yb^{3+}*in vivo* après injection sous cutanée de cellules préalablement incubées avec les dendrimères Yb-G3P-NB. Ces résultats sont la preuve de principe que les dendrimères développés par le groupe sont utilisables *in vivo* comme rapporteurs luminescents dans le proche infrarouge.

La toxicité des dendrimères Yb-G3P-NB a été évaluée *in vivo* à court et long terme chez des souris Balb/C avec une ou trois injections intraveineuses de 100 µL de dendrimères à 10 µM. Les souris ont été suivies quotidiennement et aucune perte de poids ni signe de souffrance n'ont été observés. Un mois après les injections, les souris ont été sacrifiées par inhalation de CO2 et le foie, les reins et les poumons ont été prélevés pour analyse histologique. Le rapport rendu par la société Novaxia, spécialisée dans les études histo-pathologiques, n'indique aucune modification microscopique qui traduirait la toxicité des dendrimères après 1 ou 3 injections intraveineuses.

En conclusion, les dendrimères Ln-G3P-NH_2et Ln-G3P-NB, constitués de 32 chromophores dérivés de 1,8-naphthalimide et de 8 cations lanthanides (Eu^{3+}, Yb^{3+}et Nd^{3+}), ont montré des propriétés photophysiques similaires. Ils sont capables d'être internalisés par les cellules, même si celle-ci est limitée pour les dendrimères Ln-G3P-NH_2 par leur faible solubilité dans l'eau. La stratégie visant à incorporer un grand nombre de chromophores et de lanthanides par dendrimère s'est une fois encore avérée efficace pour s'affranchir des rendements quantiques faibles et permettre de détecter le signal d'émission dans le proche infrarouge *in cellulo* et *in vivo*.

Une ou trois injections intraveineuses n'induisent pas de toxicité chez la souris, cependant, d'autres études (actuellement en cours), telles que l'étude de leur biodistribution et de leur clairance vont permettre d'envisager des applications spécifiques pour le diagnostic *in vivo*.

4-Increase of the emission intensity of 1.8-naphthalimide groups attached to polyamidoamine dendrimers

4.1-Introduction

This chapter will discuss unexpected and surprising observations obtained under the microscope on living cells labeled with luminescent dendrimers. The following experiments are related to dendrimer lanthanide complexes. For clarity, we have chosen to describe this part of the work in a separate chapter as a "different story".

After 24h of incubation with 1 µM of Eu-G3P-NB (see chapter 3 for detailed description), Hela cells were observed under an epifluorescence microscope. After 5 minutes of irradiation under 488 nm excitation light, a spectacular increase of emission signal (λ_{em}: 525/50 nm corresponding to 1,8-naphthalimide combined with Eu^{3+} emission signal) could be observed.

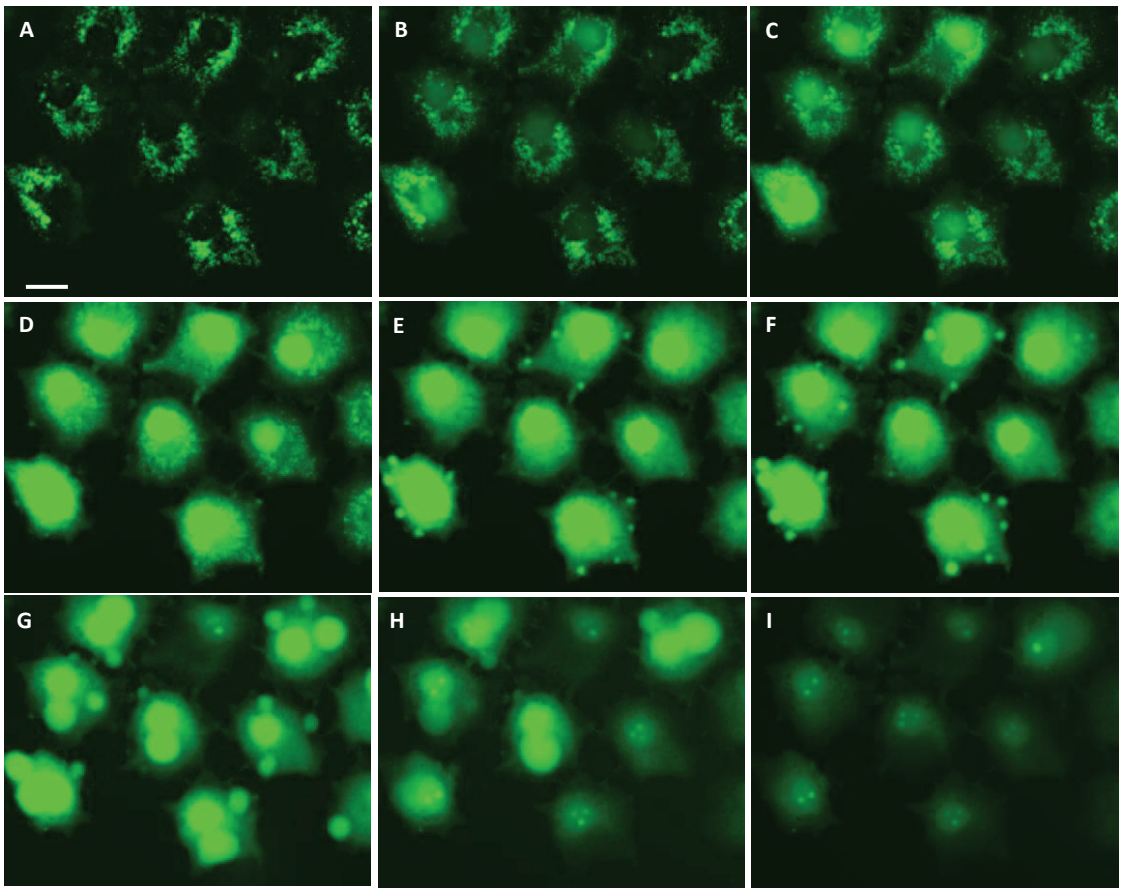

Figure 4.1. Microscopy images of HeLa cells after 24h of incubation with Eu-G3P-NB (1µM) under blue

light excitation. Images were extracted from a 15 minutes movie to represent as well as possible the evolution of cells over time. A: t0; B: t2 minutes; C: t3 minutes; D: t5 minutes; E: t8 minutes; F: t10 minutes; G: t12 minutes; H:t14 minutes; I: t15 minutes. Scale bar 20 µm.

At t0, the monitored emission signal was located in the lysosomes (as described in the Chapter 3) (Figure 4.1). When the cells loaded with the luminescent dendrimers are further continuously illuminated with 488 nm light, the emission signal increases dramatically and reaches its maximum intensity after 5 minutes. The observed emission signal is more diffuse in the cytoplasm with the maximum of intensity in the nucleus.
After 5 minutes of continuous illumination, when the maximum intensity is reached, we can observe the formation of small vesicles that keep growing to finally burst after 15 minutes inducing a major decrease of the emission signal.

This measurement was repeated several times in the same conditions with different cell lines (HeLa, U87MG, NIH 3T3, MSU 1.1). The same phenomenon was observed with more or less intensity depending on the respective cellular uptake.

4.2-Materials and methods

4.2.1-Epifluorescence microscopy

HeLa cells were incubated in 96-well black microplates (BD Biosciences, Le Pont de Claix, France) with 1 µM of Eu-G3P-NB. After 24h at 37°C, the cell culture media was changed and replaced by Opti-MEM media exempt of phenol red. A 15 minutes video of dendrimer emission (λ_{em} = 525/50 nm) was registered under continuous 485/20 nm light exposition using an Axio Observer Z1 fluorescence inverted microscope (Zeiss, Le Pecq, France) equipped with an ORCA-R2 high-resolution CCD camera linked to a computer driving the acquisition software Axiovision (Zeiss). The inverted microscope was equipped with a Zeiss immersion Plan Apochromat 20x (NA=1.4) objective. The Zeiss HXP-120 light source (metal halide) was used as excitation.

4.2.2-Dendrimers release

HeLa cells were incubated in 24-well microplateand incubated with 1 µM of Eu-G3P-NB or Eu-G3P-NH_2 for 48h to incorporate a higher quantity of dendrimers inside cells. After incubation, the cell culture media was changed and replaced by PBS. Cells were illuminated using the HGFIE HG pre-centered fiber illuminator (130W mercury) from a Nikon AZ100 Multizoom macroscope. The fluorescence channel was set with 482/35 nm filter. (Semrock, Rochester, New York, USA).

The illumination time (around 15 minutes) was controlled in the macroscope eyepieces to reach the burst of vesicles and the decrease of fluorescence intensity. The supernatant was removed and analyzed using a Jobin Yvon-Horiba Fluorolog 3-22 spectrofluorimeter to detect the chromophore emission signal.

4.2.3-ROS production

The Reactive Oxygen Species (ROS) production was determined by means of fluorescence spectrometry with 2',7'-dichlorodihydrofluorescein diacetate (DCDHF-DA) (Invitrogen, Courtaboeuf, France), a chemical probe that become fluorescent on reaction with ROS. DCDHF-DA presents the advantages to have an excitation wavelength at 488 nm and an emission wavelength at 520 nm (the same wavelengths as for 1,8 naphthalimide).

$1x10^4$ HeLa cells were seeded in a 96-well black microplate and were incubated with 1µM of Eu-G3P-NB or with the same volume of DMSO as for dendrimer treatment as a control. After 24h of incubation, the cells were washed and replaced by 10 µM of DCDHF-DA dissolved in PBS for control conditions (untreated and DMSO-incubated cells) for 30 minutes at 37°C in absence of light. Cells were then carefully washed with PBS. The fluorescence signal of the dendrimer and of DCDHF-DA was measured with a microplate reader (Victor 3V, Perkin-Elmer, Courtaboeuf, France). After the first fluorescence measurement, cells were illuminated during 5 minutes under the light of the Nikon AZ100 Multizoom macroscope combined with a 482/35 nm filter.

The fluorescence was measured for a second time after the 5 minutes of illumination.

4.2.4-Dose-light spectrofluorimetry

Dendrimers were diluted in PBS at different concentrations and were illuminated using the Nikon AZ100 Multizoom macroscope lamp combined with the 482/35nm excitation filter.
The dose of light received by the sample was controlled with the exposition time. The output of the lamp (combined with the excitation filter) was measured with the help of a power-meter and the exposition time was calculated in order to obtain a precise dose of light in J/cm².
Each solution was illuminated with the appropriate time to obtain 0, 35, 70 and 140 J/cm² of 482nm light prior to the recording of the 1,8-naphthalimide emission with the following parameters: λ_{ex}: 488 nm; λ_{em}: 498-800 nm; 0.1 s integration time.

4.2.5-cTDNA interaction

Amino and biotin dendrimers solutions were prepared with different concentration of calf Thymus DNA (cTDNA) (Sigma Aldrich, St Quentin Fallavier, France) dissolved in water. The prepared solutions were analyzed by spectrofluorimetry using the same parameters as those used for the study of light effects

4.3-Results

The kinetics observed under 488 nm excitation light can be divided in 3 phases: the first one correspond to the increase of emission intensity with apparition of emission signal in the nucleus of the cells (after 5 minutes approximately). The second step starts with the apparition of vesicles that will keep growing (around 10 minutes after the beginning of the illumination). The last step corresponds to the burst of vesicles and the decrease of the emission signal in the cells.

4.3.1-Implication of chromophore 1.8-naphthalimide

The"kinetic experiment" was conducted in the same conditions as those used for the free biotin-dendrimer ligand (G3P-NB) and the complexes formed between this ligand and Eu^{3+} or Yb^{3+} (Eu-G3P-NB or Yb-G3P-NB respectively). A systematic comparison between the behaviors of the dendrimers is possible because the monitored emitted signal is arising from the chromophore and not from the lanthanide.

In a second time, comparable experiments were done with the amino dendrimer ligand (G3P-NH_2) and the corresponding Eu^{3+}complex (Eu-G3P-NH_2).

A similar general behavior was observed with a lower intensity for the amino dendrimer because it is less uptaken by cells. However the kinetic remains the same.

Microscopy experiments were also realized with different excitation wavelengths (365, 485, 550 and 640 nm). The phenomenon appears only with UV and blue excitation wavelengths which corresponds specifically to the absorption energy of the dendrimers.

The requirement of an active cell metabolism to occur to obtain the phenomenon has been demonstrated by testing similar conditions on living and fixed cells (PFA 4%). Indeed, the emission intensity increases faster in living cells when emission signal do not change and stay in lysosomes with no increase in fixated cells.

These series of results allow concluding that the observed phenomenon is due to the presence of the 1,8-naphthalimide moiety and not from the lanthanide or from the terminal surface groups attached on the dendrimer.

4.3.1-Dendrimer release

The observation of vesicles growth and its burst under illumination followed by the decrease of emission signal can attributed to the release of dendrimers in the cell culture media.

To verify this hypothesis, HeLa cells were incubated with Eu-G3P-NB during 48h to incorporate a large amount of dendrimer inside cells in order to release a potentially higher concentration of luminescent dendrimer to facilitate its detection in cell culture media.

After incubation, the cell culture media was replaced by PBS and the dendrimer-loaded cells were illuminated for approximately 15 minutes until the burst of vesicles is observed (Figure 4.2).

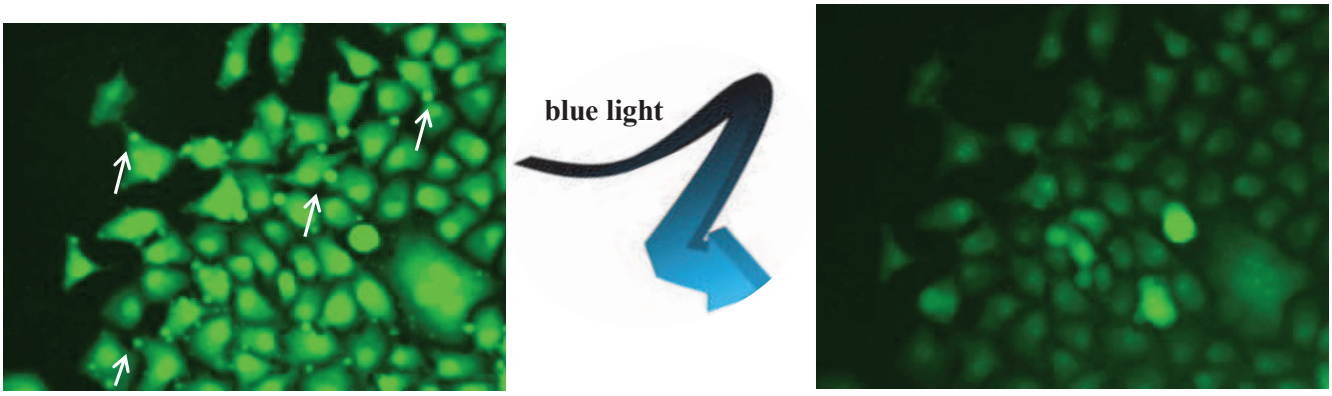

Figure 4.2. Epifluorescence microscopy of HeLa cells following the last step of the observed kinetic. Left: formation of vesicles (white arrows) after 10 minutes of illumination. Right: decrease of emission signal 15 minutes after illumination.

After illumination, supernatants were collected and analyzed by spectrofluorimetry. For both Eu-G3P-NB and Eu-G3P-NH_2, the signal arising from the 1,8-naphthalimide group appeared in the supernatant of illuminated cells. (Figure 4.3). The chromophore emission signal of Eu-G3P-NB and Eu-G3P-NH_2 is 8 times more intense in the supernatant after illumination which means that dendrimers are expelled out of the cells, in the cell culture media during the experiment. The more intense emission intensity observed for Eu-G3P-NB and Eu-G3P-NH_2 can be attributed to the higher cellular uptake of Eu-G3P-NB as described in the Chapter 3.

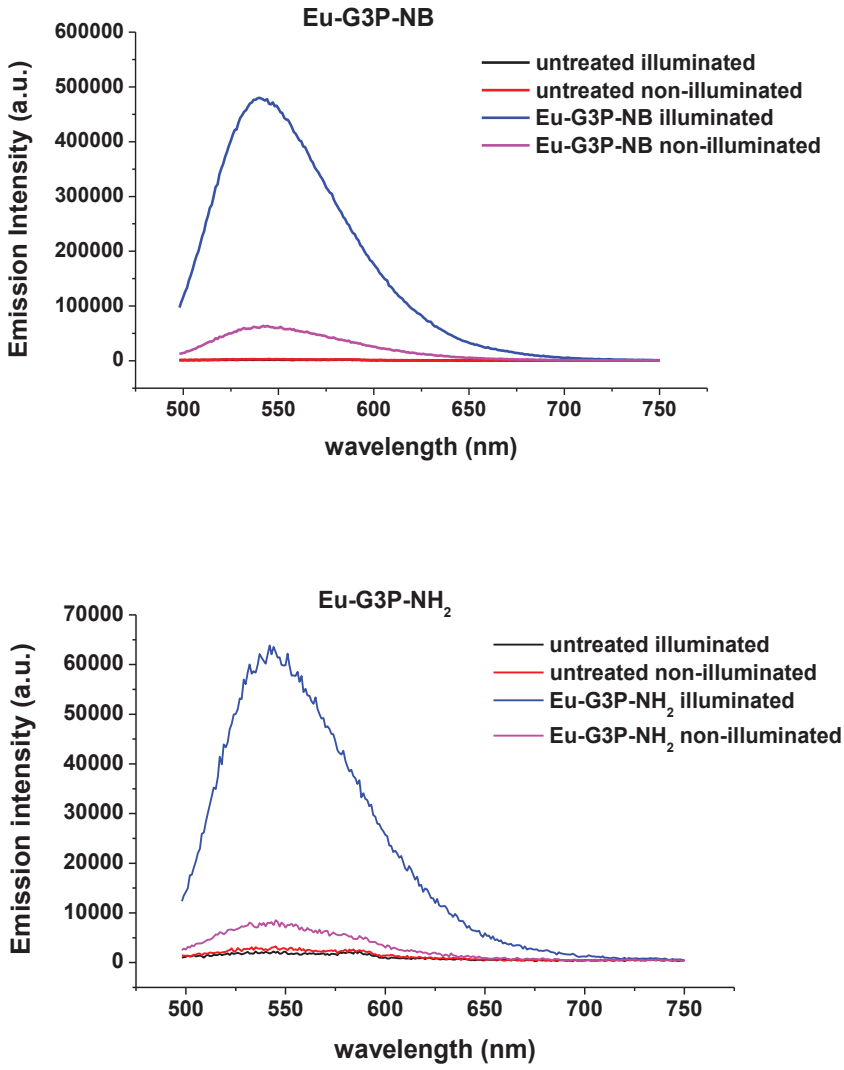

Figure 4.3. Emission spectra measured in solution of cellular supernatant with and without incubation with Eu-G3P-NB (top) and Eu-G3P-NH_2 (bottom) and with and without illumination with blue light (482/35 nm) for 15 minutes.

The control experiment with untreated HeLa cells illuminated in the same conditions as for dendrimers has showed that the vesicle formation is induced by the blue light illumination and not by the presence of the dendrimer. (Figure 4.4)

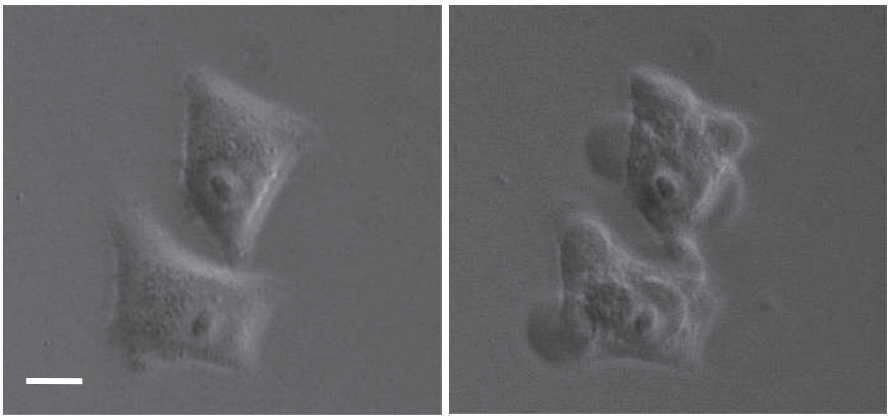

Figure 4.4. Brighfield of untreated HeLa cells before (left) and after 15 minutes of blue light illumination (right). Scale bar=20 µm.

Brightfield picture of untreated HeLa cells are presented in figure 4.4 and show the formation of vesicles induced by blue light illumination. When cells are loaded with dendrimers, these vesicles seem to allow the release of dendrimers in the cell culture media.

It is important to indicate that after the 15 minutes illumination with blue light, the cells die. Such long exposition under blue light is probably generating an excessive stressto the cells. However, after 5 minutes of illumination, when the dendrimer intensity reaches its maximum, cells are still alive and if the illumination is stopped at this moment, cells will continue to grow and divide.

4.3.2-ROS production induced by blue light illumination

Blue light (380-500 nm) has been described as inducing Reactive Oxygen Species (ROS) (Lockwood, Wataha *et al.* 2005). Moreover, Wolfbeis *et al.*, has reported the increasing of Eu^{3+} complex emission intensity in the presence of ROS (H_2O_2). (Wolfbeis, Durkop *et al.* 2002)

These parameters suggest that the observed increase of emission intensity can be due to the ROS production under blue light illumination.

In order to verify this hypothesis, ROS production was evaluated using a chemical probe that becomes fluorescent upon reaction with ROS: DCDHF-DA. This sensor possesses the similar excitation and emission wavelengths as the 1,8-naphthalimide group, what allowed to measured respective emission intensities of DCDHF-DA and of the dendrimer Eu-G3P-NB during the experiment.

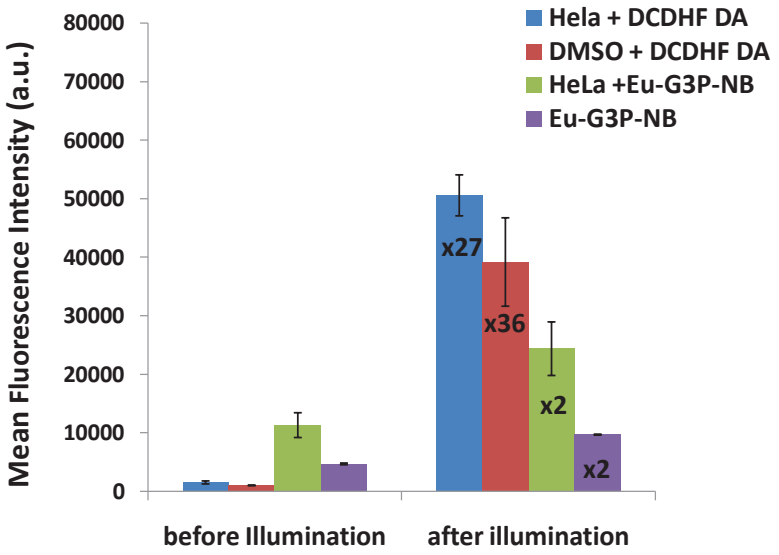

Figure 4.5. Evaluation of ROS production after 5 minutes ofblue lightillumination (λ_{ex}: 482/35 nm) and ROS effect on dendrimer emission intensity.

Results depicted in the figure 4.5 confirm the fact that 5 minutes of illumination with blue light induce ROS production. Indeed, the fluorescence intensity of untreated cells in presence of DCDHF-DA increased by a factor 27, confirming with no ambiguity the ROS induction by the blue light illumination. The emission intensity arising from HeLa cells treated with DMSO (same volume as for the dendrimer) in presence of DCDHF-DA increased by a factor 36.

The ROS sensor was not added to HeLa cells incubated for 24h with Eu-G3P-NB because they possesses similar fluorescence properties (excitation and emission wavelengths) and therefore respective signals can not be separated.

The initial observations obtained from microscopy revealed a dramatic increase of the dendrimer emission intensity which is beyond the dynamic range of the microscope camera(1:3000). From these experiments, based on the hypothesis that ROS could explain the observed phenomenon, an intensity increase of only 2 times was quantified. These results allow to conclude that ROS production induced by illumination in cells is only a marginal parameter here and is not sufficient to explain the increase in emission intensity in the global microscopy experiment.

Another experimental condition was tested during this experiment, the dendrimer Eu-G3P-NB diluted at 1µM in PBS without cells was illuminated in similar conditions for control. It is interesting to note that the emission intensity also increased 2 times.

Dendrimer in solution seems to be sensitive to illumination with blue light. Therefore other experiments were realized in spectroscopic cuvettes to observe dendrimer behavior under light exposition.

4.3.3-Effect of blue light on dendrimers emission intensity

Eu-G3P-NB and Eu-G3P-NH_2 dendrimers were illuminated with increasing dose of blue light (482/35 nm selection filter) after dilution at 1µM in PBS or in HEPES (0.1 M). Results obtained in both buffers are significantly similar and only measurements obtained in PBS are presented here.

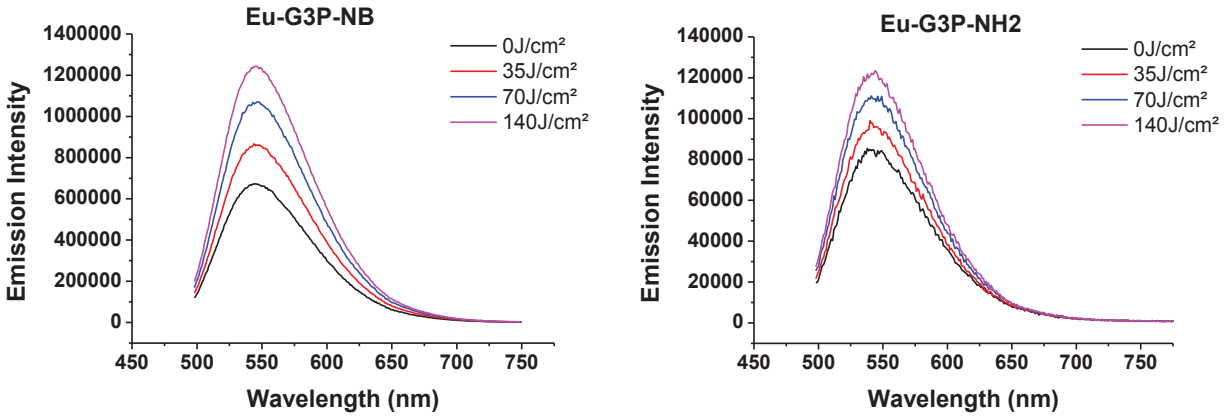

Figure 4.6. Plots depicting increases of Eu-G3P-NB (left) and Eu-G3P-NH_2 emission intensities after illumination with increasing dose of blue light (482/35 nm filter).

The emission intensity of dendrimers is increasing as soon as the first dose of blue light is received (Figure 4.6).

Values showing the increase of emission signals are reported in the table 4.1 after illumination with 140J/cm². All the tested dendrimers are sensitive to the blue light illumination and the increase of intensity is comprised between 1.5 and 3 times.

Table 4.1. Increase factor of different dendrimer emission intensities after illumination with 140 J/cm² of blue light (482/35 nm selection filter).

Dendrimers (1 µM)	Increase of emission intensity after illumination (140 J/cm²)
Yb-G3P-NB	3x
Eu-G3P-NB	2x
G3P-NB	1.5x
Eu-G3P-NH_2	1.5x

Intensities of the emission spectra of the chromophore 1,8-naphthalimide increase even for the uncomplexed dendrimer which confirm its involvement in the observed phenomenon. In addition, it is also interesting to observe the effect of the energy transfer from the 1,8-naphthalimide moiety towards the lanthanide.

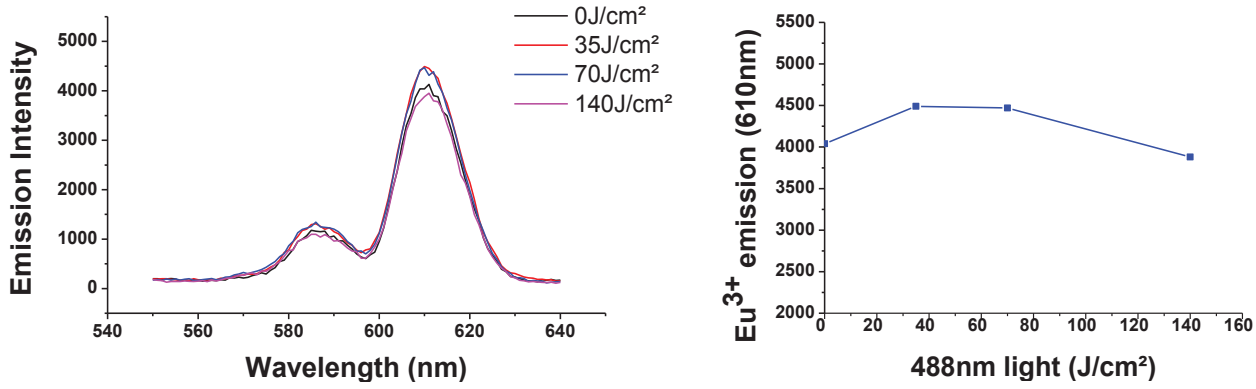

Figure 4.7. Specific Eu^{3+} emission (Eu-G3P-NB) spectra recorded by time-resolved measurements after illumination with increasing doses of blue light. Left: Overlay of the measured emission spectra. Right: maximum of Eu^{3+} emission intensity as a function of the dose of light.

Time-resolved measurements were realized to discriminate and detect the Eu^{3+} emission in absence of any chromophore emission signal (Figure 4.7). Unlike what was observed for the lanthanide sensitizer itself, the different doses of light did not affect the lanthanide emission intensity.

At this stage, no parameter can fully explain the change of intensity observed under the microscope when solutions of dendrimers are exposed to blue light but only some minor contributions.

Therefore, we decided to test the system in extreme conditions to observe its limits.

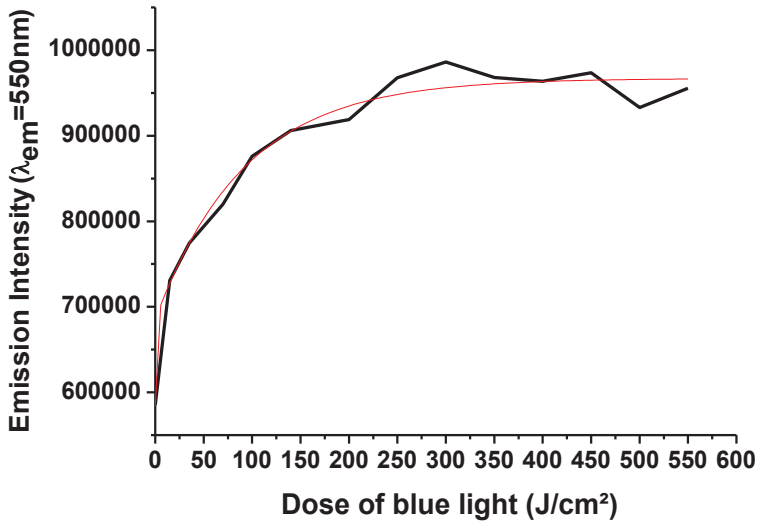

Figure 4.8. Effect of the blue light on the intensity of dendrimer Eu-G3P-NB emission

An increase of the dose of light was tested on a solution of 1 µM of Eu-G3P-NB in PBS. The figure 4.8 reports the intensity of the Eu-G3P-NB maximum of emission as function of the dose of blue light (482/35 nm). Results indicate that the increase of intensity reaches a plateau at a value corresponding to around 150 J/cm² of blue light.

The kinetic of change of emission signal over time was measured after illumination with 140 J/cm² of blue light. (Figure 4.9)

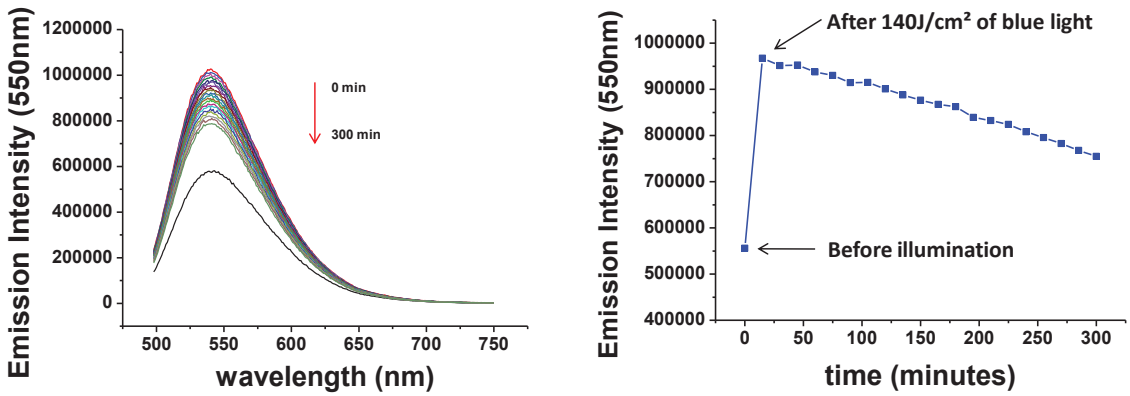

Figure 4.9. Plot describing the monitoring of the Eu-G3P-NB emission signal after illumination with 140 J/cm² of blue light. Each emission spectrum (λ_{ex}: 488 nm) was measured every 30 minutes during a total time of 5h. Left: overlay of the emission spectra. Right: maxima of

emission intensities as a function of time. The initial time corresponds to the first spectrum recorded before illumination and the second point after illumination with 140 J/cm² of blue light.

The emission intensity of dendrimers increasessignificantly (about two times) after the initial illumination. Data shown on figure 4.9 indicate that the intensity tends to return to the initial signal intensity after a certain amount of time reflecting a reversible process.

To summarize results presented here, it appears that dendrimers are sensitive to illumination with blue light (which correspond to the absorption wavelengths of the 1,8-naphthalimide groups located in the end of their branches).
This effect is observable with Eu-G3P-NH_2, but also with G3P-NB and Eu/Yb-G3P-NB dendrimers. The increase of the intensity is directly linked to the presence of the chromophore since G3P-NB emission intensity is also increasing and the emission of Eu^{3+}remains constant after illumination with an increasing dose of light.
The phenomenon appears to be reversible with a signal which tends to return to the initial intensity after a given illumination time. Other experiments have shown the reversibility of the system. Indeed, it is possible to increase emission intensity of dendrimer for a second time (with a new illumination) after emission intensity has returned to its initial value.
However the 2-fold increase of emission intensity observed after blue light illumination can still not account by the huge for the huge increase of signal observed in cells under microscopy.

4.3.4-Interactions between dendrimers and DNA

The microscopic observations of the phenomenon show high emission intensity located in the nuclei suggesting the possibility of interactions between the dendrimer complex and the DNA. (Figure 4.10).

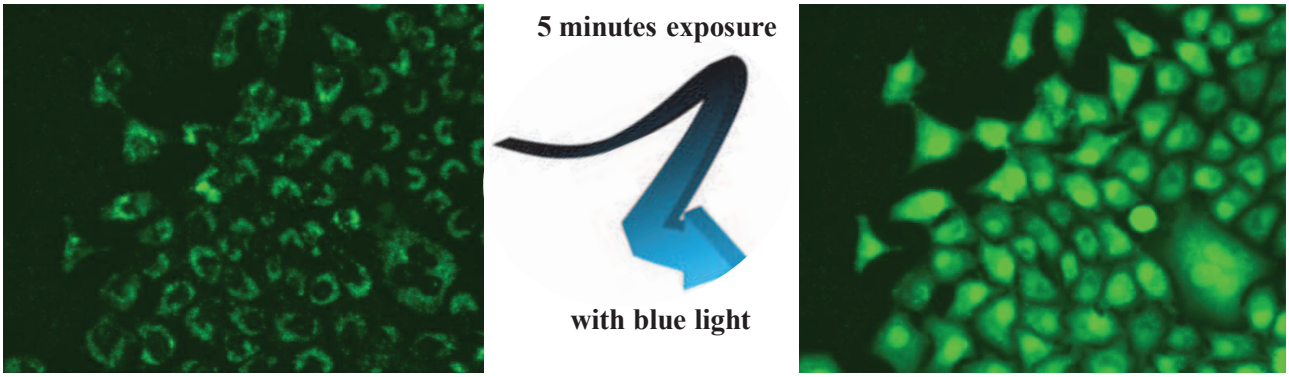

Figure 4.10. Picture of Eu-G3P-NB loaded HeLa cells during the kinetic of illumination experiment at t0 (left) with lysosomal signal and after 5 minutes of illumination(λ_{ex}:485/20nm) (right) showing the increase of the emission intensity and its location in the nuclei.

Naphthalimide groups and derivatives have been described in the literature as intercalating agents. The planarity of the aromatic core (Figure 4.11) suggests that it can bounds to DNA by insertion between pairs of the double helix (Brana and Ramos 2001; Duke, Veale *et al.* 2010).

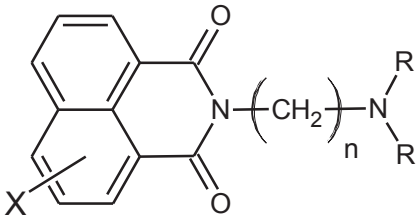

R = CH_3, $(CH_2)_3CH_3$
n = 2, 3
X = NO_2, NH_2, OCH_3

Figure 4.11. Chemical structure of 2,3-naphthalimide groups and derivatives as developed by Braña as DNA-binding agent.(Brana and Ramos 2001)

Amino (Ln-G3P-NH_2) and biotin (Ln-G3P-NB) dendrimers complexes described in this work possess 32 groups derived of the 1,8-naphthalimide group (an isomer of the 2,3-napthalimide group which is also planar). The figure 4.12 described the complete chemical structure of Ln-G3P-NB with the naphthalimide groups located at the end of dendrimer branches. The location of aromatic core in dendrimer periphery provides a good access of these groups to the exterior allowing a potential DNA intercalcation.

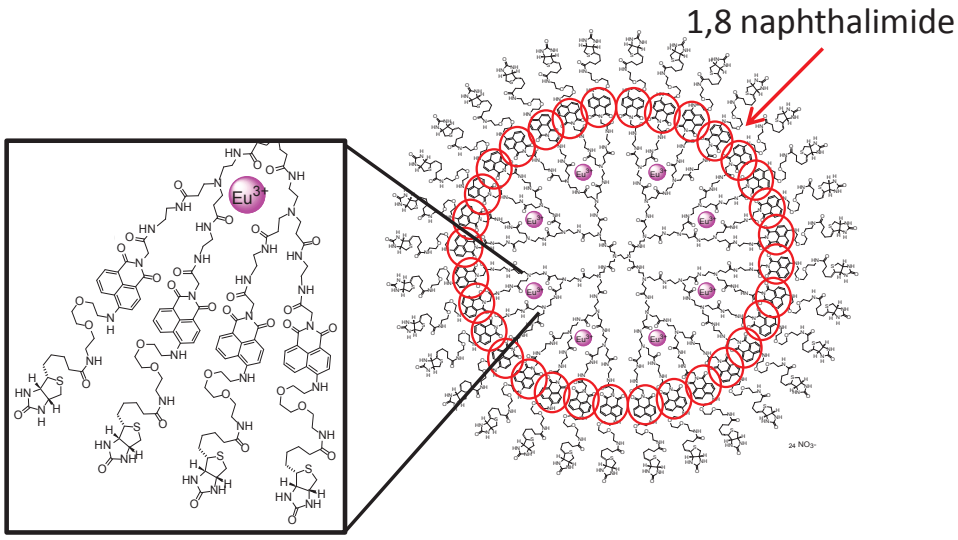

Figure 4.12. Schematic structure of the Ln-G3P-NB dendrimer complex showing the location of 1,8-naphthalimide groups.

The simulated 3D structure of Eu-G3P-NH_2 was estimated with the help of a *MM3* energy minimization mechanic software. Black arrows on the figure 4.13 indicate the position of the naphthalimide groups and indicate their availability to interact with DNA. However, the biotin groups substituted on the derivatives of the 1,8-naphthalimide groups may limit their availability for DNA interaction.

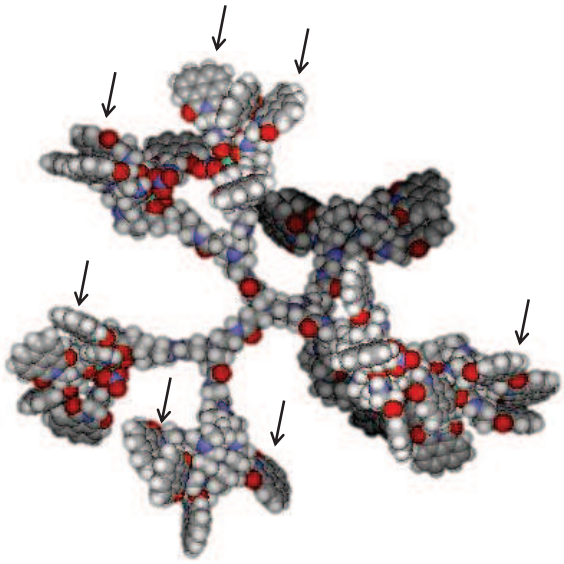

Figure 4.13. MM3 Molecular mechanic simulation of Eu-G3P-NH_2tridimensional structure. Black arrows indicate the location of 1.8-naphthalimide groups.

Interaction between Eu-G3P-NB and DNA has been evidenced by spectrofluorimetry experiments.

Firstly, 4 μM of Eu-G3P-NB and G3P-NB were diluted in water in presence of increasing concentration of calf thymus DNA (cTDNA) and the emission spectrum of the solution was measured by spectrofluorimetry (Figure 4.14). The Eu-G3P-NB emission increases when a concentration of 1mg/ml of cTDNA is reached. This result indicates that interactions are concentration dependent. The G3P-NB emission intensity increases with the lowest cTDNA tested concentration (0.1 mg/ml). The increase of the emission signal arising from the 1,8-naphthalimide in both dendrimers can be directly related to interaction with cTDNA.

These results can be explained by the hypothesis that dendrimer branches become more rigid when coordinated with lanthanides. The naphthalimide groups located on Eu-G3P-NB are less available for interactions with DNA because of the branches rigidity, explaining the increase of intensity only with concentration as high as 1 mg/ml of cTDNA. In contrast, the naphthalimide groups located on the G3P-NB ligand interact more easily with cTDNA thanks to the flexibility of the uncomplexed dendrimer ligand, inducing the increase of intensity with lower concentrations of cTDNA.

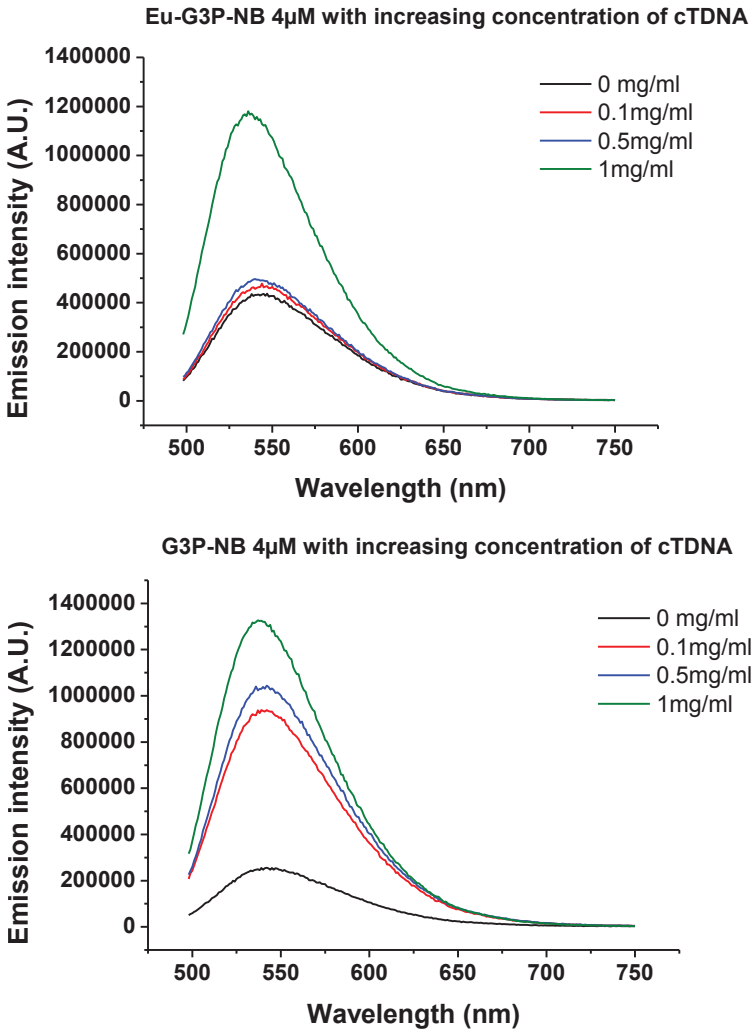

Figure 4.14. Emission spectra of Eu-G3P-NB (top) and G3P-NB (bottom) in presence of increasing concentration of cTDNA showing the increase of emission intensity in presence of DNA.

The presence of interactions taking place between naphthalimide groups and cTDNA (1 mg/ml) was tested on biotin and amino free dendrimers ligands and their respective Eu^{3+}complexes. The increase factors of emission intensities are reported in the table 4.2 for each of the tested dendrimers. The presence of cTDNA in dendrimer solutions results in a significant increase of their emission intensity. In respect to the biotin dendrimer, the increase is more important for G3P-NB (5.5 times) that for Eu-G3P-NB (3 times). These results are consistent with the hypothesis that we have made previously of the higher rigidity induced by lanthanide coordination reducing their abilities for cTDNA biding.

The increase of intensities measured on the basis of amino dendrimer (Ln-G3P-NH_2) did not follow the same trend as observed for the system based on the biotine dendrimer (3.5 times for Eu-G3P-NH_2 and 3 times for G3P-NH_2). According to its hypothesized tridimensional structure, naphthalimide groups are well exposed in the extremities of the dendrimers and can

easily create interaction with DNA. Therefore, the increase of the emission signal of amino dendrimer (Ln-G3P-NH_2) in presence of cTDNA should be more important than for the corresponding biotin dendrimer as it is less soluble in water. If it starts to aggregates after dilution in aqueous cTDNA solution, naphthalimide groups will be less accessible and this situation can explain the smaller increase of intensity than expected.

Table 4.2. Values of increase of 1,8-naphthalimide emission intensity in presence of 1 mg/ml of cTDNA for biotin and amino dendrimers as free ligand or coordinated with Eu^{3+}.

Dendrimers (4 µM)	Increase of emission intensity in presence of cTDNA (1 mg/ml)
Eu-G3P-NB	3x
G3P-NB	5.5x
Eu-G3P-NH_2	3.5x
G3P-NH_2	3x

The emission intensity of Eu^{3+} increases with a factor of almost 2 times in presence of 1mg/ml of cTDNA (Figure 4.15).

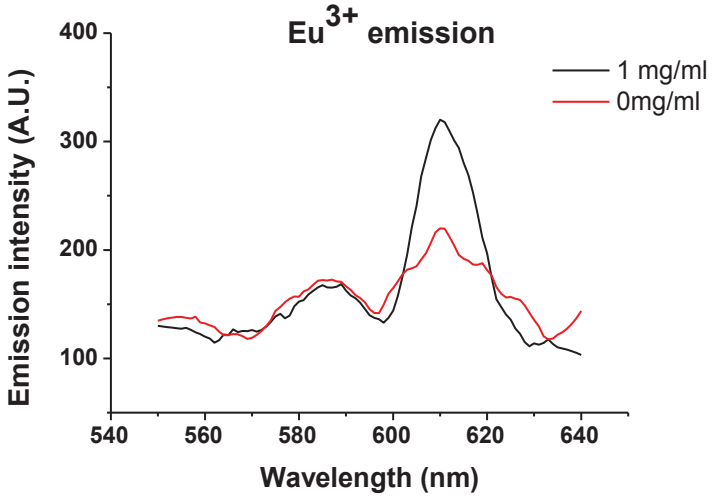

Figure 4.15. Emission spectra of Eu-G3P-NB solutions (4µM in water) showing band corresponding to the Eu^{3+} transitions in presence or not ofcTDNA.

These experiments indicate that1,8-naphthalimide emission increases significantly in presence of cTDNA and that the transfer to the lanthanide is enhanced.

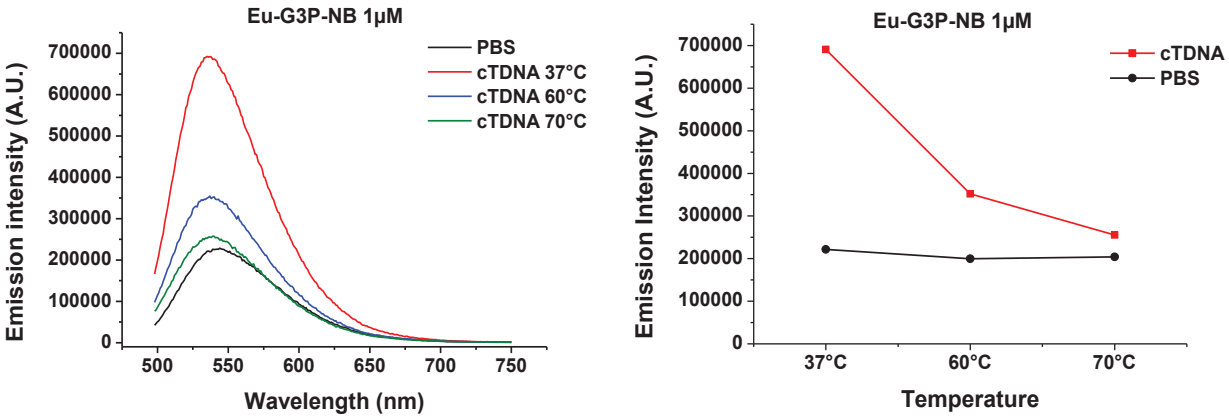

Figure 4.16. Plots showing the effect of the double strands dissociation on Eu-G3P-NB emission intensity. Left: overlay of emission spectra in PBS and with 1mg/ml of cTDNA at different temperature.

Braña has described the 1,8-naphthalimide group as being as able to bind with double strand of DNA.

A very simple experiment was realized to observe the effect of double strand dissociation on dendrimer emission intensity by increasing the temperature (Figure 4.16). At 37°C, same temperature as used for cell culture, the naphthalimide of Eu-G3P-NB emission increases with 1mg/ml of cTDNA in comparison to what is observed for the PBS solution. When the temperature is raised, the emission intensity remains stable in PBS while it decreases in presence of cTDNA and tends to return to the initial intensity in absence of cTDNA. These results confirm the fact that the emission of the 1,8-naphthalimide group increases only in presence of cTDNA and that it interact with the double strands of DNA.

4.3-Discussion-Conclusion

To summarize the surprising phenomenon described in this chapter: when dendrimers lanthanide complexes loaded-cells are illuminated with blue light, the intensity of their emission signal increases dramatically and rapidly. The majority of the luminescence signal is located in the nuclei of cells. The maximum of intensity signal is reached after 5 minutes of illumination with blue light. This increase of signal is so important that it is not contained in the dynamic range of the camera (1:3000), rendering the quantification difficult.

If the illumination continues, cells start to form vesicles which emit also a strong emission signal. When these vesicles burst, the emission signal decreases significantly.

In this chapter, different experiments were described to attempt to explain the phenomenon.

Microscopy experiments were repeated with different dendrimers (amino and biotin complexed or not with different lanthanide cations). A similar phenomenon was observed, with more or less intensity depending with the dendrimer concentration inside the cells, which has allow us to conclude that the 1,8-naphthalimide chromophore moiety was involved and not the remaining part the dendrimer structure.

The necessity to have an active cell metabolism to observe the emission increase has led to a the idea of a response to ROS species production under blue light illumination.

Experiments have confirmed the induction of ROS production under illumination conditions, but it is not sufficient to quantitatively explain the strong increase of luminescence observed in cells.

Dendrimers possess a sensitivity to the UV and blue light illumination (the same experiments were realized with 377/25 nm illumination wavelength with the same results). At the present moment, we are not able to fully explain the important light effect on dendrimer which induced an increase of emission intensity. This change occurring without shift in wavelength and appears to be reversible.

In vitro experiments have demonstrated that the increase of emission intensity is also partially induced by DNA interaction. Agarose gel electrophoresis was performed to confirm the interaction between DNA and dendrimers (data not shown) but the difficulty of migrating the described dendrimer derivatives on gels involves focusing more the experimental conditions. Interactions will have to be demonstrated by other independent techniques and if electrophoresis will not success, surface plasmon resonance analysis (Biacore) could be investigated and could allow to determine affinity constant between the dendrimers and the DNA.

All the *in vitro* experiments have raised tracks for beginning to explain this multifactorial phenomenon.

The illumination of cells leads to oxidative stress which will trigger lysosomes release. Once in the cytoplasm, dendrimers go to the nucleus and interact with DNA leading to a strong increase of the emission intensity.

An important question remains: how the dendrimer can be released from the lysosome under illumination? And how can it go to the nucleus and pass through the nuclear membrane?

Polyamidoamine (PAMAM) dendrimers are used for gene transfer as cationic polymers (see chapter 3). Their structure can help for DNA condensation, for endosomal release and to protect DNA from lysosomal degradation (Tekade, Kumar *et al.* 2009). For this type of application, the dendrimer is internalized by endocytosis and will go through the endocytosis pathway: early endosomes, later endosomes and lysosomes. The DNA has to be released from later endosomes or lysosomes to go in the nucleus before being degraded in the proteasome. Protonated residues on dendrimers may provide endosomal/lysosomal release. Indeed, the protonation of polymers in the acidic pH of endosomes/lysosomes destabilize the membranes and allow the release towards the cytoplasm.

In the present case, the lysosomes release cannot be explained only by dendrimer protonation. In fact, without illumination, dendrimers remains in lysosomes. The release is observed only under illumination. We can hypothesize that the stress induced by illumination (combined or not with dendrimer protonation) generates the destabilization of the lysosome membrane destabilization which allow the crossing to the nucleus.

PAMAM dendrimers are often referred to as "artificial proteins") (Weyermann, Gisselbrecht *et al*. 1999; Hecht and Frechet 2001; Svenson and Tomalia 2005). Dendrimer of high generation (G6) have been observed has "histone mimic" to condensate the DNA. Even if the dendrimers used in this work are of lower generation (G3), the addition of chromophores and/ or biotin group increase their size and can be compared to higher generation PAMAM dendrimers. These information are in favor of the hypothesis of the amino/biotine dendrimer interaction with DNA inside the nucleus even if the DNA is highly condensed in cells nuclei.

The exploration of the different parameters causing this huge increase of emission intensity needs to be continued as the current step by step investigation can explain a fraction of the observed change of intensity during the initial microscopy experiment. These interesting mechanisms need to be understood to control the parameters and consider potential applications such as photodynamic therapy against cancer cells under blue light exposition.

References

- Brana, M. F. and A. Ramos (2001). "Naphthalimides as anti-cancer agents: synthesis and biological activity." Curr Med Chem Anticancer Agents**1**(3): 237-255.
- Duke, R. M., E. B. Veale, *et al*. (2010). "Colorimetric and fluorescent anion sensors: an overview of recent developments in the use of 1,8-naphthalimide-based chemosensors." Chem Soc Rev**39**(10): 3936-3953.
- Hecht, S. and J. M. Frechet (2001). "Dendritic Encapsulation of Function: Applying Nature's Site Isolation Principle from Biomimetics to Materials Science." Angew Chem Int Ed Engl**40**(1): 74-91.
- Svenson, S. and D. A. Tomalia (2005). "Dendrimers in biomedical applications--reflections on the field." Adv Drug Deliv Rev**57**(15): 2106-2129.
- Tekade, R. K., P. V. Kumar, *et al*. (2009). "Dendrimers in oncology: an expanding horizon." Chem Rev**109**(1): 49-87.
- Weyermann, P., J. P. Gisselbrecht, *et al.* (1999). "Dendritic Iron Porphyrins with Tethered Axial Ligands: New Model Compounds for Cytochromes." Angew Chem Int Ed Engl**38**(21): 3215-3219.
- Wolfbeis, O. S., A. Durkop, *et al*. (2002). "A europium-ion-based luminescent sensing probe for hydrogen peroxide." Angew Chem Int Ed Engl**41**(23): 4495-4498.

Résumé Français

Le chapitre 4 rapporte un phénomène inattendu observé au microscope sur des cellules HeLa ayant internalisé le dendrimère Eu-G3P-NB. Dans un souci de clarté, il a paru préférable de présenter ces résultats séparément, même s'ils concernent les dendrimères luminescents précédemment décrit.

Lorsque des cellules HeLa ayant été incubées 24h avec le dendrimère Eu-G3P-NB sont exposées de façon continue à la lumière bleue du microscope (λ_{ex}: 485/20 nm), l'intensité de fluorescence émise par le dendrimère (λ_{em}: 525/50 nm) augmente considérablement. Au départ, le signal de fluorescence des dendrimères est localisé au niveau des lysosomes (comme décrit dans le chapitre 3), mais lorsque les cellules sont illuminées sans interruption à la lumière bleue, un intense signal apparait au niveau des noyaux cellulaires avec un maximum d'intensité atteint après 5 minutes d'illumination. Si l'exposition à la lumière se poursuit, des vésicules émettant un signal intense vont se former (environ 10 minutes après le début de l'illumination). Sous l'effet de la lumière, ces vésicules vont grossir puis éclater au bout d'une quinzaine de minutes entraînant la disparition du signal de fluorescence au niveau des cellules.

Cette cinétique peut être découpée en 3 étapes en fonction de l'illumination continue à la lumière bleue:

- augmentation du signal d'émission accompagnée de l'apparition d'un signal intense dans le noyau
- formation de vésicules émettant un fort signal de fluorescence
- disparition du signal de fluorescence associée à l'éclatement des vésicules.

Le même phénomène a été observé avec les dendrimères G3P-NB, G3P-NH_2 ainsi que les complexes Eu-G3P-NB, Eu-G3P-NH_2 et Yb-G3P-NB, indiquant l'implication du chromophore 1,8-naphthalimide dans le processus et non celle des groupes NH_2 ou biotines exposés à la surface des dendrimères. De plus, seules les longueurs d'onde absorbées par le chromophore (UV et bleue) induisent une augmentation d'intensité de fluorescence dans les cellules.

La formation des vésicules est induite par l'exposition prolongée à la lumière bleue puisque le même type de vésicules a été observé sur des cellules non traitées. Elles sont probablement

associées à une mort des cellules qui ne survivent pas à 10 minutes d'illumination à la lumière bleue.

La dernière étape du phénomène (lorsque les vésicules éclatent et que le signal disparait) s'explique par le fait que les dendrimères sont re-largués dans le milieu extracellulaire. Les spectres d'émission des dendrimères Eu-G3P-NB et Eu-G3P-NH_2ont été retrouvés dans le surnageant de cellules après 15 minutes d'illumination.

Le stress oxydatif induit par la lumière bleue pourrait être à l'origine de l'augmentation de signal observée dans les cellules. Pour vérifier cette première hypothèse, la production de ROS (« ReactiveOxygenSpecies ») a été évaluée après 5 minutes d'illumination à la lumière bleue grâce à l'utilisation d'un marqueur fluorescent spécifique. Les résultats confirment la production de ROS induite par l'illumination mais celle-ci ne suffit pas à expliquer l'augmentation d'intensité observée.

La lumière semble avoir un effet sur les dendrimères eux-mêmes. En effet, une augmentation de l'intensité d'émission du chromophore 1,8-naphthalimide a été observée sur les dendrimères G3P-NB, leurs complexes Eu^{3+} et Yb^{3+} et le dendrimère Eu-G3P-NH_2en solution. L'intensité d'émission augmente jusqu'à atteindre un plateau après avoir reçu 150 J/cm² de lumière bleue. De plus, ce phénomène est réversible. Après une illumination, l'intensité augmente puis diminue progressivement au cours du temps jusqu'à revenir à son niveau initial, une seconde illumination augmente à nouveau l'intensité d'émission du chromophore.

L'apparition d'un signal nucléaire dans les cellules après quelques minutes d'illumination recoupées avec les données de la littérature décrivant la famille des naphthalimides comme des agents intercalants de l'ADN ont conduit à l'hypothèse d'une interaction entre les dendrimères et l'ADN. Les dendrimères Ln-G3P-NH_2 et Ln-G3P-NB sont constitués de 32 groupements dérivés de 1,8-naphthalimide attachés aux extrémités des branches des dendrimères. Cependant la structure tridimensionnelle de ces molécules ainsi que la présence de biotines substituées sur les naphthalimides peut être limitante pour une interaction avec l'ADN des cellules.

Des mesures spectrofluorimétriques ont montré *in vitro* que l'interaction entre les dendrimères et l'ADN induit une augmentation de l'intensité d'émission du 1,8-naphthalimide. Le dendrimère G3P-NB réagit avec les plus petites concentrations d'ADN testées (0.1mg/ml) alors que le complexe Eu-G3P-NB réagit à partir de 1mg/ml d'ADN. De plus, l'augmentation d'intensité est plus élevée pour G3P-NB (5.5 fois) que pour Eu-G3P-NB (3 fois). Ces résultats

s'expliquent par le fait que le dendrimère devient plus rigide lorsqu'il est complexé à un lanthanide, rendant l'accessibilité des groupes naphthalimide plus difficile pour interagir avec l'ADN.

En résumé, lorsque des cellules ayant internalisé les dendimères Ln-G3P-NB ou Ln-G3P-NH_2 sont illuminées de façon continue à la lumière bleue sous le microscope, le signal d'émission de fluorescence augmente drastiquement (avec un maximum atteint après 5 minutes) et passe des lysosomes aux noyaux des cellules. Après 10 minutes d'exposition, des vésicules fluorescentes se forment et vont finir par éclater entrainant une diminution du signal dans les cellules.

Dans ce chapitre, une série d'expériences a permis d'analyser et mettre en évidence différents points essentiels dans la compréhension de ce phénomène. La production de ROS, l'exposition à la lumière des dendrimères en solution ainsi que l'interaction avec l'ADN induisent une augmentation de l'intensité d'émission du chromophore 1,8-naphthalimide. D'autres expériences seront nécessaires pour relier ces phénomènes et expliquer le mécanisme observé dans les cellules.

5- General conclusion and perspectives

Biology and medical imaging show an exponentially increasing interest for fluorescence because of its high sensitivity, spatial and temporal resolution at the cellular level, multiple detection capabilities by simultaneous use of several complementary probes, low cost, versatility and portability. Moreover, this technique requires reagents to ensure detection but in comparison to MRI, only small quantities of such imaging agents are required for the visualization of molecular events occurring at the single cell level and/or at the whole organism. In contrast to radioactive reagents used for nuclear imaging techniques such as PET or SPECT,optical probes exhibit non-ionizing radiation, do not need to be used in a short period of time and manipulated using special precautions.

Actually the main challenge is the development of fluorescent/luminescent probes that are able to detect non-ambiguously specific entities or events in a real-time. Biological systems are by nature a mixture of a broad variety of molecules and many of themare fluorescent which create a strong autofluorescence background. Many of commercially available fluorophores used today need to have very high quantum yields in order to overcome the autofluorescence signal (which is typically subtracted from the microscopy images).

In this work, another strategy was used to open new possibilities aiming at using NIR photons arising from lanthanide cations coordinated and sensitized in nanosized complexes for biological imaging in living cells and small animals. As biological systems possess reduced or no autofluorescence in the NIR, the only signal that can be observed originates from the lanthanide luminescent agents, providing a good signal to noise ratio and a good detection sensitivity. Due to this absence of background, images obtained from NIR fluorescence will not need to be treated for background subtraction. A key requirement for the use of lanthanide cations is to sensitize them using an appropriate chromophoric sensitizer.

The ideal NIR lanthanide-based imaging agent should emit a large number of photons, and should not be sensitive to photobleaching for a long time or under repeated experiments. To avoid disturbing the biological studied system, it needs to be non-toxic, should have sufficiently long blood circulation time to reach a target and should nevertheless be excreted in a reasonable amount of time.

The limitation of current NIR emitting lanthanide complexes described in the literature are the relatively modest values of quantum yields. We have based this work on the hypothesis that a major increase in NIR detection sensitivity can be obtained by using luminescent imaging

agents that are able to emit a large number of photons per unit volume. This idea can be tested by creating chemical species that possess a high density of chromophoric absorbers and lanthanide ions per unit volume.
More specifically, to test this hypothesis, two species that are very different in from a chemical point of view have been chosen: i) polymetallic lanthanide dendrimer complexes and ii) nano-Metal Organic-Frameworks.

One principal advantages of lanthanide MOFs in which both the lanthanides and the antenna are part of the well-defined structure that can be determined. In particular, antenna are located at a controlled distance and angle to the lanthanide cations that they sensitize. The nanoscale compound is formed through a one-pot synthesis that represents a major advantage and gives a possibility to obtain rapidly large quantity of nanoparticules.

The physical and photophysical characterization of nano-MOFs Yb-PVDC-3 has shown that this novel type of nanomaterial possess a crystalline structure that can be characterized with X-ray diffraction. It has been established that this nanoMOFs is able to sustain aqueous solution as well as more aggressive exposition to cell lysate without losing its luminescence properties as an indication that the chromophore to lanthanide energy transfer is maintained. We have also demonstrated in this work that Yb-PVDC-3 is not affected by photobleaching in aqueous solution. This point is important as it is often a major limitation for the use of NIR-emitting organic fluorophores in the biological world.

The reverse emulsion synthesis used to produce the nano-Yb-PVDC-3 has been efficient to obtain crystalline nanoparticles able to enter cells without modification of their surface.
The location inside of the cells has been proven by two independent techniques: confocal microscopy and ICP technique. Cytotoxicity analysis has shown that these systems can be used at a concentration that allows good detection sensitivity without generating toxicity. We have demonstrated that by the formation of this nanoscale polymetallic system, it is possible to take advantage of the NIR emission properties of lanthanide cations for cellular imaging. Experiments in this PhD thesis report for the first time the use *in cellulo* and/or *in vivo* of a luminescent reporter based on a NIR emitting lanthanide for a traditional microscopy single photon source. This is therefore a demonstration of a major importance in the field of

lanthanide coordination chemistry and spectroscopy as well as in the field of biological imaging.

In this work, it has also been shown that nano-Yb-PVDC-3 presents some drawbacks, starting with its UV excitation wavelength, which makes it less attractive for *in vivo* imaging. In addition to the damages induced by UV light, subcutaneous implants of nano-Yb-PVDC-3 were not detectable *in vivo* even with long exposition time. This limitation can be explained by the high UV light absorbance and diffusion into tissues.

Due to their crystalline structure, nano-MOFs integrity can be easily followed by X-ray diffraction analysis. Particularly interesting, it will allow determining evolution of the nano-MOFs structures after cellular uptake. Experiments are in progress to determine crystalline phase of nano-Yb-PVDC-3 on a cell pellet after incubation with the nano-MOFs (collaboration with the Argonne synchrotron in USA) and to observe nano-MOFs crystals by TEM on a nano-Yb-PVDC-3-loaded cell slice.

The actual miniaturization process of nano-Yb-PVDC-3 through the use of reverse emulsion does not allow producing nanoparticles of ideal sizes for cellular imaging and their actual size may constitute a limitation. As the next step of this project, it will be important to decrease of the size of the nano-MOFs in order to induce a higher cellular uptake.

Another perspective of this project is the surface coating of the nanoparticles to achieve specific biological targeting.

The luminescent lanthanide dendrimer complexes derived from the generation-3 polyamidoamine naphthalimide dendrimers studied in this work, Ln-G3P-NH_2 and Ln-G3P-NB, have been obtained by reacting of eight equivalent of lanthanide nitrate with one equivalent of the ligand. In contrast to the nano-MOFs the overall structure of Ln-G3P-NH_2 and Ln-G3P-NB is less rigid since lanthanide cations are wrapped by dendrimer branches possessing coordinating groups.

In a similar way to the work conducted with the nano-MOFs, we have fully characterized these systems beside the crystals structure. In respect to biological imaging, we have been able to obtain promising results confirming the possibility of using lanthanide-based dendrimers as luminescent probes not only *in cellulo* but also *in vivo* through a non-invasive imaging experiment. Even thought the chromophores has not an optimized excitation wavelength yet, we have demonstrated that we could detect the signal in the NIR range through the skin of a living mouse under 488 nm excitation.

The advantages of this system, like a highly efficient cellular uptake combined with a strong brightness of Ln-G3P-NB have been evidenced.
Emission wavelength can be tuned according the lanthanide chosen, without changing dendrimer behavior and using the same organic ligand (requiring no additional synthesis), as a function of the imaging experiment to conduct, with the help of the 1,8-naphthamilide which can sensitize several lanthanide cations (Eu^{3+}, Yb^{3+}, Nd^{3+} have been tested so far).
The limitations that have been observed for this dendrimer system is the presence of residual 1,8-naphthalimide emission in the NIR that overlap with the $Yb^{3+/}Nd^{3+}$ signal in the Ln-G3P-NH_2 and Ln-G3P-NB complexes. This may limit the ability to discriminate the signal of the lanthanide from the background. As a strategy to overpass this limitation, we could modify the structure of the dendrimer to decrease the number of chromophores or choose a different lanthanide sensitizer with no NIR emission. Another drawback of 1,8-naphthalimide-based dendrimers originates from their sensitivity to light illumination and ability to interact with DNA.

The two polymetallic systems, dendrimers and nanoMOFs, possess common advantages, they combine a large number of chromophores and lanthanide ions within relatively well defined architectures allowing to increase the number of emitted photons per unit volume). With these two independent chemical systems we have created for the first time a strong evidence that the limitation of low quantum yields of lanthanide complexes emitting in the NIR can be overcome and that they can be used in biological imaging experiments in cells and in small animals.

Both systems are versatile with the possibility to tune excitation and emission wavelengths by changing the nature of the chromophore and/or the nature of the lanthanide to be more adapted to desired applications.

Nano-MOFs and luminescent dendrimers can be functionalized for a specific targeting and efficient diagnostic. As examples of strategies, the surface of the nanoMOFs or the termini of the dendrimer can be modified by coupling with specific peptides (RGD), antibodies, or other targeting agents. The biotin terminated dendrimer complexes Ln-G3P-NB investigated in this work can not only be directly coupled with a streptavidin-antibody linkage but the termini can also be modified to keep the small size of the nanoparticles. In addition, an importance of sufficient water solubility has been demonstrated for dendrimer complexes. This is the reason

why the terminal groups of the dendrimer have to be modified to meet this requirement. As an example, experiments are in progress to synthesize a new dendrimer (with the same chromophore) possessing terminal folic acid groups able to target folate receptors overexpressed at the surface of some tumor cells.

Moreover, nano-MOFs and naphthalimide-lanthanide dendrimers can both be potentially used as drug carrier. It would be interesting as a perspective of this work to take advantage of their luminescent properties to monitor the release of drugs in order to create a new generation of theranostics agents. The nano-Yb-PVDC-3 network delivers its luminescent properties and the porous cavity remains available for a drug loading. Numerous molecules of interest can be considered, and even some more tricky such as the hydrophobic anticancer drugs (i.e. paclitaxel) to simultaneously treat tumor and follow its evolution by fluorescence imaging.

The cavities of the Ln-G3P-NB dendrimer complexes can not be loaded with therapeutic molecules due to the presence of lanthanide. However, G3 dendrimers possess 32 terminal surface groups. Some of these groups can be modified by covalent attachment of therapeutic molecules and the remaining groups with a specific targeting agent. As an example, we could imagine and synthesize a “Janus dendrimer” carrying targeting motif (folic acid or RGD peptide) in one half of the branch termini and the second half being decorated with pH activated drug which will be specifically released/activated in acidic and/or reducing tumor microenvironment.

Résumé Français

La grande sensibilité et l'excellente résolution spatio-temporelle de la fluorescence attire de plus en plus le monde de l'imagerie médicale.

A l'heure actuelle le principal challenge est de mettre au point des sondes fluorescentes/luminescentes capables de détecter de façon non ambigüe un événement donné. La sonde idéale devra, en plus d'être spécifique, résister au photoblanchiment et posséder des longueurs d'ondes d'excitation et d'émission dans le proche infrarouge pour une détection de signal plus en profondeur, sans autofluorescence des tissus.

Dans le but de s'approcher du modèle idéal, nous proposons ici de combiner les nombreux avantages des lanthanides avec les propriétés intéressantes des nano-objets que sont les dendrimères PAMAM et les nano-MOFs.

Comme précédemment décrit, ces deux familles de molécules ont été testées afin d'améliorer la sensibilité de détection par augmentation du nombre de chromophores et de lanthanides par unité de volume. Les composés obtenus ont montré leur efficacité pour sensibiliser les cations lanthanides ainsi que leurs efficacités en tant que rapporteurs luminescents proche infrarouge *in cellulo* (et *in vivo* pour les dendrimères).

La caractérisation des nano-MOFs Yb-PVDC-3 a montré leur grande stabilité ainsi que la conservation du transfert d'énergie au lanthanide dans différents milieux. La synthèse des nano-MOFs en une étape est un avantage majeur car elle permet d'obtenir rapidement de grandes quantités de produit.

Malgré ses nombreux avantages, le nano-MOFs présente des inconvénients à commencer par sa longueur d'onde d'excitation dans l'UV qui le rend inapproprié pour de l'imagerie *in vivo*. Sa taille importante peut également être limitante pour une utilisation à l'échelle cellulaire.

Les dendrimères Ln-G3P-NB/NH_2 dérivés de polyamidoamine de génération 3 ont montré des résultats très prometteurs pour des applications en imagerie proche infrarouge *in cellulo* et *in vivo*. Leur efficacité permet d'utiliser de faibles concentrations n'induisant aucune cytotoxicité tout en ayant un fort signal d'émission proche infrarouge dans les cellules. Le chromophore est actuellement la principale limitation de ce système à cause de sa longueur d'onde d'excitation qui n'est pas idéale et surtout à cause de sa sensibilité à la lumière (encore non complètement expliquée à ce jour) et de son action en tant qu'agent intercalant de l'ADN.

Les deux systèmes présentent l'avantage commun d'avoir des structures parfaitement définies et maîtrisées qui permettent d'accroitre le nombre de photons émis par unité de volume, augmentant ainsi la sensibilité de détection et s'affranchissant des rendements quantiques

faibles dans le proche infrarouge. Ils offrent également la possibilité d'adapter les longueurs d'ondes d'excitation et d'émission en fonction des besoin expérimentaux (en changeant le chromophore et/ou le lanthanide).

La preuve de principe a été établie que les nano-MOFs et dendrimères peuvent être utilisés comme rapporteurs luminescents dans le proche infrarouge.

Couplés à des agents ciblants efficaces (RGD, acide folique, anticorps..), ces composés peuvent être utilisés pour des applications de théragnostique. Des molécules thérapeutiques anti-cancéreuses type paclitaxel peuvent être incorporées dans les pores des MOFs. La surface des 32 branches des dendrimères de génération3 peut être fonctionnalisée par l'accroche de molécules ciblantes d'une part et de molécules thérapeutiques d'autre part (par exemple, une drogue pH-activable qui serait libérée dans l'environnement tumoral acide).

Appendix

Appendix 1. Synthesis of Yb-PVDC-3 and nano-Yb-PVDC-3.

In a glass vial (20 mL), a solution of 4,4'-(1*E*,1'*E*)-2,2'-(2,5-dimethoxy-1,4-phenylene)bis(ethene-2,1-diyl)dibenzoic acid (H_2-PVDC) (86.0 mg, 0.20 mmol) in DMF (4.0 mL) was added to a solution of $Yb(NO_3)_3 \cdot 5H_2O$ (22.5 mg, 0.05 mmol) in DMF (1.0 mL) and HNO_3 (1 mL, 1 M aq) to produce a neon green solution. The vial was capped and placed in a 105 ˚C isotemp oven for 12 hours to produce yellow crystalline needles of the product. The crystals were collected, washed with DMF (4 x 5 mL), and air dried (29.7 mg, 61.8%).
EA Calcd. (%) for $Yb_1(C_{26}H_{20}O_6)_{1.5}(DMF) \cdot 0.65$ DMF, H_2O: C, 55.31; H, 4.60; N, 2.42. Found: C, 54.87; H, 4.22; N, 2.51. EA. Calcd. (%) for the water exchange product, $Yb_1(C_{26}H_{20}O_6)_{1.5}(H_2O)_2 \cdot (DMF)_{0.25}(H_2O)_{2.25}$: C, 52.43; H, 4.46; N, 0.38. Found: C, 52.12; H, 3.68; N, 0.30. FT-IR (KBr 4000-700 cm^{-1}): 3424 (br), 3054 (w), 2998 (w), 2936 (w), 2830 (w), 1665 (DMF C=O, m), 1601 (m), 1544 (m), 1413 (COO^-, vs), 1338 (w), 1260 (w), 1211 (s), 1181 (m), 1108 (w), 1044 (s), 965 (m), 861 (w), 779 (trans C=C-H, s), 709 cm^{-1}(w).

The synthesis of nano-Yb-PVDC-3 procedure is based on previously reported reverse microemulsion nanoMOF syntheses (Rieter, Taylor *et al*. 2006; Rieter, Taylor *et al*. 2007; Taylor, Rieter *et al*. 2008). The methylammonium salt of the H_2-PVDC ligand (PVDC-$(NH_2CH_3)_2$) was prepared by dissolving H_2-PVDC in methylamine, removing the solvent under reduced pressure, and adding a known amount of water to achieve the desired concentration. A 0.05 M solution of CTAB was prepared by dissolving CTAB in a 9:1 (v/v) ratio of heptane/hexanol and stirring for 30 minutes. A w = 10 (where w is the H_2O/CTAB molar ratio) reaction mixture was prepared as follows. A solution of $YbCl_3 \cdot 6H_2O$ (225 µL, 0.05 M in H_2O) was added to a flask containing the CTAB mixture (25 mL, 0.05 M in heptane/hexanol). A solution of PVDC-$(NH_2CH_3)_2$ (225 µL, 0.05 M in H_2O) was added to another flask also containing the CTAB mixture (25 mL, 0.05 M). The flasks were stirred separately for at least 10 minutes until clear. The $YbCl_3 \cdot 6H_2O$ solution was then added to the PVDC solution and stirred for 24 hours at room temperature. Yellow solid was isolated via centrifugation at 4000 rpm for 30 minutes followed by washing with ethanol (3 x 35 mL).The product was purified by dialysis using a regenerated cellulose membrane (nominal MWCO

3,500; Fisher Scientific; Pittsburgh, PA, USA) in DMSO for three days. The solid recovered from the dialysis membrane was dried in a vacuum oven (40 °C, 40 mbar).

Appendix 2.^{1}H NMR of digested Yb-PVDC-3.

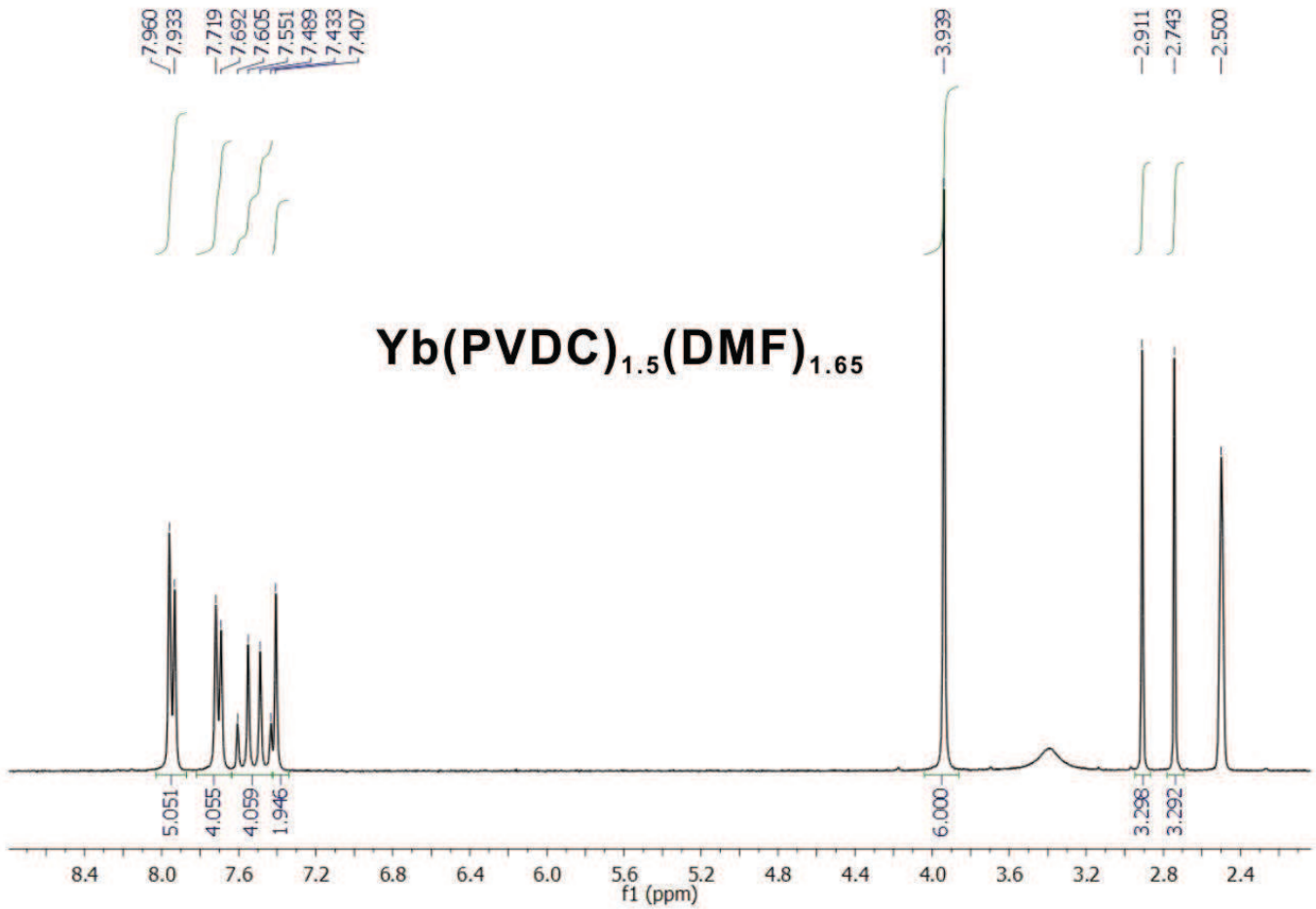

Approximately 5 mg of as-synthesized Yb-PVDC-3 was first dried under argon flow and then dissolved in 0.65 ml d_6-DMSO and 3 µl concentrate DCl mixture.Proton nuclear magnetic resonance spectra (^{1}H-NMR) were collected on Bruker Avance 300 MHz spectrometers. Chemical shifts are in parts per million using the residual solvent peak as the reference value. The value used for proton spectra is 2.5 ppm for d_6-DMSO.The integration for the six methyl hydrogen atoms in PVDC was set as 6.

Appendix 3: Single Crystal X-ray Diffraction Study for Yb-PVDC3.

An X-ray crystal structure was determined for $C_{42}H_{41}NO_{12}Yb$, **Yb-PVDC-3**, using a single crystal on a Bruker Smart Apex CCD diffractometer with graphite-monochromated MoK_α (λ= 0.71073 Å) radiation. The crystal was mounted in a glass loop with Paratone® N oil and placed in a cold N_2 stream (203 K) for data collection.

Unit-cell parameters and lack of systematic absences indicated Yb-PVDC3 crystallized in triclinic space groups P 1 or P-1; centrosymmetric P-1 was chosen based on E-values and the successful solution and refinement of the structure. Unit-cell dimensions were derived from the least-squares fit of the angular settings of 1373 reflections. Data were corrected for absorption using the Bruker program SADABS[1]. The structure was solved via direct methods, which located Yb and most of the remaining non-hydrogen atoms. Yb was found to be disordered over at least two sites. The two Yb sites are occupied at 56% and 44%. Remaining non-hydrogen atoms were gradually found from several subsequent different Fourier syntheses. All non-hydrogen atoms were refined anisotropically excepting O6, O11, C24, C27, O12, N, C40, C41, C42, O10, C39A, C39B, and O13. A total of 47 restraints were applied to optimize the bond lengths, bond angles, and atomic displacement parameters. Idealized atom positions were calculated for all hydrogen atoms (*d*-(Cmethyl-H) = 0.97 Å, *d*-(Cphenyl-H) = 0.94 Å), *U* = 1.2 *Uiso* of attached carbon). The coordinated DMF seen in other Ln-PVDC isomorphs could not be resolved in this structure, probably because of overlap with the disordered Yb sites.

All computer programs used in the data collection and refinements are contained in the Bruker program packages SMART (vers. 5.625), SAINT (vers. 6.22)[1], and SHELXTL (vers. 6.10)[2].

References

1. APEX II software suite, Bruker-AXS, 2006.
2. Sheldrick GM (2008) A short history of SHELX. *Acta Crystallogr A* 64(1):112-122.

Appendix 4: G3P-NH2 and G3P-NB dendrimer synthesis

The Synthesis of G3P-NH_2 was described in 2011 by Alcala *et al*. (Alcala, Shade *et al*. 2011)

Synthesis of G3P-NB (reported in Dr Hu thesis 2012):

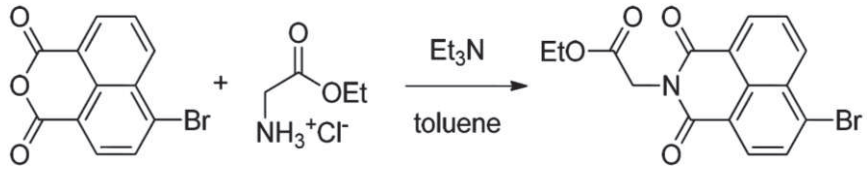

13

6-Bromo-1,3-dioxo-1H-benz[de]isoquinoline-2(3H)-acetic acid ethyl ester (**13**) was synthesized as follows: 4-Bromo-1,8-naphthalic anhydride (3.00 g, 10.8 mmol) and glycine ethyl ester hydrochloride (1.52 g, 10.9 mmol) were suspended in toluene (120 mL) and triethyl amine (2.2 g, 22 mmol) was added. The mixture was refluxed for 15 h. The precipitate was filtered off and the residual solution was concentrated *in vacuo* to afford **13** as light yellow solid (3.87 g, 10.7mmol, 99%): 1H NMR (CDCl3, 300 MHz, δ): 8.68 (dd, *J* = 7.2, 0.9 Hz, 1H, Ar H), 8.62 (dd, *J* = 8.4, 0.9 Hz, 1H, Ar H), 8.44 (d, *J* = 7.8 Hz, 1H, Ar H), 8.07 (d, *J* = 7.8 Hz, 1H, Ar H), 7.87 (dd, *J*= 8.4, 7.2 Hz, 1H, Ar H), 4.93 (s, 2H, -C*H2*COO-), 4.25 (q, *J* = 7.2 Hz, 2H,-CH_2CH$_3$), 1.30 (t, *J*= 7.2 Hz, 3H, -CH$_2$CH_3); 13C NMR (CDCl3, 75 MHz, δ): 167.99 (1C), 163.35 (1C), 163.32 (1C), 133.79 (1C), 132.50 (1C), 131.64 (1C), 131.24 (1C), 130.88 (1C), 130.74 (1C), 129.18 (1C), 128.21 (1C), 122.65 (1C), 121.79 (1C), 61.79 (1C), 41.54 (1C), 14.27 (1C); HRMS-EI (m/z): [M]+ calcd for $C_{16}H_{12}NO_4Br$, 360.9950; found, 360.9926.

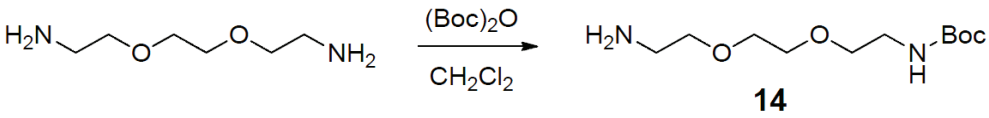

14

N-Boc-1,8-diamino-3,6-dioxaoctane (**14**) was synthesized by a reported method (Song, Ngai et al. 2009) withslight modification as follows: A solution of (Boc)2O (2.25 g, 10.3 mmol) in CH2Cl2 (50 mL)was added dropwise to a solution of 1,8-diamino-3,6-dioxaoctane (10.3 g, 69.7 mmol) in CH_2C_{l2}(70 mL) at 0 °C for 3 h. The reaction mixture was stirred at room temperature for 4 h. Theorganic layer was successively washed with sat. $NaHCO_3$ solution (60 mL), water (2 × 60 mL)and brine (80 mL), dried over anhydrous $MgSO_4$ and concentrated *in vacuo* to afford **14** as acolorless oil (2.26 g, 9.10 mmol, 88%). 1H NMR (300 MHz,

CDCl3, δ): 5.15 (br s, 1H, NH), 3.61(s, 4H, -OC*H*$_2$C*H*$_2$O-), 3.54 (t, 2H, *J* = 5.1 Hz, -OC*H*$_2$-), 3.52 (t, 2H, *J* = 5.1 Hz, -OC*H2*-), 3.31(m, 2H, -C*H2*NHBoc), 2.88 (m, 2H, -C*H2*NH2), 1.73 (br s, 2H, NH$_2$), 1.43 (s, 9H, *tert*-Bu); 13C

NMR (CDCl3, 75 MHz, δ): 155.63 (1C), 78.37 (1C), 72.60 (1C), 69.70 (3C), 41.08 (1C), 39.83 (1C), 27.97 (3C); HRMS-ESI (m/z): $[M^+Na]^+$ calcd for $C_{11}H_{24}N_2O_4Na$, 271.1634; found, 271.1617.

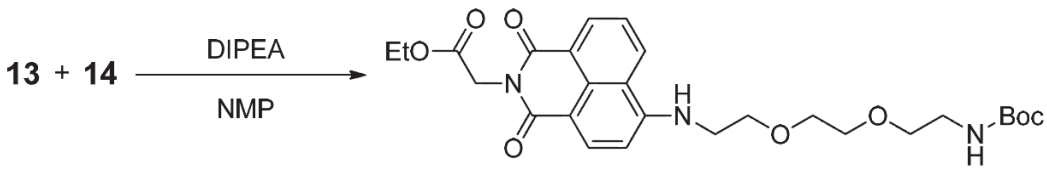

15

Compound **15** was synthesized as follows: Imide **13** (1.41 g, 3.89 mmol) and amine 14(1.96 g, 7.91 mmol) were dissolved in *N*-methylpyrrolidone (NMP, 40 mL). *N*,*N*diisopropylethylamine (DIPEA, 1.04 g, 8.04 mmol) was added and the mixture was stirred for one day at 120 °C. Then water (50 mL) was added and extracted with EtOAc (2 × 100 mL). The organic layer was washed with brine (2 × 75 mL), dried over anhydrous MgSO4, andconcentrated *in vacuo*. The mixture was purified by column chromatography on silica using EtOAc as an eluent to afford **15** as brown solid (1.70 g, 3.21 mmol, 82%): 1H NMR (300 MHz, CDCl3, ·): 8.18 (d, *J* = 7.2 Hz, 1H, Ar H), 8.10 (d, *J* = 8.4 Hz, 1H, Ar H), 7.99 (d, *J* = 8.1 Hz, 1H, Ar H), 7.28 (t, *J* = 7.8 Hz, 1H, Ar H), 6.36 (d, *J* = 8.4 Hz, 1H, Ar H), 6.18 (br s, 1H, NH), 5.15 (br s, 1H, NH), 4.83 (s, 2H, -C*H*$_2$COO-), 4.21 (q, *J* = 7.2 Hz, 2H, -C*H2*CH3), 3.74 (t, *J* = 7.2 Hz, 2H, -OC*H2*-), 3.60 (m, 4H, -OC*H2*C*H2*O-), 3.49 (t, *J* = 7.2 Hz, 2H, -OC*H2*-), 3.41 (m, 2H, - C*H*$_2$NH-), 3.25 (m, 2H, -C*H*$_2$NH-), 1.34 (s, 9H, *tert*-Bu), 1.27 (t, *J* = 7.2 Hz, 3H, -CH$_2$C*H*$_3$); 13C NMR (CDCl3, 75 MHz, ·): 169.20 (1C), 164.17 (1C), 163.39 (1C), 156.02 (1C), 150.07 (1C), 134.42 (1C), 131.06 (1C), 129.37 (1C), 127.06 (1C), 124.29 (1C), 121.58 (1C), 119.96 (1C), 108.67 (1C), 103.85 (1C), 79.21 (1C), 70.27 (1C), 70.22 (1C), 70.07 (1C), 68.62 (1C), 61.50 (1C), 43.03 (1C), 41.10 (1C), 40.23 (1C), 28.33 (3C), 14.15 (1C); HRMS-EI (m/z): [M]+ calcd for $C_{27}H_{35}N_3O_8$, 529.2424; found, 529.2432.

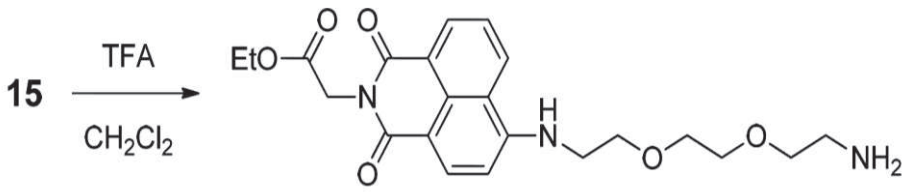

16

Compound **16** was synthesized as follows: Boc-protected amine **15** (0.202 g, 0.382mmol) was dissolved in 5 mL of CH2Cl2 and 5 mL of trifluoroacetic acid was added. The solution was stirred at 0 °C for 30 min and then at r.t. for 30 min. The solvent and trifluoroacetic acid were removed under reduced pressure. The residue was dissolved in 5 mL of CH_2C_{l2} and washed with sat. Na_2CO_3 solution (5 mL) and brine (5 mL), dried over anhydrous MgSO4, and concentrated *in vacuo* to afford **16** as brownish yellow solid (0.139 g, 0.325 mmol, 85%): 1H NMR (300 MHz, CDCl3, ・): 8.52 (d, *J* = 7.2 Hz, 1H, Ar H), 8.40 (d, *J* = 8.4 Hz, 1H, Ar H), 8.26 (d, *J* = 8.4 Hz, 1H, Ar H), 7.57 (t, *J* = 7.8 Hz, 1H, Ar H), 6.65 (d, *J* = 8.4 Hz, 1H, Ar H), 6.20 (br s, 1H, NH), 4.92 (s, 2H, -C*H*$_2$COO-), 4.24 (q, *J* = 7.2 Hz, 2H, -C*H*$_2$CH$_3$), 3.88 (t, *J* = 5.0 Hz, 2H, -OC*H2*-), 3.73-3.66 (m, 4H, -OC*H2*C*H2*O-), 3.61-3.53 (m, 4H, -OC*H*$_2$- and -C*H2*NH-), 2.90 (br s, 2H, -C*H*$_2$NH$_2$), 2.15 (br s, 2H, NH_2), 1.30 (t, *J* = 7.2 Hz, 3H, -CH2C*H3*); 13C NMR (CDCl3, 100 MHz, ・): 169.15 (1C), 164.15 (1C), 163.35 (1C), 150.09 (1C), 134.40 (1C), 131.04 (1C), 129.43 (1C), 127.09 (1C), 124.27 (1C), 121.68 (1C), 120.02 (1C), 108.76 (1C), 103.92 (1C), 72.91 (1C),70.34 (1C), 70.09 (1C), 68.63 (1C), 61.47 (1C), 43.03 (1C), 41.47 (1C), 41.10 (1C), 14.16 (1C);HRMS-ESI (m/z): $[M+Na]^+$ calcd for $C_{22}H_{27}N_3O_6Na$, 452.1798; found, 452.1760.

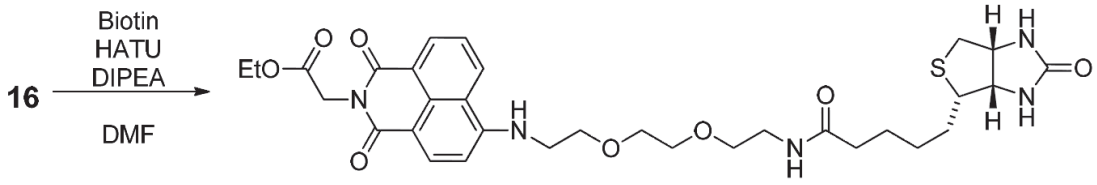

17

Compound **17** was synthesized as follows: Amine **16** (0.0520 g, 0.121 mmol), D-biotin (0.0297 g, 0.122 mmol), HATU (0.0538 g, 0.141 mmol) and DIPEA (0.0371 g, 0.287 mmol) were dissolved in 5.0 mL of DMF. The mixture was stirred at room temperature under N2

atmosphere for 20 h. DMF was removed in vacuo, then the residual solid was triturated to afford **17** as yellow solid (0.0539 g, 0.0822 mmol, 68%): 1H NMR (300 MHz, DMSO-*d6*, ・): 8.76 (d, *J*= 8.1 Hz, 1H, Ar H), 8.46 (d, *J* = 6.9 Hz, 1H, Ar H), 8.28 (d, *J* = 8.4 Hz, 1H, Ar H), 7.93 (br t, 1H, NH), 7.81 (br t, 1H, NH), 7.73 (t, *J* = 8.1 Hz, 1H, Ar H), 6.88 (d, *J* = 8.7 Hz, 1H, Ar H), 6.41 (s, 1H, NH of biotin), 6.36 (s, 1H, NH of biotin), 4.77 (s, 2H, -C*H2*COO), 4.28 (m, 1H, - NHC*H*(CH)CH2-), 4.14 (q, *J* = 7.2 Hz, 2H, -C*H2*CH3), 4.12 (m, 1H, -NHC*H*(CH)CH-), 3.73 (m, 2H, -OC*H2*-), 3.59 (m, 4H, -OC*H2*C*H2*O-), 3.53 (m, 2H, -OCH_2-), 3.38 (m, 2H, -CH_2NH-), 3.16 (m, 2H, -C*H2*NH-), 3.06 (m, 1H, -CHC*H*(CH_2)S-), 2.80 (dd, *J* = 12.5, 5.1 Hz, 1H, -CHCH_2S-), 2.56 (d, *J* = 12.0 Hz, 1H, -CHCH_2S-), 2.04 (t, *J* = 7.5 Hz, 2H, -NHC(=O)C*H*2CH2-), 1.65-1.40 (m, 4H, -NHC(=O)CH_2C$H_2$$CH_2CH_2$-), 1.27 (m, 2H, -NHC(=O)$CH_2$$CH_2CH_2$$CH_2$-), 1.21 (t, *J* = 7.2 Hz, 3H, -CH_2CH_3); 13C NMR (CDCl3, 75 MHz, ・): 172.12 (1C), 168.37 (1C), 163.52 (1C), 162.70 (1C), 162.46 (1C), 151.10 (1C), 134.61 (1C), 131.11 (1C), 129.63 (1C), 129.16 (1C), 124.50 (1C), 121.34 (1C), 120.22 (1C), 107.02 (1C), 104.19 (1C), 69.81 (1C), 69.57 (1C), 69.18(1C), 68.13 (1C), 61.02 (1C), 60.94 (1C), 59.18 (1C), 55.43 (1C), 42.80 (1C), 40.88 (1C), 40.66(1C), 38.40 (1C), 35.09 (1C), 28.19 (1C), 28.03 (1C), 25.26 (1C), 14.07 (1C); HRMS-ESI (m/z):[M+Na]+ calcd for $C_{32}H_{41}N_5O_8SNa$, 678.2574; found, 678.2632.

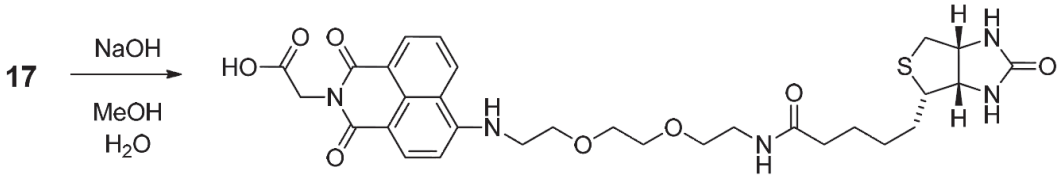

18

Compound **18** was synthesized as follows:: Ester **17** (0.355 g, 0.541 mmol) wassuspended in 20 mL of MeOH. NaOH (0.266 g, 6.65 mmol) was dissolved in 10 mL of water and added to the suspension in MeOH. Upon addition of NaOH, the suspension changed to clear solution. The mixture was stirred at 40 °C for 5 h. The solution was acidified with 7 mL of 1M HCl at 0 °C, and yellow solid was formed. The solid was filtered, washed with cold water, and dried in vacuo to afford **18** (0.286 g, 0.4562 mmol, 84%): 1H NMR (300 MHz, DMSO-*d6*, ・): 12.94 (br s, 1H, -COO*H*), 8.76 (d, *J* = 8.7 Hz, 1H, Ar H), 8.46 (d, *J* = 7.2 Hz, 1H, Ar H), 8.28

(d, *J* = 8.7 Hz, 1H, Ar H), 7.91 (br t, 1H, NH), 7.82 (br t, 1H, NH), 7.72 (t, *J* = 7.8 Hz, 1H, Ar H), 6.87 (d, *J* = 8.7 Hz, 1H, Ar H), 6.41 (s, 1H, NH of biotin), 6.36 (s, 1H, NH of biotin), 4.69 (s, 2H, -C*H*$_2$COO-), 4.28 (m, 1H, -NHC*H*(CH)CH$_2$-), 4.11 (m, 1H, -NHC*H*(CH)CH-), 3.79 (m, 2H, -OC*H2*-), 3.59 (m, 4H, -OC*H*$_2$C*H*$_2$O-), 3.53 (m, 2H, -OC*H*$_2$-), 3.39 (m, 2H, -C*H*$_2$NH-), 3.16 (m, 2H, -C*H*$_2$NH-), 3.06 (m, 1H, -CHC*H*(CH$_2$)S-), 2.80 (dd, *J* = 12.3, 5.1 Hz, 1H, -CHC*H*$_2$S-), 2.56 (d, *J* = 12.3 Hz, 1H, -CHC*H*$_2$S-), 2.04 (t, *J* = 7.4 Hz, 2H, -NHC(=O)C*H*$_2$CH$_2$-), 1.65-1.40 (m, 4H, -NHC(=O)CH$_2$C*H*$_2$CH$_2$C*H*$_2$-), 1.27 (m, 2H, -NHC(=O)CH$_2$CH$_2$C*H*$_2$CH$_2$-); 13C NMR (CDCl3, 75 MHz, ・): 172.14 (1C), 169.75 (1C), 163.56 (1C), 162.72 (1C), 162.55 (1C), 151.02 (1C), 134.53 (1C), 131.03 (1C), 129.62 (1C), 129.10 (1C), 124.48 (1C), 121.48 (1C), 120.22 (1C), 107.18 (1C), 104.14 (1C), 69.81 (1C), 69.59 (1C), 69.18 (1C), 68.13 (1C), 61.03 (1C), 59.18 (1C), 55.45 (1C), 42.79 (1C), 40.87 (1C), 40.51 (1C), 38.41 (1C), 35.11 (1C), 28.21 (1C), 28.05 (1C), 25.28 (1C); HRMS-ESI (m/z): [M+Na]+ calcd for $C_{30}H_{37}N_5O_8SNa$, 650.2261; found 650.2259.

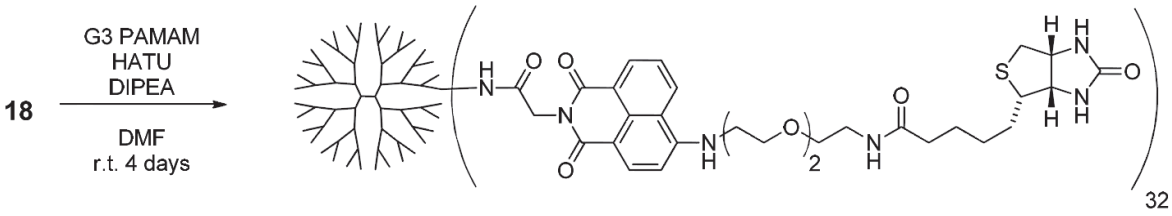

19

Biotin conjugated dendrimer **19** was synthesized as follows: 283.5 mg (4.516 × 10-4 mol)of **18** was added to a solution of 78.90 mg (1.142 × 10-5 mol) of G3 PAMAM dendrimer in 25mL of DMF. 197.9 mg (5.205 × 10-4 mol) of HATU and 300 µL (223 mg; 1.72 × 10-3 mol) of DIPEA were added. The reaction mixture was stirred at room temperature for two days under nitrogen atmosphere while monitoring for the disappearance of G3 PAMAM dendrimer by TLC. The compound was purified by dialysis using a regenerated cellulose membrane (nominal MWCO 12,000-14,000) in DMSO for four days. The solution recovered from the dialysis membrane was dried in a vacuum oven (40 °C, 50 mbar) to yield dendrimer **19** as brown solid (144 mg, 48%).

Appendix 5: Emission intensity variations of Eu-G3P-NB (A.U.) as function of pH

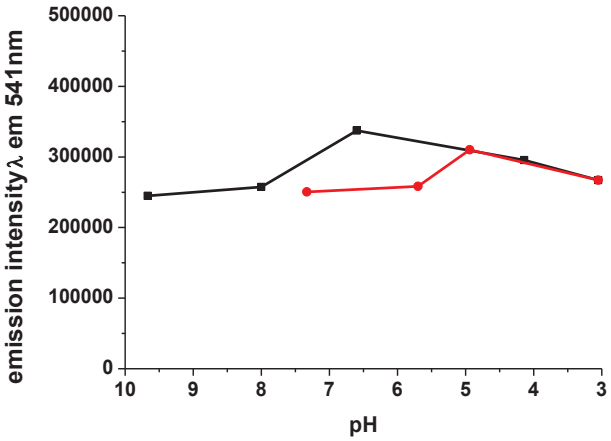

Emission intensity values correspond to the maximum of chromophore emission (550 nm) at different pH during the acidification (black) and the basification (red).

Appendix 6: excitation and emission spectra of Nd^{3+} dendrimers.

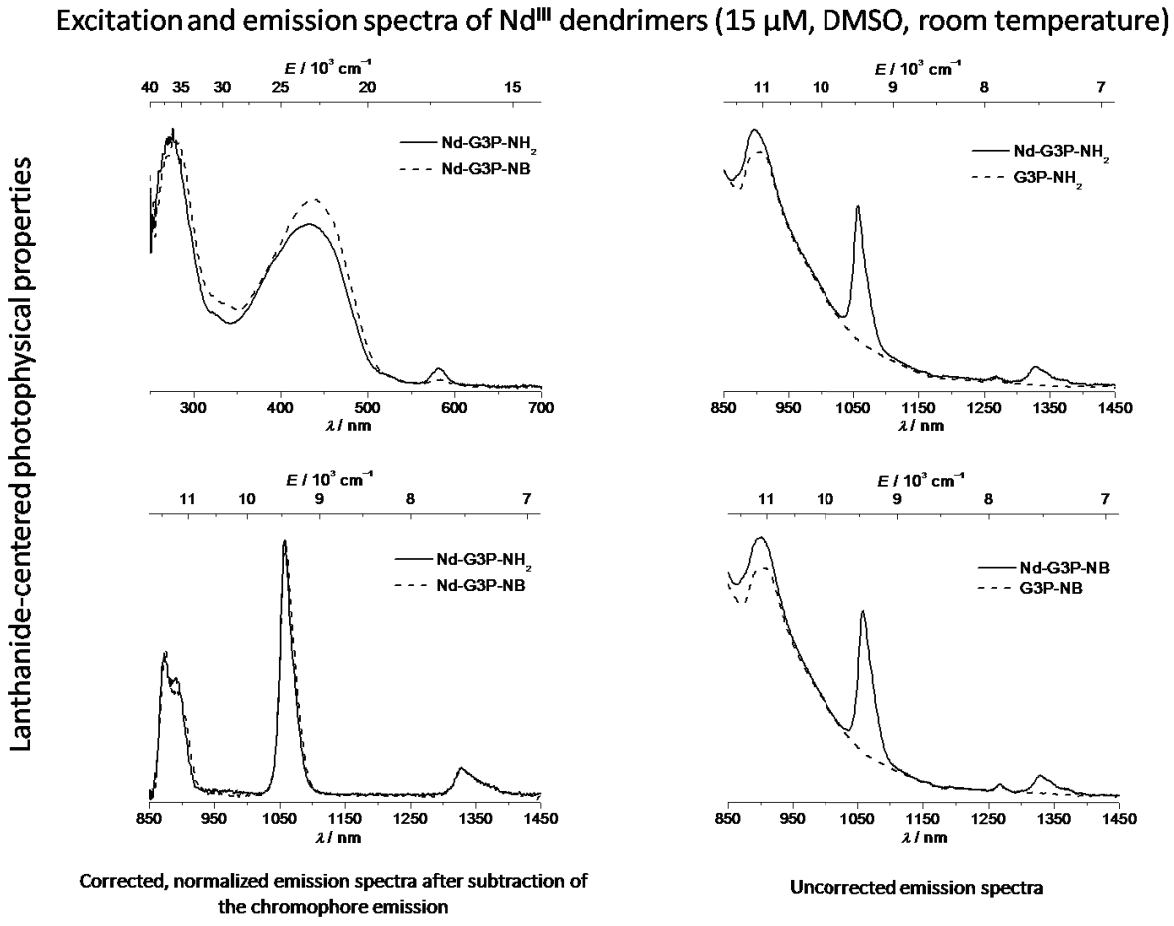

Appendix 7: Emission and excitation spectra of Yb^{3+} dendrimers.

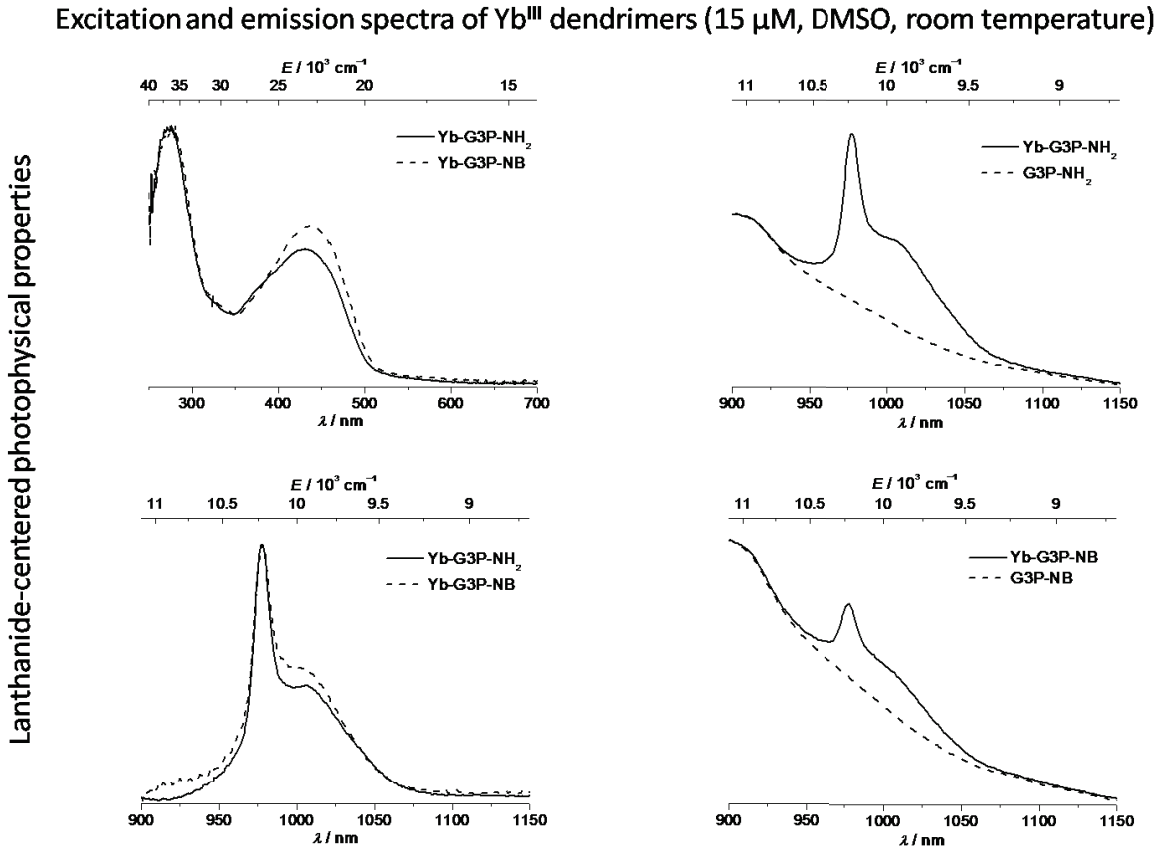

Appendix 8. Decay of the intensity with time of the luminescence arising from Eu^{3+} cations located in the polymetallic complex formed by reaction of a generation-3 PAMAM dendrimer whose branches have been functionalized with 32 2,3-naphthalimide groups. The concentration of the complex is 10^{-10} M in DMSO, λ_{ex}= 360 nm, λ_{em}=615 nm.

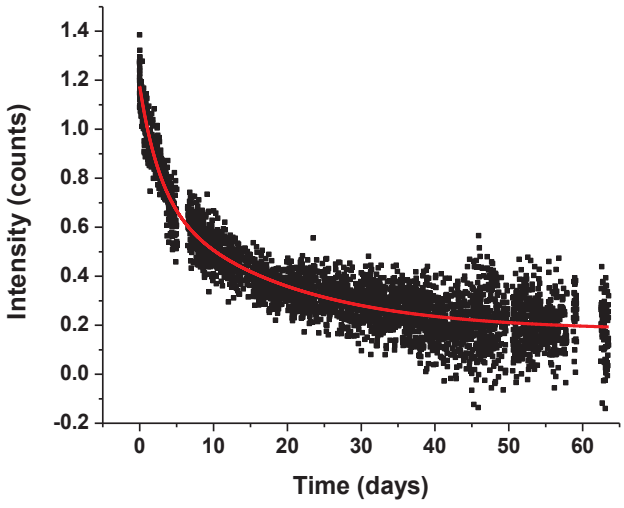

Lanthanide near infrared imaging in living cells with Yb^{3+} nano metal organic frameworks

Alexandra Foucault-Collet[a], Kristy A. Gogick[b], Kiley A. White[b], Sandrine Villette[a], Agnès Pallier[a], Guillaume Collet[a], Claudine Kieda[a], Tao Li[b], Steven J. Geib[b], Nathaniel L. Rosi[b,1], and Stéphane Petoud[a,b,1]

[a]Centre de Biophysique Moléculaire, Centre National de la Recherche Scientifique, 45071 Orléans, France; and [b]Department of Chemistry, University of Pittsburgh, Pittsburgh, PA 15260

Edited* by Kenneth N. Raymond, University of California, Berkeley, CA, and approved August 26, 2013 (received for review April 8, 2013)

We have created unique near-infrared (NIR)–emitting nanoscale metal-organic frameworks (nano-MOFs) incorporating a high density of Yb^{3+} lanthanide cations and sensitizers derived from phenylene. We establish here that these nano-MOFs can be incorporated into living cells for NIR imaging. Specifically, we introduce bulk and nano-Yb-phenylenevinylenedicarboxylate-3 (nano-Yb-PVDC-3), a unique MOF based on a PVDC sensitizer-ligand and Yb^{3+} NIR-emitting lanthanide cations. This material has been structurally characterized, its stability in various media has been assessed, and its luminescent properties have been studied. We demonstrate that it is stable in certain specific biological media, does not photobleach, and has an IC_{50} of 100 μg/mL, which is sufficient to allow live cell imaging. Confocal microscopy and inductively coupled plasma measurements reveal that nano-Yb-PVDC-3 can be internalized by cells with a cytoplasmic localization. Despite its relatively low quantum yield, nano-Yb-PVDC-3 emits a sufficient number of photons per unit volume to serve as a NIR-emitting reporter for imaging living HeLa and NIH 3T3 cells. NIR microscopy allows for highly efficient discrimination between the nano-MOF emission signal and the cellular autofluorescence arising from biological material. This work represents a demonstration of the possibility of using NIR lanthanide emission for biological imaging applications in living cells with single-photon excitation.

luminescence | bioimaging | nanoparticle | bioanalysis | sensitization

Luminescent reporters emitting in the near-infrared (NIR) region of the electromagnetic spectrum are highly advantageous for biological imaging applications for several reasons. Biological material has low autofluorescence in the NIR window, which allows facile discrimination between the desired signal of the reporter and the background, leading to an enhanced signal-to-noise ratio and improved detection sensitivity (1). Additionally, NIR light scatters less than visible light, and therefore results in increased optical imaging resolution (2, 3). Finally, NIR photons interact less with biological material compared with visible photons, thus decreasing the risk of disturbing or damaging the biological systems being observed.

NIR reporters, such as cyanine dyes (4, 5) and quantum dots (6), have previously been shown to be useful for biological imaging applications. However, these materials have broad emission bands that limit their ability to be easily discriminated from the background fluorescence. Additionally, cyanine dyes exhibit limited photostability and quantum dots can display blinking emission, making it difficult to conduct repeated or long-term experiments for such purposes as tracking a moiety or monitoring a process.

Several lanthanide cations emit in the NIR and have some advantages with respect to organic fluorophores and semiconductor nanocrystals. Lanthanide cations have narrower emission bandwidths than organic fluorophores and semiconductor nanocrystals. Their emission wavelengths are not affected by the environment, allowing them to be used in a broad range of conditions, including varied pH, and biological environments. Most luminescent lanthanide reporters are more resistant to photobleaching than organic fluorophores, which enables them to be used repeatedly and/or over long periods of time (7–9).

Free lanthanide cations have low extinction coefficients due to the forbidden nature of the $f \rightarrow f$ transition. Therefore, lanthanides must be sensitized using a photonic converter, such as an organic chromophore, through the "antenna effect" (10). "Antennae" must be placed in sufficiently close proximity to the lanthanide to provide sensitization, resulting in the compound emitting a sufficient number of photons for detection. Lanthanides must also be protected from −OH, −NH, and −CH vibrational overtones, which can quench lanthanide luminescence (11).

Despite the fact that several lanthanide complexes emitting in the NIR have been described in the literature because they have exciting properties for biological imaging in vivo (11–16), we are aware of only one example used for imaging in living cells (17). In that example, two-photon excitation was used, requiring specialized laser equipment.

We have tested a newly developed strategy by designing unique NIR-emitting lanthanide metal-organic frameworks (MOFs) that overcome these limitations by incorporating a large number of NIR-emitting Yb^{3+} cations and phenylenevinylene dicarboxylate (PVDC) sensitizers in a small volume. Using lanthanides as the metal in a MOF allows for the creation of well-defined crystalline species that can emit a large number of photons per unit volume to promote sensitive detection. This method provides an avenue for both the sensitization and the protection of the lanthanide cations, simultaneously fulfilling their requirement for large coordination numbers.

We previously reported Yb^{3+}-PVDC NIR-emitting lanthanide MOFs that exhibit tunable photophysical properties (18, 19) as bulk materials. To take advantage of using the PVDC ligand/sensitizer, we modified the synthesis and created a unique crystalline framework in the bulk phase, Yb-PVDC-3. Through a reverse microemulsion synthesis (20–22), we were able to create a nanoscale version of the same MOF, and in proof-of-principle experiments, we demonstrate its ability to operate as a NIR imaging agent in living HeLa and NIH 3T3 cells.

To date, there have been reports of nanoscale MOFs and coordination polymers for use as biosensors (20), as contrast agents for MRI (21–25) and computed tomography (26), and in drug delivery (24, 25, 27); in this report, we demonstrate that NIR-emitting nanoMOFs can be designed as imaging agents for biological systems.

Author contributions: A.F.-C., K.A.G., K.A.W., N.L.R., and S.P. designed research; A.F.-C., K.A.G., K.A.W., S.V., A.P., G.C., C.K., T.L., and S.J.G. performed research; A.F.-C. and K.A.G. contributed new reagents/analytic tools; A.F.-C., K.A.G., K.A.W., S.V., T.L., S.J.G., N.L.R., and S.P. analyzed data; and A.F.-C., K.A.G., N.L.R., and S.P. wrote the paper.

The authors declare no conflict of interest.

*This Direct Submission article had a prearranged editor.

Data deposition: The atomic coordinates and X-ray structure have been deposited in the Cambridge Structural Database, Cambridge Crystallographic Data Centre, Cambridge CB2 1EZ, United Kingdom (CSD reference no. 931598).

[1]To whom correspondence may be addressed. E-mail: nrosi@pitt.edu or stephane.petoud@cnrs-orleans.fr.

This article contains supporting information online at www.pnas.org/lookup/suppl/doi:10.1073/pnas.1305910110/-/DCSupplemental.

Results and Discussion

Yb-PVDC-3 crystallizes in the low-symmetry space group *P*-1 and exhibits infinite Yb-carboxylate secondary building units (SBUs) along the *a*-crystallographic direction (*SI Appendix*, Tables S2–S6). The SBU consists of octacoordinated Yb^{3+} with six carboxylates from three ligands and two oxygen atoms from two dimethylformamide molecules. The Yb-PVDC-3 nano-MOF is isostructural to the corresponding bulk material, as evidenced by powder X-ray diffraction (PXRD) pattern comparisons (Fig. 1). Compared with the previously reported Yb-PVDC-1 and Yb-PVDC-2 (18), Yb-PVDC-3 has lower symmetry and its structure is significantly more condensed, with 1D channels along the *a*-crystallographic direction measuring ~43 × 9 Å (Yb^{3+}-Yb^{3+} center-to-center distances). The 1D channels are very narrow: close contacts (e.g., 0.281, 0.637, and 0.706 Å) exist between the PVDC linkers lining opposite channel walls. SEM was used to study the size of nano-Yb-PVDC-3. The nano-MOFs exhibit a block-like morphology (Fig. 1), having average dimensions of 0.5 (±0.3) μm (length) by 316 (±156) nm (width) by 176 (±52) nm (thickness) (*SI Appendix*, Fig. S1).

Spectroscopic Characterization of Nano-Yb-PVDC-3. Luminescence properties of the material were studied in water (*SI Appendix*, Fig. S5) and 0.1 M Hepes buffer (pH 7.3) (Fig. 2). In both environments, nano-Yb-PVDC-3 exhibits Yb^{3+} luminescence centered at 970 nm upon excitation of the PVDC sensitizer. The overlap of the absorption spectrum of H_2-PVDC with the excitation spectrum of the MOF indicates that sensitization is occurring via the antenna effect. Because Yb^{3+} does not have accepting levels in the visible, the observed Yb^{3+} luminescence must result from the sensitization provided by PVDC located in sufficiently close proximity to the lanthanide cations. Quantum yields were recorded to quantify the efficiency of the energy transfer between the antenna and Yb^{3+} and the protection of the lanthanide cations against sources of nonradiative deactivation. Upon excitation at 450 nm, the quantum yield values for the nano-Yb-PVDC-3 are, respectively, 1.0 (±0.3) × 10^{-4} in water and 5.2 (±0.8) × 10^{-5} in 0.1 M Hepes buffer (pH 7.3) (Table 1). These values are relatively small in comparison to the best luminescent lanthanide compounds (11–16), but our approach of using a MOF system to maximize the number of chromophores and lanthanide cations per unit volume is expected to reduce the negative impact of this limitation.

Luminescence lifetime experimental data (Table 1) were best fit with a biexponential decay curve, indicating that the Yb^{3+} cations are present within two distinct environments. All the Yb^{3+} ions have a coordination number of eight (octacoordinate), and the different environments are attributed to the Yb^{3+} present in the interior of the nano-MOF and the Yb^{3+} on the edges/faces of the crystallites (exterior). Exterior Yb^{3+} is more susceptible to nonradiative deactivation and is likely responsible for the shorter lifetime values.

Ideally, reagents for bioanalytical applications and for imaging should emit a constant number of photons over time, and their signals should not be affected by species and parameters other than the targeted analyte. A common limitation for organic fluorophores is their tendency to photobleach when exposed to light. Photobleaching test experiments were performed by exposing a suspension of nano-Yb-PVDC-3 in 0.1 M Hepes buffer (pH 7.3) to light over a period of 13 h. Results showed that the signal does not significantly change (Fig. 2), a strong indication that the material is stable in these conditions and usable over this extended period.

Material Stability Studies. We rigorously evaluated the stability of Yb-PVDC-3 and nano-Yb-PVDC-3 in various conditions, including water, 0.1 M Hepes buffer (pH 7.3), and cellular media. First, samples of Yb-PVDC-3 were soaked in water or 0.1 M Hepes. At different time points, SEM images were collected to visualize bulk structure and PXRD patterns were obtained to confirm retention of crystallinity (*SI Appendix*, Figs. S2–S4). In general, SEM images indicate that the crystals remain intact after soaking in water or Hepes for up to 4 wk; however, crystallite fragmentation occurs during this time, and the average crystallite size consequently decreases. Notably, the faces of the crystallites remain smooth, and no significant pitting was observed on the crystal surfaces. PXRD patterns of crystallites collected after soaking in either water or Hepes buffer for different time intervals indicate retention of crystallinity.

We emphasize that to preserve the luminescence properties of the NIR-emitting reagent and to prevent the release of free lanthanide cations in cellular media, the nano-Yb-PVDC-3 must remain intact. Therefore, crystallite stability was quantitatively

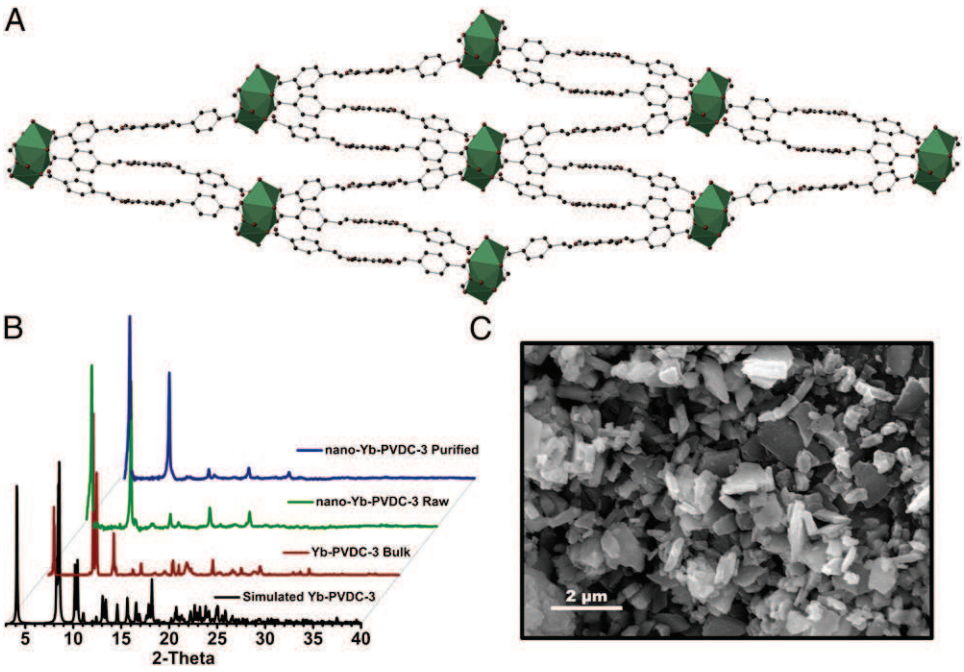

Fig. 1. (*A*) Crystal structure of Yb-PVDC-3 viewed along the *a*-crystallographic axis. Yb^{3+} is shown as a polyhedron (C, dark gray; O, red; Yb^{3+}, green). (*B*) PXRD patterns for simulated and bulk Yb-PVDC-3 and raw and purified nano-Yb-PVDC-3. (*C*) SEM image of nano-Yb-PVDC-3; average dimensions (±SD) are 0.5 (±0.3) μm (length), 316 (±156) nm (width), and 176 (±52) nm (thickness).

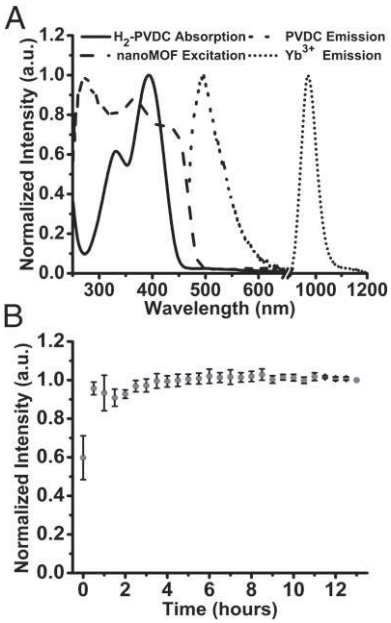

Fig. 2. Spectroscopic characterization of nano-Yb-PVDC-3 (30 μg/mL) in 0.1 M Hepes buffer (pH 7.3). (*A*) H_2-PVDC absorbance spectrum (solid line), nano-Yb-PVDC-3 excitation spectrum (long-dashed line, λ_{em} = 980 nm), and emission spectra for both the ligand (short-dashed line) and lanthanide (dotted line) obtained by exciting nano-Yb-PVDC-3 at 355 nm. (*B*) Photobleaching study monitoring the emission at 970 nm over a period of 13 h. Error bars represent SD based on three independent experiments. a.u., arbitrary unit.

evaluated in cellular media by monitoring the Yb^{3+} emission signal upon excitation of the antenna. The signal of the lanthanide cation can only be generated if the antenna effect is present and only if the sensitizer is located sufficiently close to the lanthanide. Therefore, if the MOF dissociates via hydrolysis of the Yb-carboxylate bonds, one should expect a significant decrease in the luminescence. Signal arising from Yb^{3+} was measured at regular time intervals after dilution of nano-Yb-PVDC-3 in cell lysate (HeLa or NIH 3T3 cells) and in water as a control. Intensities of the emission bands compared with initial intensity (recorded upon monitoring the Yb^{3+} band at 970 nm) are reported in Fig. 3. The emission intensity remains constant over time, which suggests that the nano-Yb-PVDC-3 structure is not significantly modified by cellular components. Indeed, the constant total intensity of the Yb^{3+} emission signal is a quantitative indication that the measured nano-MOFs retain most of their integrity in this environment. Therefore, we expect that nano-Yb-PVDC-3 will be intact inside of the cell.

Nano-Yb-PVDC-3 Cytotoxicity. A principal aim of this study is to test nano-Yb-PVDC-3 in cells as NIR imaging agents. Human cancer (HeLa) and mouse (NIH 3T3) cells were chosen as representative cell lines. The nano-Yb-PVDC-3 cytotoxicity was first evaluated for both cell lines using the Alamar Blue assay. The cell proliferation test presented in Fig. 4 indicated a similar effect on the two cell lines after 24 h of incubation. The compound is found to have relatively low toxicity for concentrations up to 50 μg/mL. A working concentration was chosen on the criterion of 90% of cellular viability (30 μg/mL).

Table 1. Relative quantum yields (Φ) and luminescent lifetimes (τ_x) of Yb^{3+}-centered emission at 980 nm

	Solvent*	Φ_{Yb}[†]	τ_1[‡], μs	τ_2[‡], μs
Nano-Yb-PVDC-3	H_2O	1.0 (±0.3) × 10^{-4}	7.01 (±0.07)	1.51 (±0.01)
	0.1 M Hepes	5.2 (±0.8) × 10^{-5}	4.6 (±0.1)	1.04 (±0.02)

*Nano-MOFs as a crystalline solid under solvent.
[†]λ_{ex} = 450 nm.
[‡]λ_{ex} = 355 nm.

Cellular Uptake. Internalization of nano-Yb-PVDC-3 by the cells was confirmed with confocal microscopy and inductively coupled plasma (ICP) spectrometry experiments. Microscopy images in Fig. 5 show that nano-Yb-PVDC-3 is internalized by cells. Optical slices of 1 μm (less than cell thickness) were obtained for NIH 3T3 cells after incubation with nano-Yb-PVDC-3 at 30 μg/mL. Despite the fact that untreated cells generate autofluorescence at these wavelengths (λ_{ex} = 365 nm, λ_{em} = 445/50 nm), we could unambiguously detect the chromophore signal inside cells. This fluorescence signal is located preferentially in the cytoplasm (and not in the nucleus). To confirm results of confocal microscopy, the quantity of nano-Yb-PVDC-3 associated with 1 × 10^6 cells was measured by ICP (*SI Appendix*, Table S1). More specifically, the amount of Yb^{3+} in cells was measured after 24 h of incubation of HeLa and NIH 3T3 cells with nano-Yb-PVDC-3. ICP results confirm the presence of nano-Yb-PVDC-3 in the cells. For both cell lines, the Yb^{3+} amount in cells increases with the amount of nano-Yb-PVDC-3 present in cell incubation medium. No saturation of cellular uptake has been observed at these concentrations. The uptake is more pronounced in NIH 3T3 cells than in HeLa cells. The mechanism of cell uptake has not been analyzed at this time and is currently under investigation.

Spectral Microcopy. Several cellular compounds are excited by UV light and emit in the visible, such as tryptophan (λ_{ex} = 275 nm, λ_{em} = 335 nm), collagen (λ_{ex} = 335 nm, λ_{em} = 405 nm), and NAD(P)H (λ_{ex} = 340 nm, λ_{em} = 460 nm) (28). To confirm that the detected signal observed with confocal microscopy is arising from PVDC emission, we conducted spectral fluorescence microscopy analysis on cells after 24 h of incubation with nano-Yb-PVDC-3. At each individual point of the image (step size = 3 μm), an emission spectrum was recorded. The intensity value averaged between 400 and 600 nm was used to create an intensity map of the cell (Fig. 6). This spectral fluorescence microscopy experiment permits the discrimination of nano-Yb-PVDC-3 emission from cellular autofluorescence. The signal obtained from untreated cells (*SI Appendix*, Fig. S6) can be attributed to cellular autofluorescence with a maximum of the emission band located at 420 nm. Spectra obtained from treated cells result from the overlay of autofluorescence emission and PVDC emission signals (λ_{em} = 455 nm). This result is a third confirmation that the nano-MOF is able to enter incubated cells.

NIR Epifluorescence Microscopy. The ability to use nano-Yb-PVDC-3 as a NIR lanthanide-based imaging agent was tested in a NIR microscopy experimental setup. HeLa and NIH 3T3 cells were incubated with 30 μg/mL nano-Yb-PVDC-3 for 24 h. Visible chromophore PVDC and NIR Yb^{3+} emission signals were both

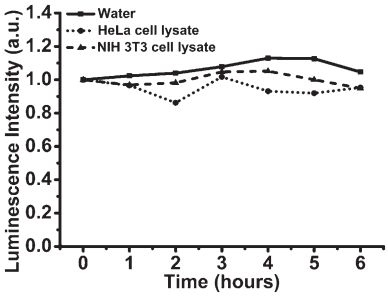

Fig. 3. Spectroscopic evaluation of the nano-Yb-PVDC-3 stability in cell lysate. Emission intensity values correspond to the maximum of Yb^{3+} emission (970 nm) after dilution of nano-Yb-PVDC-3 at 30 μg/mL in water (solid line), HeLa cell lysate (dotted line), or NIH 3T3 cell lysate (dashed line).

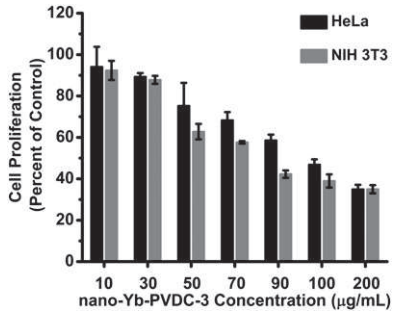

Fig. 4. Cellular viability by Alamar Blue assay on HeLa and NIH 3T3 cells after 24 h of incubation with increasing concentrations of nano-Yb-PVDC-3.

observed by epifluorescence microscopy in the same field (Fig. 7). In the NIR microscopy mode, the specific Yb^{3+} emission signal was collected with good sensitivity (1-s exposure time can be considered as short for NIR signals) as the result of a high signal-to-noise ratio. In parallel, switching to visible detection mode, the specific fluorescence arising from the PVDC was observed in addition to the cellular autofluorescence, and the resulting images were used as a comparison. The difference observed between the PVDC and Yb^{3+} emission signal results from the discrimination of the NIR signal from the visible autofluorescence arising from the biological material.

The images presented in Fig. 7 report NIR microscopy experiments obtained with a lanthanide compound in living cells using a conventional excitation source.

Conclusion

We have designed and synthesized nano-Yb-PVDC-3, a unique nano-MOF emitting in the NIR, and we have tested its ability to operate as a NIR imaging agent in cells. The overlap of the excitation spectra of nano-Yb-PVDC-3 with the absorbance spectra of H_2-PVDC demonstrates that the Yb^{3+} is sensitized through the antenna effect, where the sensitizers embedded in the MOF structure are excited and transfer energy to the accepting level of the Yb^{3+} cations.

The nanoscale material was shown to be luminescent in water and Hepes buffer. As expected, the nano-MOF quantum yield is low in water, likely due to the energy level of the −OH overtone vibration being so close to that of Yb^{3+}. It further decreases when the nano-MOF is placed in Hepes, likely due to the increase in number of moieties with −OH vibrations in solution. This low quantum yield does not prevent imaging applications because of the polysensitizer and polymetallic design.

The energy transfer is conserved after 24 h of incubation in cellular media, indicating that crystalline nano-Yb-PVDC-3 remains in the cells. This stability, combined with cytotoxicity results, is promising for using nano-Yb-PVDC-3 as a biological probe for in vivo applications.

We have been able to observe NIR microscopy images in living cells based on the signal arising from Yb^{3+}, sensitized via the antenna effect. This achievement has been realized by the use of a unique nano-MOF that is able to incorporate a large number of lanthanide sensitizers (PVDC) and a large number of NIR-emitting lanthanide cations, resulting in an increase in the number of emitted NIR photons per unit volume.

Materials and Methods

Reagents. Reagents were obtained from commercial sources and used as received without further purification. The H_2-PVDC was synthesized according to a previously published method (18). The 1,4-dimethoxybenzene (99%), paraformaldehyde (PFA; 95%), sodium methoxide (0.05 M in methanol), anhydrous methanol (99.8%), anhydrous benzene (99.8%), methylamine (40 wt% in water), hexadecyltrimethylammonium bromide (CTAB; >98% powder), heptane (Reagent Plus, 99%), $Yb(NO_3)_3{\cdot}5H_2O$ (99.999%), $YbCl_3{\cdot}6H_2O$ (99.998%), and DMSO (ACS Reagent, >99.9%) were purchased from Sigma–Aldrich. Hydrobromic acid (33 wt% in acetic acid) was purchased from Fluka. Anhydrous chloroform (99.8%) and anhydrous toluene (99.8%) were purchased from Acros. Triphenylphosphine was purchased from MCB Reagents. Methanol (Certified ACS), tetrahydrofuran (Certified ACS), and potassium hydroxide (Certified ACS pellets) were purchased from Fisher. Methyl 4-formylbenzoate (>98%) was purchased from TCI. N,N-dimethylformamide [DMF, American Chemical Society (ACS) grade] was purchased from Emmanuel Merck Darmstadt. Nitric acid (HNO_3, ACS Reagent, 36.5–38.0%) and glacial acetic acid (Baker Analyzed Reagent) were purchased from J. T. Baker. Hexanol (purified) was purchased from Spectrum. Ethanol (200 proof) was purchased from Decon Laboratories, Inc.

Synthesis of Yb-PVDC-3. In a 20-mL glass vial, a solution of 4,4′-(1*E*,1′*E*)-2,2′-(2,5-dimethoxy-1,4-phenylene)bis(ethene-2,1-diyl)dibenzoic acid (H_2-PVDC; 86.0 mg, 0.20 mmol) in DMF (4.0 mL) was added to a solution of $Yb(NO_3)_3{\cdot}5H_2O$ (22.5 mg, 0.05 mmol) in DMF (1.0 mL) and HNO_3 (1 mL, 1 M aqueous) to produce a neon green solution. The vial was capped and placed in a 105 °C isotemp oven for 12 h to produce yellow crystalline needles of the product. The crystals were collected, washed with DMF (4 × 5 mL), and air-dried (29.7 mg, 61.8%).

Elemental analysis (EA) calculated (%) for $Yb_1(C_{26}H_{20}O_6)_{1.5}(DMF){\cdot}0.65$ DMF, H_2O was C, 55.31; H, 4.60; and N, 2.42. EA found was C, 54.87; H, 4.22; and N, 2.51. EA calculated (%) for the water exchange product, $Yb_1(C_{26}H_{20}O_6)_{1.5}(H_2O)_2{\cdot}(DMF)_{0.25}(H_2O)_{2.25}$, was C, 52.43; H, 4.46; and N, 0.38. EA found was C, 52.12; H, 3.68; and N, 0.30. FTIR (KBr, 4,000 to 700 cm^{-1}) was as follows: 3,424 [broad (br)], 3,054 [weak (w)], 2,998 (w), 2,936 (w), 2,830 (w), 1,665 [DMF C = O medium (m)], 1,601 (m), 1,544 (m), 1,413 [COO^-, very strong (vs)], 1,338 (w), 1,260 (w), 1,211 (s), 1,181 (m), 1,108 (w), 1,044 (s), 965 (m), 861 (w), 779 (trans C = C − H, s), and 709 cm^{-1} (w).

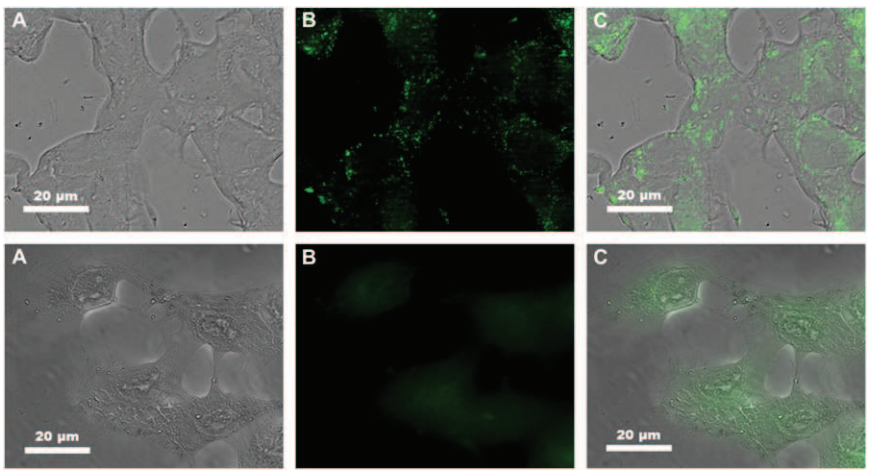

Fig. 5. Cellular uptake of nano-Yb-PVDC-3. Confocal microscopy of NIH 3T3 cells after incubation with nano-Yb-PVDC-3 at 30 μg/mL (*Upper*) and of untreated cells (*Lower*). Bright-field (*A*), H_2-PVDC emission (λ_{ex} = 365/12 nm, λ_{em} = 445/50 nm) (*B*), and merged (*C*) images are shown.

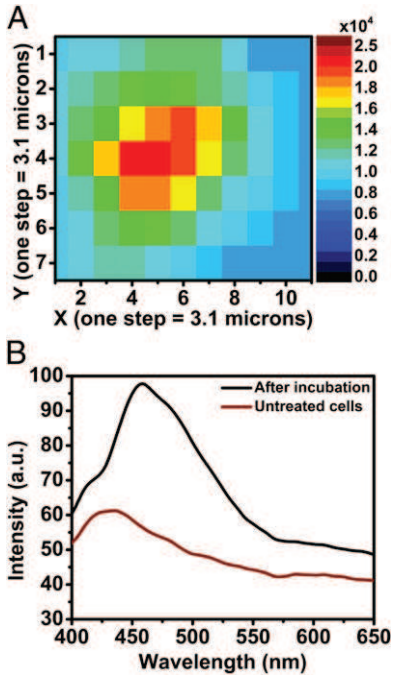

Fig. 6. Spectral microscopy of nano-Yb-PVDC-3 in the visible region. (*A*) Fluorescence intensity map of NIH 3T3 cells after incubation with 30 μg/mL nano-Yb-PVDC-3 (λ_{ex} = 340 nm, λ_{em} = 390–650 nm). (*B*) Spectra correspond to the mean of intensity of each map.

Synthesis of Nano-Yb-PVDC-3. This procedure is based on previously reported reverse microemulsion nano-MOF synthesis (20–22). The methylammonium salt of the H_2-PVDC ligand [PVDC-$(NH_2CH_3)_2$] was prepared by dissolving H2-PVDC in methylamine (40 wt% in water) removing the solvent under reduced pressure, and adding a known amount of water to achieve the desired concentration. A 0.05 M solution of CTAB was prepared by dissolving CTAB in a 9:1 (vol/vol) ratio of heptane/hexanol and stirring for 30 min. A w = 10 (where w is the H_2O/CTAB molar ratio) reaction mixture was prepared as follows. A solution of $YbCl_3{\cdot}6H_2O$ (225 μL, 0.05 M in H_2O) was added to a flask containing the CTAB mixture (25 mL, 0.05 M in heptane/hexanol). A solution of PVDC-$(NH_2CH_3)_2$ (225 μL, 0.05 M in H_2O) was added to another flask also containing the CTAB mixture (25 mL, 0.05 M). The flasks were stirred separately for at least 10 min until clear. The $YbCl_3{\cdot}6H_2O$ solution was then added to the PVDC solution and stirred for 24 h at room temperature. Yellow solid was isolated via centrifugation at 3,313 × g for 30 min, followed by washing with ethanol (3 × 35 mL).

The product was purified by dialysis using a regenerated cellulose membrane (nominal molecular weight cut off of 3,500; Fisher Scientific) in DMSO for 3 d. The solid recovered from the dialysis membrane was dried in a vacuum oven (40 °C, 40 mbar).

FTIR. FTIR spectra were measured on a Nicolet Avatar 360 FTIR spectrometer using KBr pellet samples. Absorptions are described as vs, s, m, w, shoulder, and br, and stretches are labeled as symmetrical or asymmetrical. Data were analyzed using the Omnic Software Package (Thermo Scientific).

PXRD. PXRD patterns for the bulk material were collected using a Bruker AXS D8 Discover powder diffractometer at 40 kV, 40 mA, for Cu Kα (λ = 1.5406 Å) with a scan speed of either 0.20 s per step or 0.50 s per step and a step size of 0.02018°. PXRD patterns for the nano-MOFs were collected using a Philips PW1830 diffractometer at 40 kV, 40 mA, for Cu Kα (λ = 1.54056 Å) with a scan speed of 0.50 s per step and a step size of 0.020°.

SEM. Samples were coated with palladium for 60 s before analysis with a Philips XL 30 scanning electron microscope. ImageJ 1.47f software (National Institutes of Health) was used to measure the particle dimensions, and OriginPro 8.6 software (OriginLab Corporation) was used to process the data.

Spectroscopic Characterization. Excitation and emission spectra were measured using a HORIBA Jobin Yvon Fluorolog 3-22 spectrofluorometer equipped with a R928 Hamamatsu detector for visible detection and with a DSS-IGA020L detector (Electro-Optical Systems, Inc.) for the NIR domain on colloidal suspension at 30 μg/mL in Hepes 0.1 M (pH 7.3). An integrating sphere developed by Frédéric Gumy and Jean-Claude G. Bünzli (Laboratory of Lanthanide Supramolecular Chemistry, École Polytechnique Féderale de Lausanne, Lausanne, Switzerland) as an accessory to the Fluorolog 3-22 spectrofluorometer (patent pending) using quartz tube sample holders was used for determination of quantum yield and was commercialized and manufactured by GMP (29). Spectra were corrected for variations in lamp intensity over the spectra range, as well as for excitation monochromator, emission monochromator, and detector responses.

Relative quantum yields were measured with the Fluorolog 3-22 setup described above using ytterbium tropolonate ($[Yb(trop)_4]^-$) in DMSO [Φ_{Yb} = 1.9 (±0.1) × 10^{-3}] as a reference (12).

Using the Fluorolog 3-22 setup described above, emission spectra (λ_{ex} = 355 nm) were collected every 30 min for a photobleaching study. The samples were exposed to white light from the xenon lamp of the Fluorolog 3-22 between collection of emission spectra.

Luminescence Lifetimes. Luminescence lifetimes were measured using a neodymium yttrium aluminum garnet Continuum Powerlite 8010 laser (355 nm, third harmonic) as the excitation source. Emission was collected at a right angle to the excitation beam, and wavelengths were selected by a Spectral Products CM 110 1/8 m monochromator. The signal was monitored by a Hamamatsu R316-02 photomultiplier tube and collected on a 500-MHz bandpass digital oscilloscope (Tektronix TDS 754D). Signals from >1,000 flashes were collected and

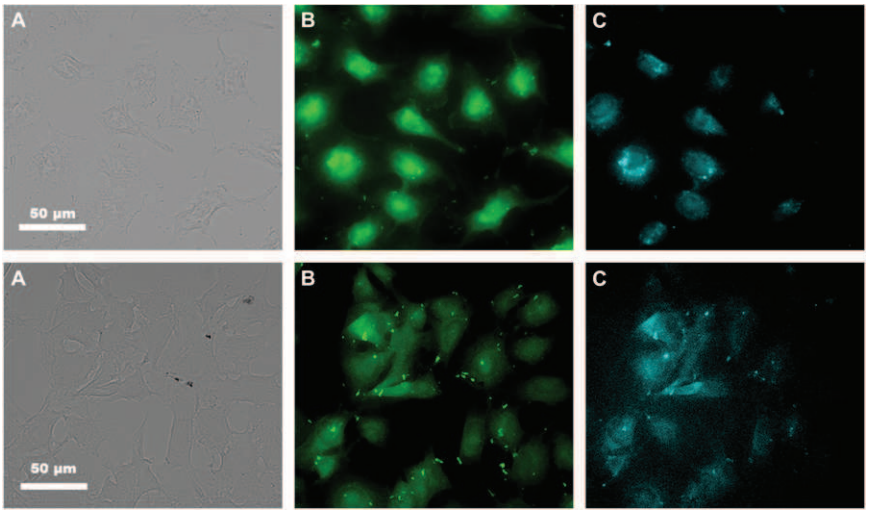

Fig. 7. Visible and NIR microscopy images of nano-Yb-PVDC-3 in HeLa cells (*Upper*) and NIH 3T3 cells (*Lower*) (λ_{ex} = 340 nm). Bright-field (*A*), H_2-PVDC emission (λ_{ex} = 377/50 nm, λ_{em} = 445/50 nm) (*B*), and Yb^{3+} emission (λ_{ex} = 377/50 nm, λ_{em} = long pass 770 nm) (*C*) images are shown.

averaged. Three decay curves were collected for each sample, and the data were analyzed using OriginPro 8.6 software with exponential fitting modes.

Cell Culture. HeLa (human epithelial ovarian carcinoma) and NIH 3T3 (mouse embryonic fibroblast) cell lines obtained from the American Type Culture Collection were grown at 37 °C in a 5% CO_2-humidified atmosphere. Every 3–4 d, 5×10^5 cells were seeded into a 25-cm^2 plastic flask. Cells were cultivated in MEM and in DMEM, respectively, supplemented with 10% FBS and, for HeLa cells, 1% L-glutamine, 1% penicillin/streptomycin, and 1% of a 100-fold nonessential amino acid solution.

Alamar Blue Assay. For the cytotoxicity test, 1×10^4 cells per well were seeded in a 96-well microplate. After 24 h of cell attachment, the cells were treated with increasing concentrations of nano-Yb-PVDC-3 diluted for 24 h at 37 °C. The cytotoxicity was evaluated with the Alamar Blue assay (Invitrogen). Alamar Blue was added to the medium (10% vol/vol), and its fluorescence (λ_{ex} = 530 nm, λ_{em} = 590 nm) was measured after 4 h at 37 °C with a microplate reader (Victor 3V; PerkinElmer). This assay compares the fluorescence of untreated cells with the fluorescence of cells after incubation with nano-Yb-PVDC-3.

Stability in Cell Biological Media. The emission of nano-Yb-PVDC-3 was followed during 6 h in cell lysate. For this, 1×10^6 cells (HeLa and NIH 3T3) were collected. After centrifugation, the pellets were resuspended in water and cell membranes were lysed using a 25-gauge syringe for a mechanical lyse. The lysates were centrifuged again to exclude cell membrane fragments. Nano-Yb-PVDC-3 was diluted in the supernatant, and the emission spectra were measured using the Fluorolog 3-22.

ICP for Cellular Uptake Quantification. To quantify the concentration of Yb^{3+} in cells, 1×10^6 cells were seeded in a six-well microplate. After 24 h of attachment, the cells were incubated with 20, 30, or 40 mg/L of nano-Yb-PVDC-3 for 24 h at 37 °C. Cells were trypsinized and centrifuged for 5 min at $423 \times g$. The pellets were resuspended in nitric acid overnight before adding PBS buffer to achieve a final concentration of 5% nitric acid. The measurements were taken on an ICP (Ultimate; Jobin Yvon) coupled with a photomultiplier tube and high dynamic detection system.

Confocal Images. Confocal fluorescence imaging was realized with an Axio Observer Z1 fluorescence inverted microscope (Zeiss) equipped with an ORCA-R2 high-resolution CCD camera linked to a computer driving the Axiovision (Zeiss) acquisition software. Confocality was obtained by means of a Zeiss-ApoTome module of optical sectioning using structured illumination by grids oscillations. The Zeiss HXP-120 light source (metal halide) was used as an excitation system and was combined with a UV cube filter unit as follows: λ_{ex} = 365/12 nm, λ_{em} = 445/50 nm to observe phenylene emission. Optical sections were recorded at magnifications of 20× and 40× with Zeiss Plan-APOCHROMAT 20×/0.8 and 40×/1.4 objectives, respectively.

NIR Microscopy. NIR epifluorescence microscopy was realized on the same microscope as for confocal images, except that the microscope was equipped with an EMCCD Evolve 512 Photometrics camera. The Zeiss HXP 120 was combined with a cube filter as follows: λ_{ex} = 365/12 nm, λ_{em} = 445/50 nm to observe phenylene emission with 280 ms of exposition and λ_{ex} = 377/50 nm, λ_{em} = long pass 770 nm to observe Yb^{3+} emission with 1 s of exposition.

Spectral Fluorescence Microscopy. Cells were plated onto 25-mm round quartz coverslips and incubated for 24 h with 30 μg/mL nano-Yb-PVDC-3 before fixation with 4% PFA. Fluorescence spectra were recorded on the POLYPHEME, the deep ultraviolet inverted microspectrofluorometer installed at the DISCO (Dichroïsme, Imagerie, Spectrométrie de masse pour la Chimie et la biOlogie) beamline at Synchrotron SOLEIL (30). Excitation at 280 or 340 nm was provided by the continuous emittance from the DISCO beamline bending magnet and focused on the sample using a 100× microscope objective (Zeiss).

One full fluorescence emission spectrum was recorded on each point of the image (6 × 10 pixels) with an acquisition time of 10 s. A fluorescence intensity map was reconstructed in the spectral region of interest.

ACKNOWLEDGMENTS. We thank the staff of the DISCO at SOLEIL synchrotron for beam time allocation and assistance during data collection (Proposal 20110179). We thank David Gosset and the Centre de Biophysique Moléculaire cytometry platform for the microscope access. We thank the University of Pittsburgh Department of Chemistry support services, the Mechanical Engineering and Materials Science Department for SEM and PXRD access, and the Petersen Nanoscale Fabrication and Characterization Facility for PXRD access. S.P. acknowledges support from the Institut National de la Santé et de la Recherche Médicale. K.A.G. acknowledges support from the Mary E. Warga Predoctoral Fellowship. We thank La Ligue contre le Cancer and La Région Centre for funding. The work in France was carried out in the framework of European Cooperation in Science and Technology Action TD1004 and CM1006. N.L.R. acknowledges partial support from the National Science Foundation (DMR-0954380).

1. Mahmood U, Weissleder R (2003) Near-infrared optical imaging of proteases in cancer. *Mol Cancer Ther* 2(5):489–496.
2. Lim YT, et al. (2003) Selection of quantum dot wavelengths for biomedical assays and imaging. *Mol Imaging* 2(1):50–64.
3. Frangioni JV (2003) In vivo near-infrared fluorescence imaging. *Curr Opin Chem Biol* 7(5):626–634.
4. Mujumdar RB, Ernst LA, Mujumdar SR, Lewis CJ, Waggoner AS (1993) Cyanine dye labeling reagents: Sulfoindocyanine succinimidyl esters. *Bioconjug Chem* 4(2):105–111.
5. Roederer M, Kantor AB, Parks DR, Herzenberg LA (1996) Cy7PE and Cy7APC: Bright new probes for immunofluorescence. *Cytometry* 24(3):191–197.
6. Sargent EH (2005) Infrared quantum dots. *Adv Mater* 17(5):515–522.
7. Alcala MA, et al. (2011) Preferential accumulation within tumors and in vivo imaging by functionalized luminescent dendrimer lanthanide complexes. *Biomaterials* 32(35): 9343–9352.
8. Alcala MA, et al. (2011) Luminescence targeting and imaging using a nanoscale generation 3 dendrimer in an in vivo colorectal metastatic rat model. *Nanomedicine* 7(3):249–258.
9. Nockemann P, et al. (2005) Photostability of a highly luminescent europium β-diketonate complex in imidazolium ionic liquids. *Chem Commun (Camb)* (34):4354–4356.
10. Weissman SI (1942) Intramolecular energy transfer the fluorescence of complexes of europium. *J Chem Phys* 10(4):214–217.
11. Eliseeva SV, Bünzli J-CG (2010) Lanthanide luminescence for functional materials and bio-sciences. *Chem Soc Rev* 39(1):189–227.
12. Zhang J, Badger PD, Geib SJ, Petoud S (2005) Sensitization of near-infrared-emitting lanthanide cations in solution by tropolonate ligands. *Angew Chem Int Ed Engl* 44(17):2508–2512.
13. Zhang J, Petoud S (2008) Azulene-moiety-based ligand for the efficient sensitization of four near-infrared luminescent lanthanide cations: Nd^{3+}, Er^{3+}, Tm^{3+}, and Yb^{3+}. *Chemistry* 14(4):1264–1272.
14. Comby S, Imbert D, Chauvin AS, Bünzli JC (2006) Stable 8-hydroxyquinolinate-based podates as efficient sensitizers of lanthanide near-infrared luminescence. *Inorg Chem* 45(2):732–743.
15. Korovin YV, Rusakova NV, Popkov YA, Dotsenko VP (2002) Luminescence of ytterbium and neodymium in complexes with bis-macrocyclic ligands. *J Appl Spectrosc* 69(6):841–844.
16. Bünzli J-CG, Eliseeva SV (2013) Intriguing aspects of lanthanide luminescence. *Chem Sci* 4(5):1939–1949.
17. D'Aléo A, et al. (2012) Ytterbium-based bioprobes for near-infrared two-photon scanning laser microscopy imaging. *Angew Chem Int Ed Engl* 51(27):6622–6625.
18. White KA, et al. (2009) Near-infrared emitting ytterbium metal-organic frameworks with tunable excitation properties. *Chem Commun (Camb)* (30):4506–4508.
19. White KA, et al. (2009) Near-infrared luminescent lanthanide MOF barcodes. *J Am Chem Soc* 131(50):18069–18071.
20. Rieter WJ, Taylor KML, Lin W (2007) Surface modification and functionalization of nanoscale metal-organic frameworks for controlled release and luminescence sensing. *J Am Chem Soc* 129(32):9852–9853.
21. Taylor KML, Rieter WJ, Lin W (2008) Manganese-based nanoscale metal-organic frameworks for magnetic resonance imaging. *J Am Chem Soc* 130(44):14358–14359.
22. Rieter WJ, Taylor KML, An H, Lin W, Lin W (2006) Nanoscale metal-organic frameworks as potential multimodal contrast enhancing agents. *J Am Chem Soc* 128(28): 9024–9025.
23. Taylor KML, Jin A, Lin W (2008) Surfactant-assisted synthesis of nanoscale gadolinium metal-organic frameworks for potential multimodal imaging. *Angew Chem Int Ed Engl* 47(40):7722–7725.
24. Taylor-Pashow KML, Della Rocca J, Xie Z, Tran S, Lin W (2009) Postsynthetic modifications of iron-carboxylate nanoscale metal-organic frameworks for imaging and drug delivery. *J Am Chem Soc* 131(40):14261–14263.
25. Horcajada P, et al. (2010) Porous metal-organic-framework nanoscale carriers as a potential platform for drug delivery and imaging. *Nat Mater* 9(2):172–178.
26. deKrafft KE, et al. (2009) Iodinated nanoscale coordination polymers as potential contrast agents for computed tomography. *Angew Chem Int Ed Engl* 48(52): 9901–9904.
27. Rieter WJ, Pott KM, Taylor KML, Lin W (2008) Nanoscale coordination polymers for platinum-based anticancer drug delivery. *J Am Chem Soc* 130(35):11584–11585.
28. Wagnières GA, Star WM, Wilson BC (1998) In vivo fluorescence spectroscopy and imaging for oncological applications. *Photochem Photobiol* 68(5):603–632.
29. Aebischer A, Gumy F, Bünzli J-CG (2009) Intrinsic quantum yields and radiative lifetimes of lanthanide tris(dipicolinates). *Phys Chem Chem Phys* 11(9):1346–1353.
30. Giuliani A, et al. (2009) DISCO: A low-energy multipurpose beamline at synchrotron SOLEIL. *J Synchrotron Radiat* 16(Pt 6):835–841.

Alexandra Foucault-Collet

Réseaux Metallo-organiques et Complexes de Dendrimères luminescents à base de lanthanides pour imagerie optique

Les composés à base de lanthanides luminescents possèdent des propriétés uniques offrant de nombreux avantages pour l'étude de problèmes biologiques et pour le diagnostic. Ils résistent notamment à la photodécomposition, possèdent des temps de vie de luminescence longs ainsi que des bandes d'émissions étroites qui ne se recouvrent pas.
De plus, certains lanthanides émettent dans le proche infrarouge, ce qui les rend particulièrement intéressants pour des applications d''imagerie *in vivo*.
De part l'interdiction des transitions $f \rightarrow f$, les cations lanthanides ont des coefficients d'extinction très faibles. C'est la raison pour laquelle, il est nécessaire d'utiliser un ou plusieurs sensibilisateur(s) (comme un chromophore organique) pour exciter le lanthanide par « effet antenne ».
Nous proposons ici de nouveaux composés émettant dans le proche infrarouge dont la structure permet d'incorporer une densité importante de lanthanides et de sensibilisateurs par unité de volume : i) les nano-MOF Yb-PVDC-3 constitués de chromophores dérivés de dicarboxylates de phenylènevinylène qui sensibilisent les cations Yb^{3+} du réseau. ii) les complexes formés avec des ligands dendrimères dérivés de polyamidoamine de génération 3 capables de sensibiliser 8 lanthanides (Eu^{3+}, Yb^{3+}, Nd^{3+}) par le biais de 32 antennes dérivées du groupe 1,8-naphthalimide.
La caractérisation physique, photophysique et la biocompatibilité de ces composés ont été réalisées. Ils ont montré une bonne stabilité dans différents environnements. Leur faible cytotoxicité a permis d'obtenir des images de microscopie proche infrarouge sur cellules vivantes.
La preuve de principe que les nano-MOFs et les dendrimères complexant des lanthanides peuvent être utilisés comme rapporteurs luminescents *in cellulo* et *in vivo* a été ici établie. Les résultats obtenus valident la stratégie d'utiliser ce type de matériel pour augmenter le nombre de photons émis par unité de volume afin d'obtenir une meilleure sensibilité de détection.

Mots clés: **imagerie - proche-infrarouge - lanthanides - dendrimères - réseaux métallo-organiques**

Luminescent lanthanide Metal-Organic Frameworks and Dendrimer Complexes for Optical Biological Imaging

Unique properties of luminescent lanthanides reporters explain their emergence for bioanalytical and optical imaging applications. Lanthanide ions possess long emission lifetimes, a good resistance to photodecomposition and sharp emission bands that do not overlap.
In addition, several lanthanides emit in the near infrared (NIR) region of the electromagnetic spectrum making them very interesting for *in vivo* imaging. Free lanthanide cations have low extinction coefficients due to the forbidden nature of the $f \rightarrow f$ transition. Therefore, lanthanides must be sensitized using a photonic converter such as an organic chromophore through the "antenna effect".
We report here new near-infrared emitting compounds whose structure allows to incorporate a high density of lanthanide cations and sensitizers per unit volume: i) nano-MOF Yb-PVDC-3 based on Yb^{3+} sensitized by phenylenevinylene dicarboxylates. ii) polymetallic dendrimer complexes formed with derivatives of new generation-3 polyamidoamine dendrimers. In these complexes, 8 lanthanide ions (Eu^{3+}, Yb^{3+}, Nd^{3+}) can be sensitized by the 32 antenna derived from 1,8-naphthalimide.
These two families of compounds were fully characterised for their physical, photophysical properties as well as for their biological respective compatibilities. They are stable in various media and their low cytotoxicity and emission of a sufficient number of photons are suitable for near-infrared live cell imaging.
One of the main goal outcomes of this work is the establishment of the proof of principle that nano-MOFs and lanthanide derived dendrimers can be used for the sensitization of NIR emitting lanthanides to create a new generation of NIR optical imaging agents suitable for both *in cellulo* and *in vivo*applications.The present work also validates the efficiency of the strategy to use both types of nanoscale systems described here to increase the number of emitted photons per unit volume for an improved detection sensitivity and to compensate for low quantum yields.

Key words: **imaging - near-infrared - lanthanides - dendrimers - Metal Organic Frameworks.**

Centre de Biophysique Moléculaire
Rue Charles Sadron
45071 Orléans Cedex 2